Title
Biomechanics of Compartmentalized Mechanical Properties of Extraocular Muscle and Tendon

Author
Shin, KWANG SUP

Publication Date
2014

Peer reviewed|Thesis/dissertation

UNIVERSITY OF CALIFORNIA

Los Angeles

Biomechanics of Compartmentalized Mechanical Properties of Extraocular Muscle and Tendon

A dissertation submitted in partial satisfaction of the

requirements for the degree Doctor of Philosophy

in Mechanical Engineering

by

Kwang Sup Shin

2014

ABSTRACT OF THE DISSERTATION

Biomechanics of Compartmentalized Mechanical Properties of Extraocular Muscle and Tendon

by

Kwang Sup Shin

Doctor of Philosophy in Mechanical Engineering

University of California, Los Angeles, 2014

Professor Joseph L. Demer Co-Chair

Professor Vijay Gupta Co-Chair

A controversial issue in the eye movement field involves the compartmentalization of extraocular muscle (EOM). Conventionally, it has been believed that each individual EOM is innervated uniformly by its motor nerve, and behaves uniformly. However, recent studies have revealed that motor nerves innervating horizontal rectus EOMs are bifurcated into two divisions that control, respectively, the superior and inferior zones of muscle fibers. This finding has motivated the proposition that each of the two compartments of these EOMs might be controlled independently, so that each EOM could behave as it were two parallel but independent actuators. The compartmental independence postulate requires a mechanically low degree of transverse force coupling among parallel EOM and extraocular tendon (EOT) fibers. This project aimed to employ biomechanical characterization to EOM and EOT to test the plausibility of this hypothesis.

The first study described the biomechanical characterization of EOT, in both at the level of individual fibers and whole tendon. Nano indentation of EOT fiber bundles analyzed within the Hertzian framework effectively characterized the transverse Young's modulus for bovine EOT fiber bundles using atomic force microscopy (AFM). A precise estimate of the Poisson ratio (PR) of bovine EOTs was calculated using optical coherence tomography (OCT) during tensile loading.

The second study investigated mechanical potential for independent compartmental behavior in EOM and EOT. Extensive experimental study was performed to examine the passive mechanical interaction between sets compartments using a custom fabricated dual channel micro-tensile load cell. Independent active contractile behavior of EOM compartments was also examined using calcium-induced EOM contraction. Both passive loading and active contraction findings indicate that EOM and tendon have a high degree of biomechanical independence, sufficient to support the proposed functional diversity of actions in distinct neuromuscular compartments of the horizontal rectus EOMs.

Finally, biomechanical effects of Z-tenotomy and Z-myotomy, surgical techniques employing transverse incisions for EOT or EOM weakening to correct strabismus (misalignment of the eyes), were characterized using tensile loading. Both Z-tenotomy and Z-myotomy demonstrated minimal shear force coupling, which confirms and extends the findings of independent compartmental behavior in second study, and explains the surgical effects of the procedure. Additional viscoelastic characterization was performed using EOM specimens.

The dissertation of Kwang Sup Shin is approved.

Christopher Lynch

William Klug

Joseph L. Demer, Committee Co-Chair

Vijay Gupta, Committee Co-Chair

University of California, Los Angeles

2014

DEDICATION

I would like to dedicate my PhD thesis to my parents. My father, Young-gook Shin, has always been a perfect role model of my life as a successful entrepreneur, politician, and father. He used to encourage me when I was a kid by saying that "You are such a talented boy, and everything will come true if you want and try to make it." He has always been supporting the decisions I have made in the past without any skepticism and has always provided needed help and advice. He made me who I am today, and I am so proud to be his son. While my father had a great impact on shaping up the core of myself, my mother, Kyung-ae Kang, actually has been the person who added flesh and blood to my sense, morals and even work ethics. She has been taught me how to meet and communicate with people by heart. Her warm and benevolent smile always gives me more comfort and encouragement than thousands of words, so I truly appreciate everything you have done for me.

I also dedicate my PhD thesis to my children and wife. My son, Matthew Shin, was born when I began the PhD, so he is very special to my PhD career. As he grew, my research also has been developed, and I would like to thank him for giving me the motivation. My daughter, Olivia Shin, is a lovely girl who gives me a pleasure every time when I see her charming acts. It is great we can celebrate both my graduation and her 2nd birthday: Happy birthday Olivia! My wife, Suyoun Park, always has been a perfect shelter whenever I had difficulties throughout my PhD course. She has sacrificed her personal life for me and children although she is an established professional baker. I know she has a dream to have her own bakery someday, and I promise I will give my support to make it come true. I would like to express my appreciation and sincere love to her for her all efforts toward me.

TABLE OF CONTENTS

LIST OF FIGURES AND TABLES

ACKNOWLEDGEMENTS

First, I would like to express my gratitude toward my research adviser, Professor Joseph L. Demer for his invaluable guidance for my PhD work. I admire his intelligence and integrity as a scholar. Furthermore, his limitless enthusiasm towards the research always has motivated me, and driven me to perform the research with passion. It has been my honor to have such a great mentor during the course of my PhD work and I can only hope that my work has met his standards over these past few years.

Secondly, I would like to convey my appreciation toward my co-advisor, Professor Vijay Gupta. His concrete and technical guidance on biomechanical characterization work has had an enormous impact on my research. Not only has he broadened my knowledge in the field of biomechanics but also he has introduced me to technology beyond the field of solid mechanics. Professor's generosity and kindness will never be forgotten.

I would also like to thank both Professor Lynch and Professor Klug for all of the guidance they have given me as my committee members. They have provided many critical advice and suggestions with a lot of interests about my PhD works and great intuition out of professional experiences.

Lastly, I want to express my deep appreciation to senior research fellow, Lawrence Yoo, who has given me endless help throughout my entire PhD career. It has been my pleasure to work with him, and the quality of my PhD dissertation could be improved owing to his valuable advice. Also, I truly appreciate Manning Beef, LLC, Los Angeles, CA, for their generous contribution of bovine specimens, and special thanks to Alan Le for assistance with photography and preparation of samples for experiments.

VITA

EDUCATION

2006	B.S., Mechanical Engineering, Hanyang University Seoul, South Korea
2008	M.S., Mechanical Engineering, Korea Advanced Institute of Science and Technology (KAIST) Daejeon, South Korea

RESEARCH EXPERIENCE

2006-2008	Research Assistant Korea Advanced Institute of Science and Technology (KAIST) Daejeon, South Korea
2009-2014	Research Assistant University of California Los Angeles, California

PRESENTATIONS

1. Shin, A., Yoo, L., and Demer, J. L. Mechanical Creep in Passive Bovine Extraocular Muscles (EOMs), The poster presentation at ARVO, Fort Lauderdale, May 2010.

2. Shin, A., Yoo, L., and Demer, J. L. Mechanical Creep in Passive Bovine Extraocular Muscles (EOMs), The poster presentation at Jules Stein Eye Institute Conference, Lake Arrowhead, Oct 2010

3. Shin, A. Biomechanical Characterization of Orbital Tissues, The oral presentation at KSEA-SC, Los Angeles, Feb 2011

4. Shin, A., Yoo, L., Kim H., and Demer, J. L. Micro-CT During Tensile Loading: Accurate Determination of the Poisson Ratio (PR) of Passive Bovine Extraocular Muscles (EOMs), The poster presentation at ARVO, Fort Lauderdale, May 2011.

5. Shin, A. Independent Passive Mechanical Behavior of Bovine Extraocular Muscle (EOM) Compartments, The oral presentation at Jules Stein Eye Institute Conference, Lake Arrowhead, Oct 2011

6. Shin, A. Independent Passive Mechanical Behavior of Bovine Extraocular Muscle (EOM) Compartments, The oral presentation at Jules Stein Eye Institute basic and clinical science seminar, UCLA, Jan 2012

7. Shin, A., Yoo, L., and Demer, J. L. Mechanical Study of Compartmentalization in Passive Bovine Extraocular Muscles (EOMs), The poster presentation at AAPOS, San Antonio, Apr 2012

8. Shin, A., Yoo, L., Chaudhuri Z., and Demer, J. L. Highly Independent Passive Mechanical Behavior of Bovine Extraocular Muscle (EOM) Compartments. The poster presentation at ARVO, Fort Lauderdale, May 2012

9. Shin, A., Independent Passive Mechanical Behavior of Bovine Extraocular Muscle Compartments, The oral presentation at Jules Stein Eye Institute award, UCLA, Jun 2012

10. Shin, A., Yoo, L., and Demer, J. L. Biomechanics of Superior Oblique Z-tenotomy: Is It Different From Unguarded Tenotomy?, The poster presentation at AAPOS, Boston, Apr 2013

11. Shin, A., Yoo, L., and Demer, J. L. Poisson Ratio Measurements of Extra-ocular Muscle and Tendon. The poster presentation at ARVO, Seattle, May 2013

12. Shin, A., Yoo, L., and Demer, J. L. Biomechanical Characterization of Z-myotomy. The poster presentation at AAPOS, Palm Springs, April 2014

13. Shin, A., Yoo, L., and Demer, J. L. Viscoelastic Biomechanical Characterization of Z-myotomy, An Extraocular Muscle (EOM) Weakening Surgery. The oral presentation at ARVO, Orlando, May 2014

PUBLICATIONS

1. Reddy NSK, Shin KS, Yang MY. Experimental study of surface integrity during end milling of Al/SiC particulate metal matrix composites, Journal of Materials and processing technology, 2008

2. Yoo L., Reed J., Shin A., Kung J., Goldberg RA., Mancini R., Taban M., Gimzewski JK., and Demer JL. Characterization of ocular tissues using micro-indentation and Hertzian viscoelastic models, Invest Ophthalmol Vis Sci., 2011; 52:3475-82.

3. Yoo L., Kim H., Shin A., Gupta V., Demer JL. Creep behavior of passive bovine extraocular muscle. J Biomed Biotechnol., 2011.

4. Shin A., Yoo L., Chaudhuri Z., Demer JL. Independent passive mechanical behavior of bovine extraocular muscle compartments. Invest Ophthalmol Vis Sci., 2012; 53:8414-23.

5. Kim H., Yoo L., Shin A., Demer JL. Determination of Poisson ratio of bovine extraocular muscle by computed X-ray tomography. Biomed Res Int., 2013.

6. Shin A., Yoo L., Demer JL. Biomechanics of Superior Oblique Z-tenotomy. J AAPOS., 2013; 17(6):612-7.

7. Yoo L., Reed, J., Shin A., and Demer, J. L. Atomic force microscopy determination of Young's modulus of bovine extra-ocular tendon fiber bundles. J of Biomechanics., 2014; 47(8): 1899-1903.

AWARDS

1. Top and Honor scholarship by Hanyang University, 2003

2. Honor scholarship by Hanyang University, 2005

3. Best of Show at AAPOS meeting, San Antonio, 2012

4. Excellence in Research Award, Jules Stein Eye Institute, 2012

5. Best of Show at AAPOS meeting, Boston, 2013

Chapter 1

Introduction

1.1. Structure of the Orbit and Eye Movement

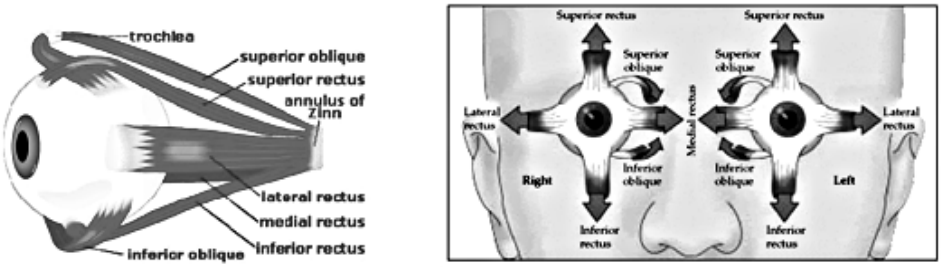

Fig. 1.1. Extraocular muscles (EOMs) and eye movement

Eye rotation is accomplished by the integrated action of ocular tissues such as extraocular muscles (EOMs), extraocular tendons (EOTs), and connective tissues. Human have six oculorotary EOMs: the lateral rectus (LR), medial rectus (MR), superior rectus (SR), inferior rectus (IR), superior oblique (SO), and inferior oblique (IO) EOMs. These six EOMs, which are shaped as broad straps, are stimulated to be contracted by nerve commands, and produce horizontal, vertical, and torsional eye rotations. Most of the EOMs are connected to the eyeball by an EOT that transfers the contractile force; an exception is the IO, which has a direct connection between EOM and eyeball in human. Other tissues, including pulley connective tissues and fatty tissue, are located inside the orbit (eye socket). Complex eye movements are

thereby executed, ranging from pursuit, which tracks smooth object movement, to saccades, the rapid, ballistic eye movements that are the fastest of any body motions.[1]

1.2. Compartmentalized Innervation of Horizontal EOM

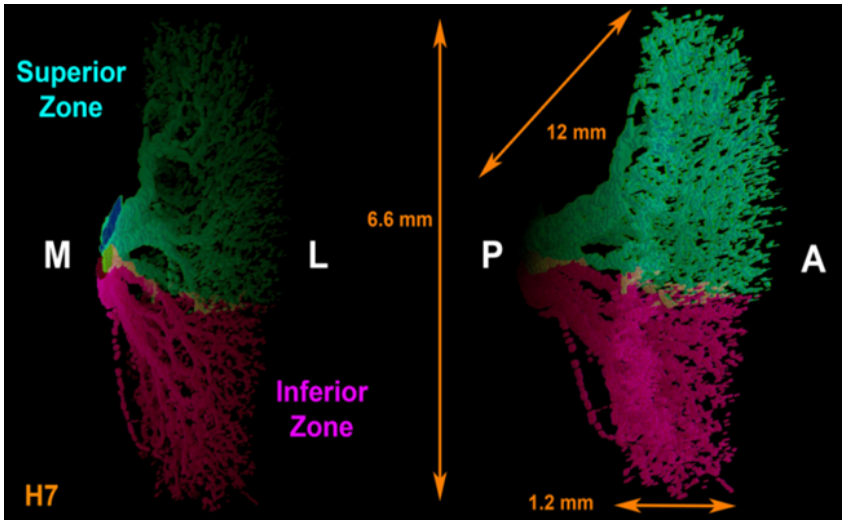

Fig. 1.2. Compartmentalized innervation of horizontal EOM (from Costa et al.)[2]

There are several controversial issues in the eye movement field, and compartmentalization of EOM is one of the most recent. Conventionally, it has been believed that each individual EOM was innervated uniformly by its motor nerve. However, recent anatomical tracing studies have found that there is a bifurcation of the abducens nerve into two parts prior to entry into the LR EOMs of monkey and human, and that the two nerve subdivisions arborize within non-overlapping regions of generally parallel muscle fibers.[3] A later study revealed both horizontal rectus (LR, MR) motor nerves are bifurcated into two divisions that control, respectively, the superior and inferior zones of muscle fibers in each of these EOMs.[2] .

Recently, functional evidence for differential compartmental activation of the human LR was obtained from magnetic resonance imaging (MRI) during ocular counter-rolling induced by head tilt,[4, 5] and LR palsy.[6] This finding suggested the possibility that each of the two compartments of these EOMs might be controlled independently, so that each EOM could behave as it were two parallel but independent actuators. A critical but untested assumption of this notion was that parallel bundles of EOM fibers could generate and transmit tension independently from the EOM origin to the EOM insertion on the sclera. That is, the compartmental independence postulate requires a low degree of transverse force coupling among parallel EOM and EOT fibers. Until the current study, this question had never been investigated through biomechanical characterization.

1.3. Biomechanical Characterization

Biomechanical characterization can define the behavior of tissue for clinical or research purposes. Theoretical models have been developed to describe the mechanical behavior of tissues, including artery,[7] brain,[8-13] heart muscle,[14-16] kidney,[17-20] liver,[21, 22] and skin.[23-25] Several different mechanical techniques and modeling methods have been applied to various tissues such as EOM,[26-31] orbital connective tissue and fat,[32] cornea,[33] and sclera.[34] The output from the biomechanical characterization can be of value both to clinicians, enhancing surgical insight by knowing target tissue properties, and to engineers by providing mechanical properties for fabricating artificial tissues or prediction using finite element models (FEMs).

Viscoelastic materials, ranging from polymers to biological tissues, can be modeled for describing their stress or strain interactions, and their temporal dependencies. Many experimental studies of soft tissue have been framed in the linear theory of viscoelasticity, relating stress and strain using Voigt, Maxwell, or Kelvin models. Buchthal et al. formulated a model having an infinite number of Voigt (parallel circuit of dampers and springs) and Maxwell (serial circuit of dampers and springs) elements.[35] A nonlinear Kelvin model was proposed by Viidik as a sequence of springs of different natural lengths, so that the number of participating springs increases with increasing strain.[36]

1.4. Overview

1.4.1. Biomechanical Study of Extraocular Tendon (EOT)

1.4.1.1. Nano-mechanical Analysis of Tendon Fiber Bundles Using Atomic Force Microscopy

Atomic force microscopy (AFM) is a widely used scanning probe microscopy having very high resolution (10^{-9} m), which is more than 1000 times better than the optical diffraction limit. AFM has been used for the purpose of imaging, measuring, and manipulating material at the nano scale. We employed AFM to characterize the Young's modulus, a measure of the stiffness of an elastic isotropic material for characterizing materials,[37] of the fiber bundles of bovine EOTs using the Hertzian theoretical framework. Indentation experiments were performed to extract Young's modulus from the force-displacement data. The flowchart below shows the sequential procedure.

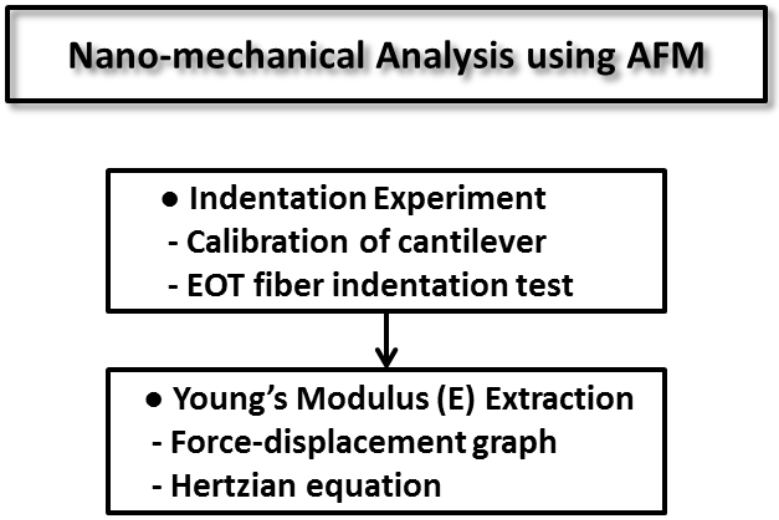

Fig. 1.3. Flowchart of nano-mechanical analysis using AFM

1.4.1.2. Poisson Ratio Measurement of EOT Using Optical Coherence Tomography

Optical coherence tomography (OCT) is an optical signal acquisition and processing methodology that can capture micrometer-resolution, three-dimensional images from within optical scattering media. Precise estimates of PRs of bovine EOTs were calculated using OCT. Tensile loading was imposed during the determination of cross sectional area change all along the specimens using OCT B-scans (two-dimensional images) enhanced by an image processing algorithm. Transverse areal strain was obtained using Green's theorem from cross sectional images, so that the PR could be extracted from axial and transverse strain data. The flowchart below describes the procedure.

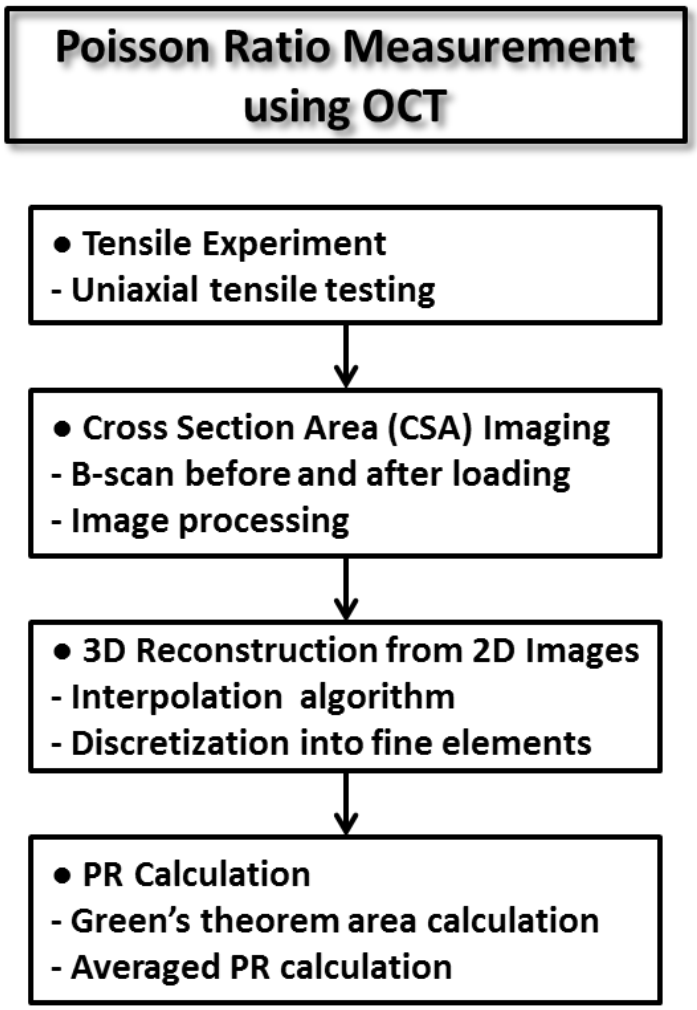

Fig. 1.4. Flowchart of Poisson ratio measurement of EOT using OCT

1.4.2. Independent Mechanical Behavior of EOM Compartments

Based on previous findings and hypotheses, mechanical evidence for independent compartmental movement was investigated. Extensive experimental study was performed to examine the independent passive mechanical interaction between sets compartments (the two transverse compartments, and global layer vs. orbital layer compartment) using a custom fabricated dual channel micro-tensile load cell assembled from pairs of linear motors and strain

gauges, housed in an environmental chamber for performing two channel tensile testing in an independent manner. Independent active behavior of EOM compartments was also investigated by calcium-induced contraction experiments. The following flowchart shows the procedure.

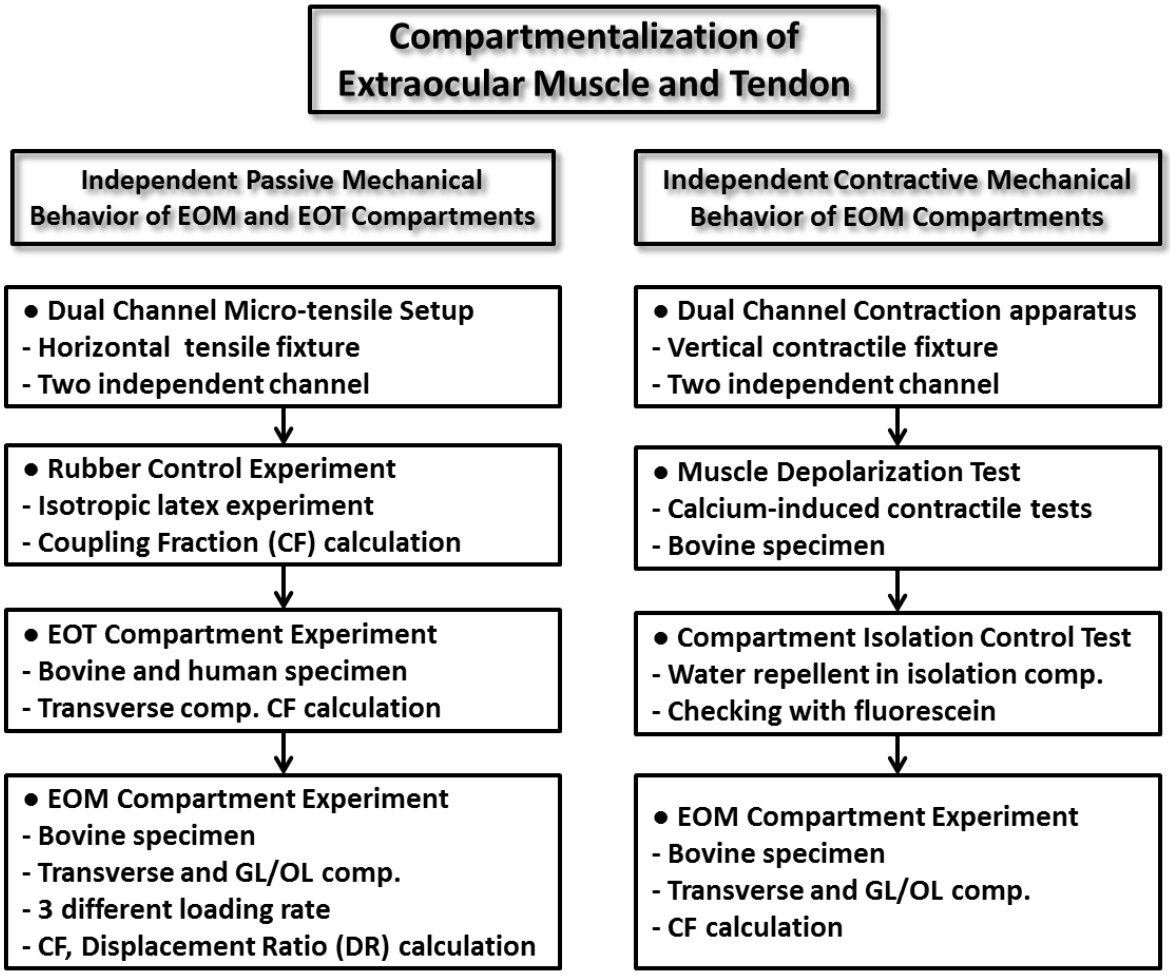

Fig. 1.5. Flowchart of independent mechanical behavior of EOM compartments

1.4.3. Biomechanics of Z-tenotomy and Z-myotomy

Z-tenotomy and Z-myotomy are surgical techniques that can weaken EOT and EOM, lengthening them as appropriate to treat strabismus. These procedures are performed by making

overlapping incisions, spaced some distance apart, from opposite sides of the EOT or EOM. Biomechanical effects of Z-tenotomy and Z-myotomy were characterized using tensile loading. For Z-tenotomy, tensile loading experiments were performed with different Z-tenotomy cut ratios, from 20 to 80% cut of specimen width, and failure forces of EOT were compared to isotropic rubber material. The same procedure was employed for Z-myotomy. Since specimen cross sections become irregular after Z-myotomy, additional viscoelastic characterization was performed by empirically determining uniform EOM cross sections with equivalent failure force to specimens subjected to various degrees of Z-myotomy. These equivalent specimens were then analyzed in a theoretical viscoelastic framework. The following flowchart shows the procedure.

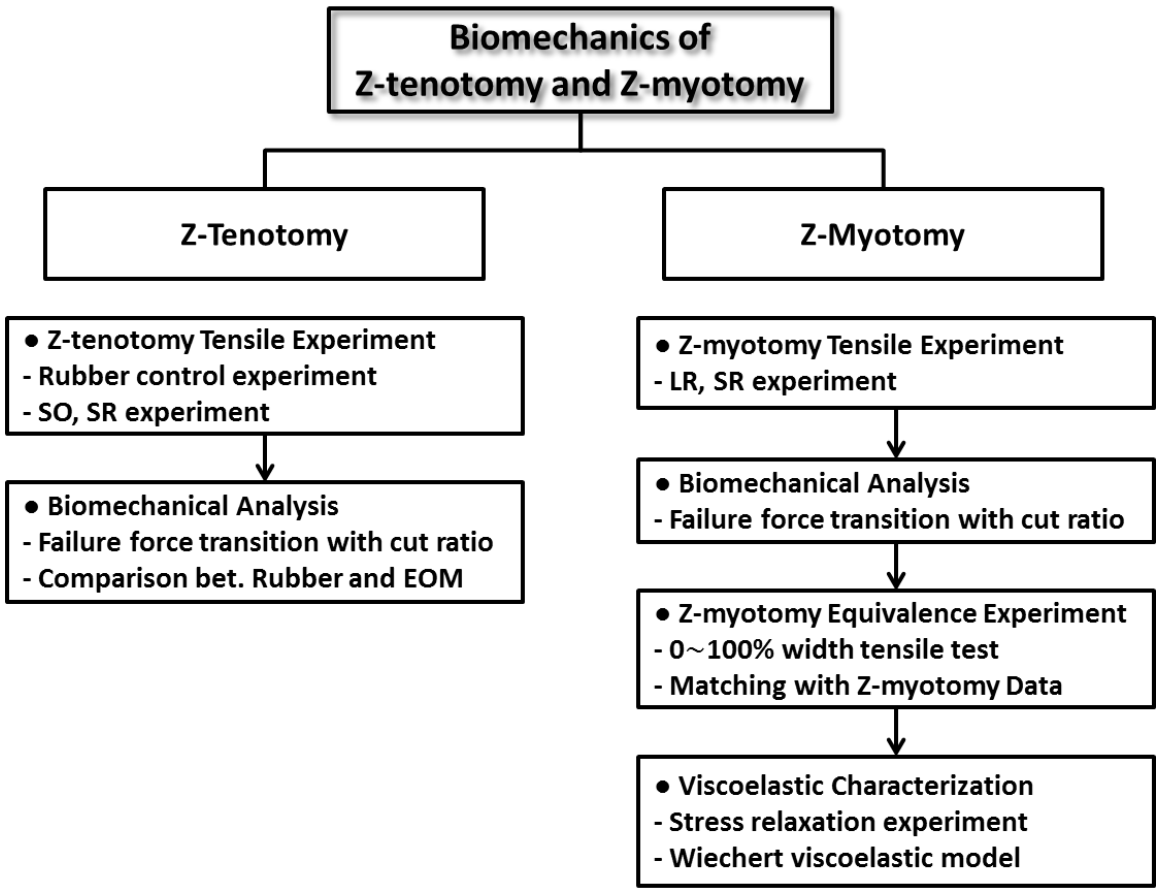

Fig. 1.6. Experiments for study of biomechanics of Z-tenotomy and Z-myotomy

1.5. References

1. Demer JL. Extraocular muscles. *In: Duane's Ophthalmology 2010 Edition by William Tasman; Lippincott Williams & Wilkins; Philadelphia.* 2010;Chapter 1, Volume 1

2. Costa RMdS, Kung J, Poukens V, Yoo L, Tychsen L, Demer JL. Intramuscular innervation of primate extraocular muscles: Unique compartmentalization in horizontal recti. *Invest Ophthalmol Vis Sci.* 2011;52:2830-2836.

3. Peng M, Poukens V, da Silva Costa RM, Yoo L, Tychsen L, Demer JL. Compartmentalized innervation of primate lateral rectus muscle. *Invest Ophthalmol Vis Sci.* 2010;51:4612-4617.

4. Demer JL, Clark RA, da Silva Costa RM, Kung J, Yoo L. Expanding repertoire in the oculomotor periphery: Selective compartmental function in rectus extraocular muscles. *Ann N Y Acad Sci* 2011;1233:8-16.

5. Clark RA, Demer JL. Differential lateral rectus compartmental contraction during ocular counter-rolling. *Invest Ophthalmol Vis Sci.* 2012;53:2887-2896.

6. Clark RA, Demer JL. Lateral rectus superior compartment palsy. *Am J Ophthalmol* 2014;157:479-487.e472.

7. Holenstein R, Niederer P, Anliker M. A viscoelastic model for use in predicting arterial pulse waves. *Journal of Biomechanical Engineering-Transactions of the Asme* 1980;102:318-325.

8. Galford JE, McElhaney JH. A viscoelastic study of scalp, brain, and dura. *Journal of Biomechanics* 1970;3:211-221.

9. Estes MS, McElhaney JH. Response of brain tissue to compressive loading. *ASME*. Washington, D.C.; 1970.

10. Pamidi M, Advani S. Nonlinear constitutive equations for human brain tissue. *J Biomech Eng* 1978;100:44–48.

11. Mendis K, Stalnaker R, Roberts V. A constitutive relation for large deformation finite element modeling of brain tissue. *J Biomech Eng* 1995;117:279–285.

12. Bilston LE, Liu Z, Phan-Thien N. Linear viscoelastic properties of bovine brain tissue in shear. *Biorheology* 1997;34:377-385.

13. Miller K, Chinzei K. Constitutive modelling of brain tissue: Experiment and theory. *Journal of Biomechanics* 1997;30:1115-1121.

14. Pinto JG, Patitucci PJ. Visco-elasticity of passive cardiac-muscle. *Journal of Biomechanical Engineering-Transactions of the Asme* 1980;102:57-61.

15. Huyghe J, Van Campen D, Arts T, Heethaar R. The constitutive behaviour of passive heart muscle tissue: A quasilinear viscoelastic formation. *J Biomech* 1991;24:841–849.

16. May-Newman K, McCulloch AD. Homogenization modeling for the mechanics of perfused myocardium. *Progress in Biophysics & Molecular Biology* 1998;69:463-481.

17. Schmidlin F, Schmid P, Kurtyke T, Iselin C, P G. Force transmission and stress distribution in a computer simulated model of kidney: An analysis of the injury mechanisms in renal trauma. *J Trauma* 1996;40:791–796.

18. Farshad M, Barbezat M, Flueler P, Schmidlin F, Graber P, Niederer P. Material characterization of the pig kidney in relation with the biomechanical analysis of renal trauma. *Journal of Biomechanics* 1999;32:417-425.

19. Phan-Thien N, Nasseri S, Bilston LE. Oscillatory squeezing flow of a biological material. *Rheologica Acta* 2000;39:409-417.

20. Nasseri S, Bilston LE, Phan-Thien N. Viscoelastic properties of pig kidney in shear, experimental results and modelling. *Rheologica Acta* 2002;41:180-192.

21. Liu Z, Bilston L. On the viscoelastic character of liver tissues: Experiments and modeling of the linear behavior. *Biorheology* 2000;37:191–201.

22. Kruse SA, Smith JA, Lawrence AJ, et al. Tissue characterization using magnetic resonance elastography: Preliminary results. *Physics in Medicine and Biology* 2000;45:1579-1590.

23. Lanir Y. The rheological behavior of the skin: Experimental results and a structural model. *Biorheology* 1979;16:191-202.

24. Shoemaker PA, Schneider D, Lee MC, Fung YC. A constitutive model for two-dimensional soft tissues and its application to experimental data. *J Biomech* 1986;19:695-702.

25. Chaudhry HR, Bukiet B, Findley T, Ritter AB. Evaluation of residual stress in rabbit skin and the relevant material constants. *J. Theor. Biol.* 1998;192:191-195.

26. Yoo L, Kim H, Shin A, Gupta V, Demer JL. Creep behavior of passive bovine extraocular muscle. *Journal of Biomedicine and Biotechnology* 2011.

27. Kim H, Yoo L, Shin A, Demer JL. Determination of poisson ratio of bovine extraocular muscle by computed x-ray tomography. *Biomed Research International* 2013.

28. Yoo L, Kim H, Gupta V, Demer JL. Quasilinear viscoelastic behavior of bovine extraocular muscle tissue. *Invest Ophthalmol Vis Sci* 2009;50:3721-3728.

29. Quaia C, Ying HS, Nichols AM, Optican LM. The viscoelastic properties of passive eye muscle in primates. I: Static forces and step responses. *Plos One* 2009;4.

30. Quaia C, Ying HS, Optican LM. The viscoelastic properties of passive eye muscle in primates. Ii: Testing the quasi-linear theory. *Plos One* 2009;4.

31. Quaia C, Ying HS, Optican LM. The viscoelastic properties of passive eye muscle in primates. Iii: Force elicited by natural elongations. *Plos One* 2010;5:A236-A254.

32. Yoo L, Gupta V, Lee C, Kavehpore P, Demer JL. Viscoelastic properties of bovine orbital connective tissue and fat: Constitutive models. *Biomechanics and Modeling in Mechanobiology* 2011;10:901-914.

33. Yoo L, Reed J, Gimzewski JK, Demer JL. Mechanical interferometry imaging for creep modeling of the cornea. *Invest Ophthalmol Vis Sci* 2011;52:8420-8424.

34. Yoo L, Reed J, Shin A, et al. Characterization of ocular tissues using microindentation and hertzian viscoelastic models. *Invest Ophthalmol Vis Sci* 2011;52:3475-3482.

35. Buchtal F, Kaiser E. The rheology of the cross striated muscle fiber with particular reference to isotonic conditions. *Dan Biol Med.* 1951;21:328-336.

36. Viidik A. Biomechanics and functional adaptation of tendons and joint ligaments. *Evans FG (ed) Studies on the Anatomy and Function of Bone and Joints. New York: Springer.* 1966;17-39.

37. Euler L. The rational mechanics of flexible or elastic bodies: Introduction to leonhardi euleri opera omnia, vol. X and xi, seriei secundae. *Orell Fussli.* 1638 - 1788.

Chapter 2

Biomechanical Study of Extraocular Tendon (EOT)

2.1. Introduction

Although several different mechanical testing techniques and modeling methods have been applied to various tissues, extraocular tendons (EOTs) have been neglected in comparison with other ocular tissues. Although ligament and tendon from other regions has been studied and theoretical models developed,[1-4] EOT has its own characteristics, and must be investigated. EOT is composed of a network of relatively thick, longitudinal collagen fiber bundles arranged in parallel, and wrapped like a cable by thinner, transverse fibers. We characterized individual fibers using a nano-scale method, and whole EOT using tensile loading during optical imaging.

2.1.1. Nano-mechanical Analysis of EOT Fiber Bundles Using Atomic Force Microscopy

A basic structural component of ligaments and tendons including EOT is the collagen fibril. Fibrils are closely packed within an extrafibrillar proteoglycan rich matrix to form a fiber. And, individual fibers are encased in the endotendinous sheath and packed into fasicular units, which then become the constituents of the whole tendon or ligament complex.[5, 6] Since EOTs are manipulated by strabismus surgery for correction of binocular misalignment, it is important to understand their mechanical properties. Although some non-ocular tendon properties have been reported[7-9], mechanical properties for EOTs have not yet been defined. In the absence of

biomechanical data, the best current computational model of the biomechanics of the EOMs and orbital tissues assumes that the EOTs are infinitely stiff.[10] This obviously unrealistic assumption might cause erroneous simulation results, and highlights the need to obtain actual data on EOTs. Investigators in the field have employed various techniques to accurately determine the biomechanical properties of other orbital tissues, including conventional tensile elongation,[11-15] and micro/nano indentation[16, 17] methodologies. Although there have been studies in some tissues,[12, 15-21] many material parameters of orbital tissues have yet to be defined.

Atomic force microscopy (AFM) is a very high-resolution type of scanning probe microscopy having nanometer (10^{-9} m) resolution, which is more than 1,000 times better than the optical diffraction limit. AFM has been widely used for the purpose of imaging, measuring, and manipulating material at the nano scale. As another application of AFM, force spectroscopy, has been developed based upon the direct measurement of tip-sample interaction forces as a function of the gap between the tip and sample. In the present method, while AFM tip is indenting the surface, the displacement of cantilever is measured using a piezoelectric sensor. These measurements have been used to measure nanoscale contacts, atomic bonding, Van der Waals forces, and Casimir forces, dissolution forces in liquids and single molecule stretching and rupture forces.[22] AFM force spectroscopy also has been applied for determining intermolecular forces,[23, 24] stiffness of cells[25], and cancer cell research.[26] Most current formulations used to compute mechanical parameters have been based on the Hertz model, as modified to match experimental conditions such as indenter shape or specimen thickness.[27, 28] This study employed AFM to characterize, using the Hertzian theoretical framework, the Young's modulus of the fiber bundles that comprise the fundamental building blocks of EOTs.

2.1.2. Poisson Ratio Measurement of EOT Using Optical Coherence Tomography (OCT)

The Poisson ratio (PR) is a critical mechanical parameter required to define comprehensively the elastic behavior of a material. The PR is the ratio of the transverse contraction strain to the axial extension strain, which can be obtained during tensile elongation. Normally, the PR of a material ranges between 0 and 0.5, depending on the material's compressibility. However, the PR can be higher than 0.5 or lower than 0 for materials having complex matrices and inner structures.[29] Most tissues are considered to be elastomeric materials with high bulk modulus relative to Young's modulus, so the PR is expected to approximate 0.5. In general, the PR can be measured by static or dynamic methods. Static methods, such as classical tensile or compressive testing, are most widely used in solid mechanics.[30, 31] In static determinations, the PR is calculated from transverse and axial deformations due to uniaxial stress. For dynamic determination, the PR is determined from the natural frequency of the transverse and axial waves in the material,[32-34] most commonly elicited by ultrasound perturbation. The PR has been typically assumed to be between 0.35 and 0.49 for soft tissues.[35-37] However, it has been estimated that a 20% error in the PR would result in errors of 3.8% and 4.4% in the biaxial flexural strength and the indentation modulus of a material, respectively.[30] Such errors could propagate and compound during the iterative computations in FEA. There is a need to minimize errors by accurate experimental determination of the PR. By employing a novel optical coherence tomography (OCT) imaging method for precise determination of strain, accurate static PR for EOT can be determined.

2.2. Method

2.2.1. Nano-mechanical Analysis of EOT Fiber Bundles Using AFM

Hertzian Model. The Hertzian method approximates specimens as isotropic and linear elastic solids occupying an infinitely extending half space, and contacted by an indenter on one surface. It is assumed that the indenter is not deformable, and that there are no additional interactions between indenter and sample. If these conditions are met, the Young's modulus (E) of the specimen, which is a measure of the stiffness of an elastic isotropic material and a quantity used to characterize material,[38] can be determined using the Hertzian model. Since the Hertzian model assumes the indentation to be negligible in comparison to sample thickness, indentation depth must be optimized for physically available biomaterial samples. The Hertzian model is valid for small indentations (up to 3% of specimen thickness) so that the substrate does not influence the calculations. For the geometry of an inverted pyramid tip indenting a flat sample, the relation between the indentation (δ) and the loading force (F) is given by:

$$F = \frac{E}{1-\upsilon^2}\frac{\tan\alpha}{\sqrt{2}}\delta^2 \qquad \text{Eq 2.1}$$

where, $\boldsymbol{\upsilon}$ is the Poisson ratio (PR), E is the Young's modulus, and α is the side angle of the inverted pyramid tip. More detailed discussion on the calculation and application of this model to mechanical properties of soft tissues have been published.[39-43] For calculation of elastic behavior, the PR of the specimen was assumed to be 0.5, as is typical for soft biological material where incompressibility is assumed.

Specimen Preparation. Bovine specimens were obtained fresh from a local abattoir (Manning Beef LLC, Pico Rivera, CA). Total preparation time including transportation time for specimens was about 1 hour and 30 minutes. Fig. 2.1 shows an EOT extraction site. All six EOTs were extracted, and cylindrical fiber bundles were extracted from each under an optical dissecting microscope.

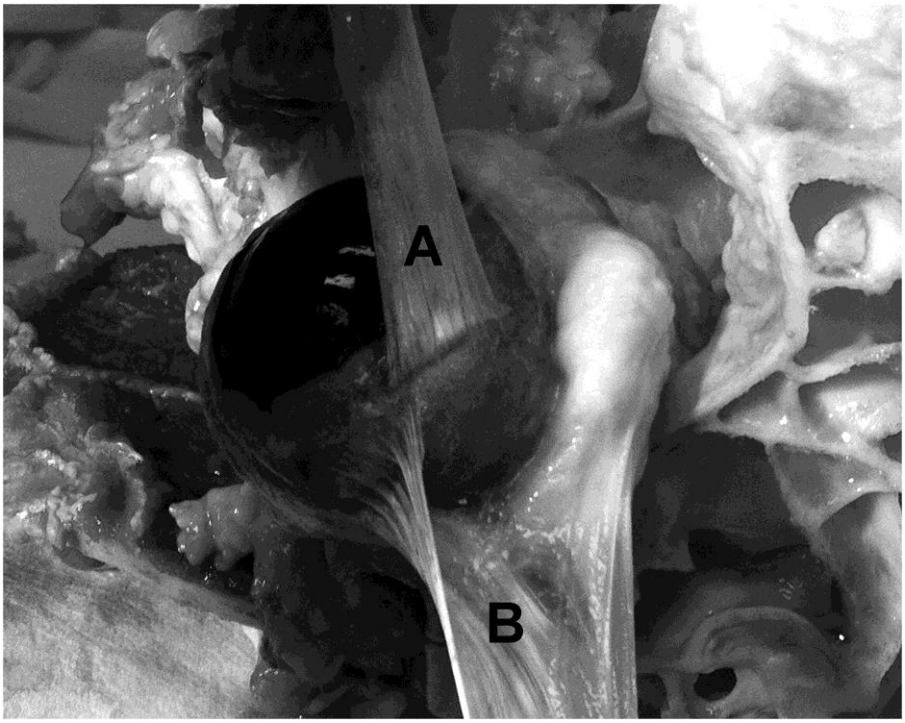

Fig. 2.1. Illustration of EOT extraction from bovine orbit. Two different bovine EOTs during extraction from this dissected orbit, illustrating their composition from numerous thin, parallel fiber bundles.[44] A. Superior rectus EOT has been reflected anteriorly (upward in the photograph) over the cornea that is to the left. B. Superior oblique EOT has been reflected laterally (downward in the photograph) away from the sclera after fracture of the trochlea at upper right.

Fiber bundles had thickness ranging from 16 to 20 μm and the length ranging from 10 to 15 mm. Fig. 2.2A shows a bovine EOT at low magnification.

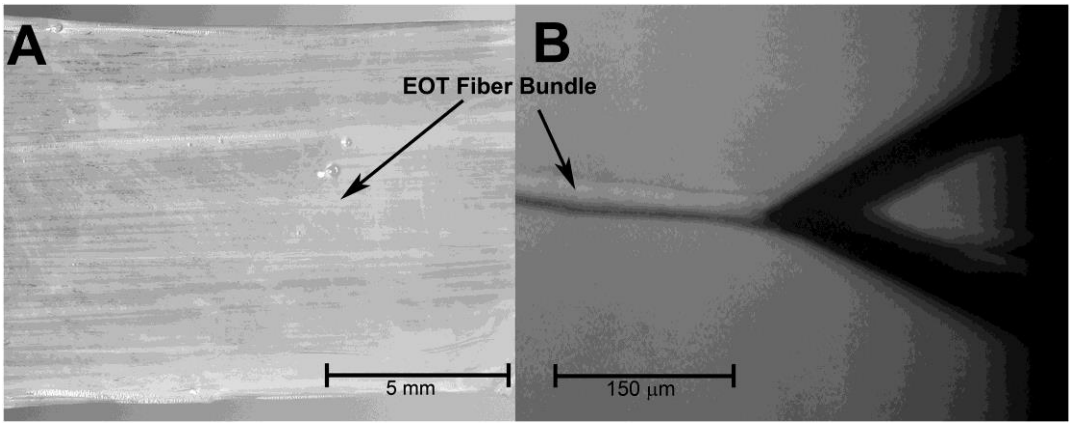

Fig. 2.2. Bovine EOTs magnification view. A. Bovine lateral rectus EOT showing horizontal grain composed of parallel fiber bundles.[44] B. Extracted EOT fiber bundle contacted by AFM indenter at the tip of triangular cantilever whose shadow appears at right.

In order to prevent any substrate effect, the extracted tendon fibers were glued to glass bottom of Petri dish. Ten fiber bundle specimens were prepared from each of 6 different bovine extra-ocular tendons.

Atomic Force Microscopy (AFM). Experiments were conducted using a Dimension 5000 Scanning Probe Microscope (Veeco digital instruments, Plainview, NY) in contact mode. The spring constant of the cantilever was determined to be 0.02 Nm^{-1} by fitting the first resonance of the thermally-actuated spectrum. For distance calibration of the deflection signal, the sharpened silicon nitride cantilever bearing an inverted pyramid tip with 35° side angle was pushed against a glass substrate, for which zero indentation was assumed, to a known distance of 1 μm.

Experimental Procedure. AFM indentations of 100 nm were recorded at three different locations within each specimen. Measurements were obtained at 37° C at 100% humidity at 1 Hz indentation rate. Force–displacement curves were recorded to determine the transverse stiffness (Young's modulus, E) of EOT fiber bundles. For the case of many materials, energy delivered by the indenter that is not completely released on unloading, but dissipated due to viscoelastic or plastic behavior, appears as hysteresis between the loading and the unloading phases of the force curve (Fig. 2.3).

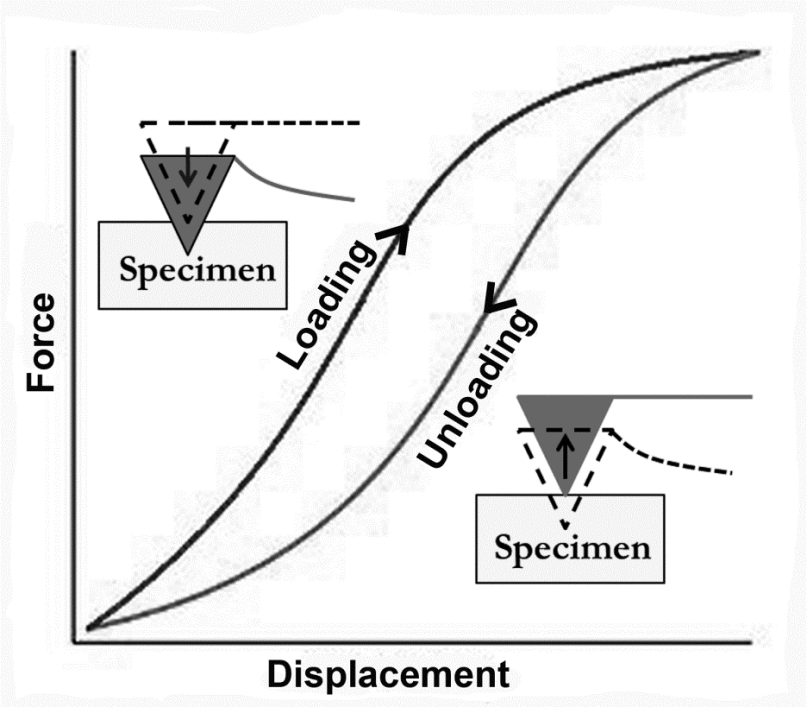

Fig. 2.3. Hypothetical force-displacement curve for viscoelastic specimens.[44] Difference between loading and unloading phases represents energy dissipated through viscosity.

However, through the series of preliminary experiments it was discovered that EOT fiber bundles exhibited purely elastic mechanical behavior; loading and unloading phases overlap in force-displacement curves, justifying the use of the Hertzian contact model (Fig. 2.4.)

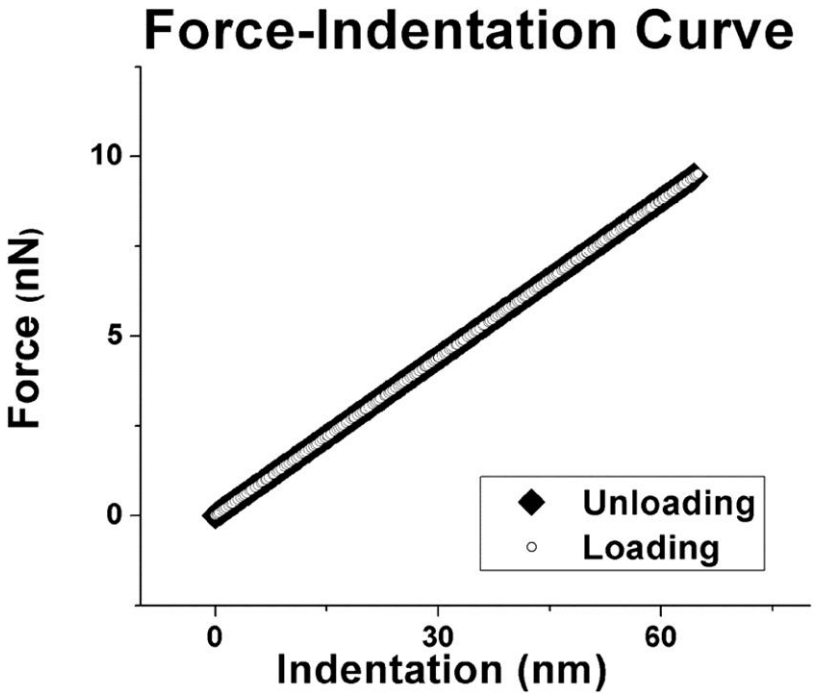

Fig. 2.4. Sample graph of loading and unloading phases of lateral rectus EOT.[44] Loading and unloading phases exhibited the same behavior for of all EOTs, indicating pure elasticity to the limit of measurement error.

Young's modulus was calculated by converting force–displacement curves into force–indentation curves and fitting with the Hertz model, which describes the indentation of an elastic sample using a stiff indenter. Analysis was restricted to low force ranges resulting in shallow indentations (<100 nm) to prevent damage to the specimen surface and to reduce any possible influence from substrate induced effects.[42, 45]

2.2.2. Poisson Ratio Measurement of EOT Using OCT

Poisson Ratio. The PR ν for materials undergoing deformations exceeding greater 1%[46] is expressed as the negative ratio of transverse to axial true strain:[47, 48]

$$\nu = -\frac{ln(1+\varepsilon_T)}{ln(1+\varepsilon_A)} \qquad \text{Eq 2.2}$$

Where, ε_T and ε_A are transverse and axial engineering strains, respectively. Eq 2.2 can be rearranged and can be expressed as shown in Eq 2.3:

$$ln(1+\varepsilon_A)^{-\nu} = ln(1+\varepsilon_T) \qquad \text{Eq 2.3}$$

Recognizing that an infinitesimal element in the cross-section area (CSA) undergoes a plane deformation when the EOM is subjected to loading, the transverse strain in Eq 2.3 can be represented as $ln\left({}^{\delta x}/_{\delta x_o}\right)$, and Eq 2.3 can be rearranged as Eq 2.4 with δx_o and δx being the length of side of the element in undeformed and deformed configurations:

$$\delta x = \delta x_o(1+\varepsilon_A)^{-\upsilon} \qquad \text{Eq 2.4}$$

Eq 2.4 is valid under the assumption of isotropy or transverse isotropy, which is appropriate for an EOT.[48] Hence for the CSA of the square in the deformed configuration can be expressed as Eq 2.5 where δA_o is the initial CSA:

$$\delta A = \delta {x_o}^2 (1 + \varepsilon_A)^{-2\upsilon} = \delta A_o (1 + \varepsilon_A)^{-2\nu}. \quad \text{Eq 2.5}$$

As reported by Vergari et al.,[48] the instantaneous CSA can be expressed as Eq 2.6 by summation of all the elements in the specimen CSA:

$$A = A_o (1 + \varepsilon_A)^{-2\upsilon} \quad \text{Eq 2.6}$$

where, A and A_o are the instantaneous and initial specimen CSA values, respectively.

Finally, the PR for each discretized element was calculated using Eq 3.7:

$$\nu = -0.5 \frac{ln\left({A}/{A_o}\right)}{ln(1+\varepsilon_A)}. \quad \text{Eq 2.7}$$

Green's Theorem for Calculating CSA. Green's Theorem gives the relationship between a line integral around a simple closed curve C and a double integral over the plane region D bounded by C. Let C be a positively oriented, piecewise-smooth, simple closed curve in the plane and let D be the region bounded by C. If P and Q have continuous partial derivatives on an open region that contains D, then

$$\oint_C (P\,dx + Q\,dy) = \iint_D \left(\frac{\partial Q}{\partial x} - \frac{\partial P}{\partial y}\right) dA \quad \text{Eq 2.8}$$

One of the applications of Green's Theorem is in computing areas. Since the area of D is $\iint_D 1\, dA$, we wish to choose P and Q so that $\frac{\partial \mathrm{Q}}{\partial \mathrm{x}} - \frac{\partial \mathrm{P}}{\partial \mathrm{y}} = 1$.

There are several possibilities:

$$P(x,y) = 0 \; and \; Q(x,y) = x, \qquad P(x,y) = -y \; and \; Q(x,y) = 0,$$

$$or \;\; P(x,y) = -\frac{1}{2}y \; and \; Q(x,y) = \frac{1}{2}x$$

Then Green's Theorem gives the following formulas for the area of D:

$$\mathrm{A} = \oint_C x\, dy = -\oint_C y\, dx = \frac{1}{2}\oint_C (-y\, dx + x\, dy) \qquad \text{Eq 2.9}$$

The CSA for each element was computed using the above equation (right side).

Specimen Preparation. All six EOTs were extracted from the bovine orbits, and each whole tendon was used for tensile testing. Since cross section areas before and after loading were measured within each specimen for every PR calculation, identical dimensions were not required for all specimens.

Optical Coherence Tomography (OCT). Cross section area (CSA) measurements for Poisson ratio measurement of EOT were conducted using an OCS 1300SS swept source optical OCT imaging system (Thorlabs Inc, Newton, NJ). This system employed an infrared coherent laser light source (1325 nm wavelength, and 6.0 mm coherent length). Scanning dimensions

were 10 x 10 x 3 mm. Imaging resolutions were 25 μm in transverse, and 9 μm in axial directions at a 16 kHz scan rate. Using this OCT system, numerous consecutive B scans that constitute two-dimensional cross-sectional views, were performed before and after tensile loading (Fig 4.5). The arrows show the increase in the width of the specimen under tensile elongation.

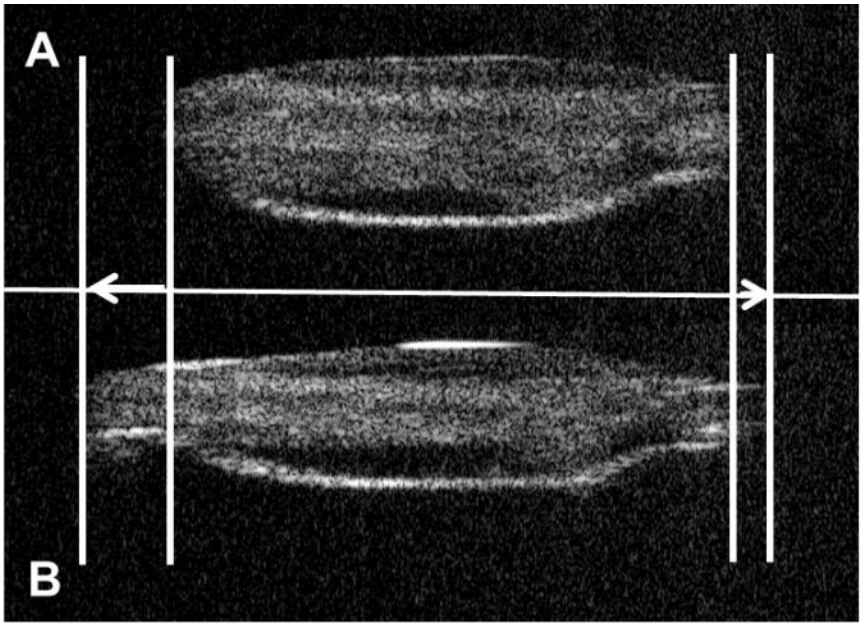

Fig. 2.5. Sample OCT images of bovine EOT specimen before (A) and after (B) elongation.

Experimental Procedure. Fresh bovine EOT specimens were clamped in a tensile fixture within the OCT imaging system under physiologic temperature and humidity control, and stretched up to 25% of initial length. Sets of 512 OCT images were obtained at 10 micron resolution before and after tensile loading. From these 2-D images, digital 3-D models were then built and discretized into 1-1.25 μm thick elements. Changes in longitudinal thickness of each

microscopic element were computed from overall specimen elongation to calculate longitudinal strain. Green's theorem was used to calculate areal strain transverse to stretching.

2.3. Result

2.3.1. Nano-mechanical Analysis of Tendon Fiber Bundles Using AFM

These results for AFM indentation testing have been published in *Journal of Biomechanics*.[44]

A total of 60 EOT fiber bundle specimens were prepared (10 specimens from each of six EOTs) and three different locations were chosen along each fiber bundle specimen to obtain 10 force-indentation recordings per site. Most of specimens revealed behavior close to linearly, albeit not perfectly. Since the Hertzian model for a pyramidal indenter relates force to the square of indentation distance, fitting to any perfectly linear result produced more errors than fits to nonlinear results. Fig. 2.6 shows samples of the best and worst fits of the model to the results.

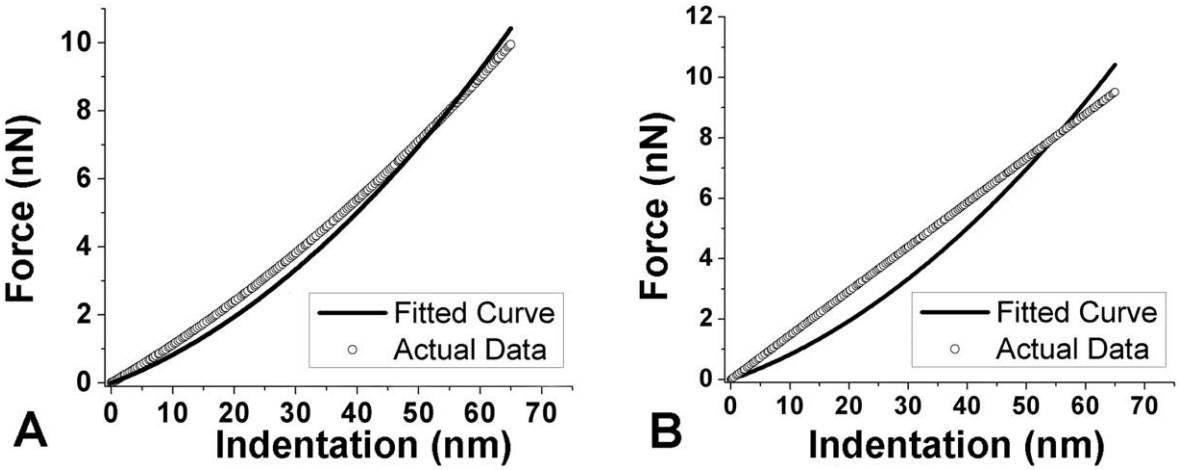

Fig. 2.6. Indentation curve fitting results. A. Best curve fitting to result. B. Worst curve fitting result that occurred when the behavior was purely linear.[44]

Young’s modulus is a measure of the stiffness of an elastic isotropic material and is a quantity used to characterize materials. It is defined as the ratio of the stress along an axis over the strain along that axis in the range of stress from curve fitting. Values of Young’s modulus were averaged for fiber bundles of each of the six anatomical EOTs, and are plotted in Fig. 2.7.

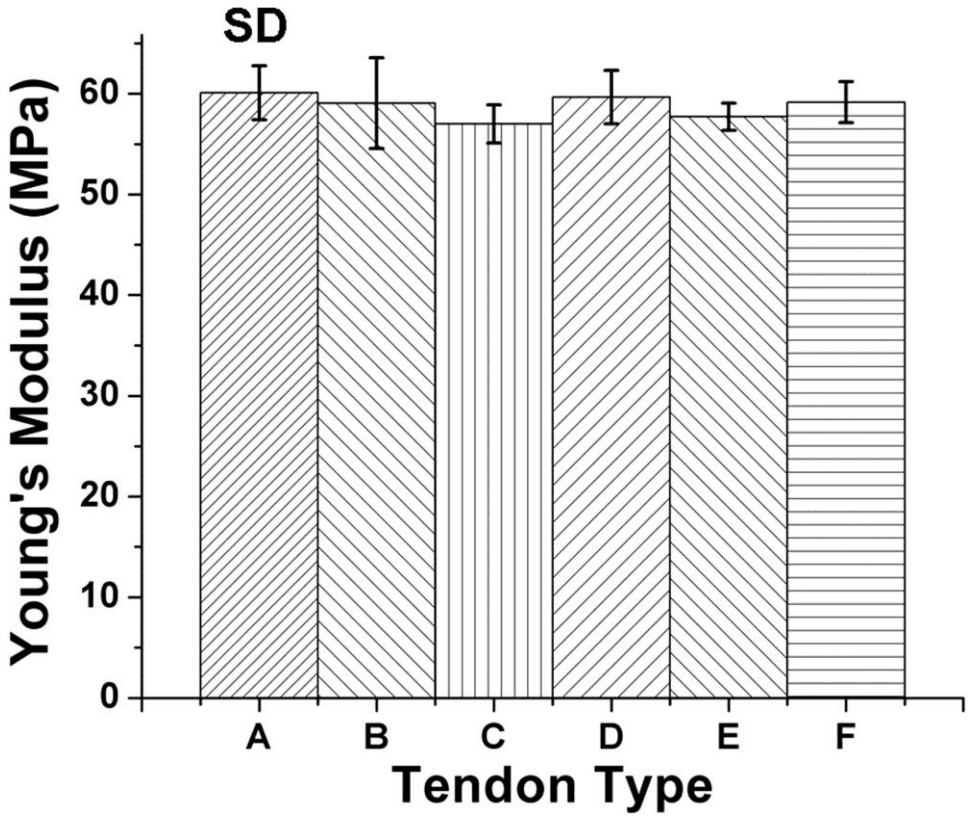

Fig. 2.7. Mean Young's modulus of fiber bundles for the 6 anatomical EOTs.[44] (N=300 measurements each) A. Lateral rectus. B. Inferior rectus. C. Medial rectus. D. Superior rectus. E. Inferior oblique. F. Superior oblique.

Young’s moduli among the six different anatomical EOTs did not differ significantly (t-test, $P > 0.25$). Since there was no significant variation in Young's modulus among anatomical EOTs, so the data were pooled for all of them to give a value of 58.88 ± 3.35 MPa.

2.3.2. Poisson Ratio Measurement of EOT Using OCT

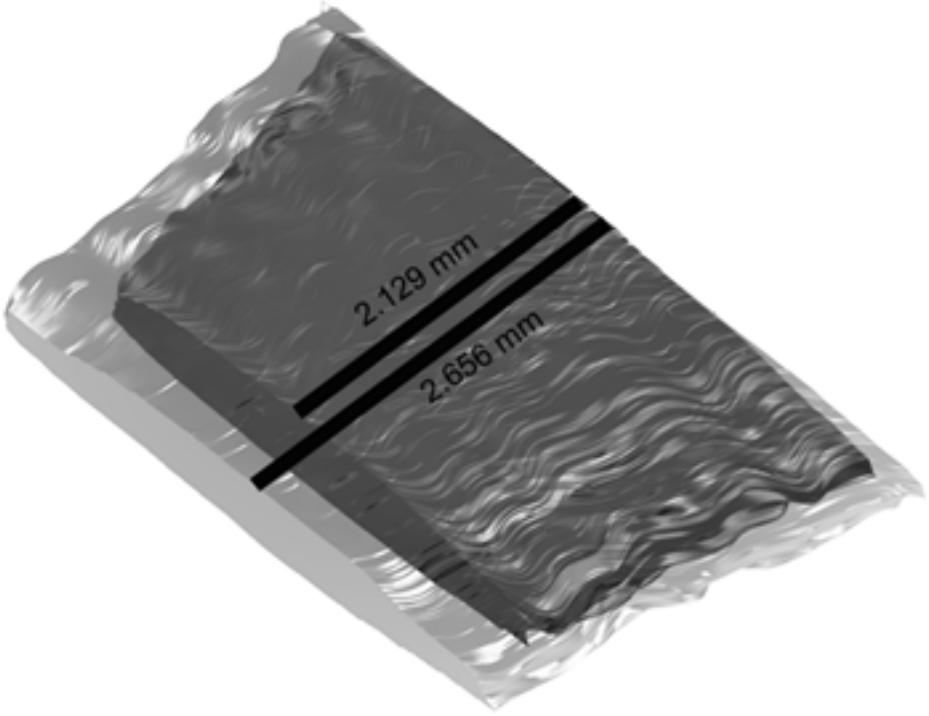

Fig. 2.8. Three-dimensional model of EOT before and after deformation

The mean PR from discretized 3-D models for each microscopic element in 7 bovine EOT specimens averaged 0.542 ± 0.011 (SD, n=7). The PR for EOT significantly ($P < 0.0001$) exceeded 0.5, which is the PR of an ideal incompressible material. This indicates that EOT volume decreases during tensile deformation. Assuming mass conservation, we may conclude that EOT density increased during tensile elongation.

2.4. Discussion

Nano indentation of EOT fiber bundles analyzed within the Hertzian framework effectively characterized the transverse Young's modulus, a critical mechanical parameter, for bovine EOT fiber bundles. The present investigation might be the first to do so by nano indentation characterization in EOT. Transverse Young's modulus for fiber bundles from LR, IR, MR, SR, IO and SO EOTs were all similar and averaged 58.88±3.35 MPa, and did not vary significantly according to the anatomical EOM from which the EOTs were obtained.

Fig. 2.9 shows previously reported Young's modulus for a wide range of materials.[45, 49-51] Fibers from EOT have a transverse Young's modulus between stiff gelatin and protein such as collagen, and significantly higher than for cells or gelatin. Since EOT fiber bundles are comprised mainly of collagen, the observation that the Young's modulus of EOT fiber bundles is appreciably less than that of collagen implies a more compliant micro-structure. Tendon fibers have been reported to have a helical microstructure that gives arise to volume loss under axial tensile loading.[46, 52] It is also generally accepted that the helical structure of fiber bundles causes the fiber-aligned modulus to be one to two orders of magnitude larger than the transverse modulus.[53-55] The presentation determination of EOT fiber bundle transverse Young's modulus as one to two orders of magnitude less than the axial modulus of collagen is thus consistent with known properties of non-ocular tendons. The difference between transverse and axial Young's moduli can result from an endotendinous sheath that provides a stress shielding effect.[55]

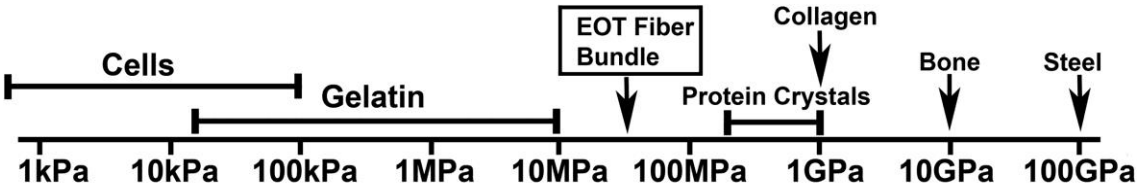

Fig. 2.9. Young's moduli for various materials,[45, 49-51] including EOT fiber bundles.

Unlike other ocular and orbital tissues,[15, 17] single fibers from EOT exhibit much higher stiffness and purely elastic, rather than viscoelastic, behavior. From previous investigations on viscoelastic characteristic of orbital/ocular tissues, it was reported that Young's modulus of most of orbital tissues does not exceed 120 kPa.[17] Perhaps the purely elastic behavior of EOT facilitates the eye movements known as saccades, which are not only the fastest movements achieved by any part of the body, but are regulated by neural commands that appear optimized to minimize the time required to shift from one eye position to the next.[56] Saccades must be brief because vision during the flight of a saccade is nearly impossible as saccade speed typically ranges from 300°/s to 600°/s; saccade durations range from 20 – 200 ms.[57] Since EOTs are in series with the actuating EOMs, any viscous behavior of EOTs would have the undesirable effect of damping peak saccade acceleration and prolonging the intra-saccadic period of impaired vision. Moderately high EOT stiffness would also be desirable, since elongation under load would dissipate the muscle force required to rotate the eye.

The highly reproducible determination of transverse Young's modulus of EOT fiber bundles reported in the present study not only gives us an insight to the axial stiffness of EOTs, but also should facilitate quantitative modeling of ocular motor biomechanics. It would be reasonable to model all EOTs similarly, reducing the complexity of models representing

interactions among multiple EOMs. Such a representation might ultimately be represented using finite element analysis in a theoretical framework practical for graphical simulation of quasi-static strabismus and its surgical treatment.

The current investigation employed AFM to determine the transverse Young's modulus of bovine EOT fiber bundles, and to demonstrate that they have negligible viscous properties. As anticipated, the determined value of Young's modulus for EOT fiber bundles was significantly lower than that of collagen, suggesting that EOT fiber bundles incorporate fine structural features that increase compliance without introducing viscosity. Since the transverse properties of EOTs in macroscopic scale involve multi constituents such as collagen as well as components that comprise connective tissue sheath around the EOTs, the value of Young's modulus reported in current investigation does not reflect the macroscopic properties of EOTs. However, the value reported in the current study can serve as the low threshold for EOT transverse properties in macroscopic characterization.

A PR across 0.5 has two opposite implications on tendon behavior: a PR smaller than 0.5 means an increase in volume during loading, based upon the mass conservation assumption, decreasing density. On the contrary, a PR value higher than 0.5 implies volume decrease and an increase in density. In this study, averaged PR value was 0.542 ± 0.011, which means that volume decreased during tensile loading. Other studies also reported PR values from rat[58] and sheep[53] tendon as over 0.5 (0.8 and 2.99, respectively). While Lynch et al. suggested that the small volume variations measured might be caused by water loss,[53] Reese et al. suggested that volume change might depend on the tendon microstructure, which is characterized by a helical organization of fibrils within crimped fibers.[46] Employing OCT measurement for cross section area change has higher precision than alternative measurement methodologies. The precise PR

estimate for EOT reported in the present study should facilitate quantitative modeling of ocular motor biomechanics and is represented in a theoretical framework practical for graphical simulation of quasistatic ocular motility using FEM.

2.5. References

1. Lin H, Kwan M, Woo S. On the stress relaxation properties of the anterior cruciate ligament (acl). *Adv Bioeng* 1987;5–6.

2. Pradas MM, Calleja RD. Nonlinear viscoelastic behavior of the flexor tendon of the human hand. *Journal of Biomechanics* 1990;23:773-781.

3. Johnson GA, Livesay GA, Woo SLY, Rajagopal KR. A single integral finite strain viscoelastic model of ligaments and tendons. *Journal of Biomechanical Engineering-Transactions of the Asme* 1996;118:221-226.

4. Jung HJ, Fisher MB, Woo SL. Role of biomechanics in the understanding of normal, injured, and healing ligaments and tendons. *Sports Med Arthrosc Rehabil Ther Technol* 2009;1:9.

5. Kastelic J, Galeski A, Baer E. The multicomposite structure of tendon. *Connect Tissue Res.* 1978;6:11-23.

6. Kannus P. Structure of the tendon connective tissue. *Scand J Med Sci Sports.* 2000;10:312-320.

7. Maganaris CN, Paul JP. In vivo human tendon mechanical properties. *The Journal of Physiology.* 1999;521:307-313.

8. Maganaris CN, Paul JP. Tensile properties of the in vivo human gastrocnemius tendon. *Journal of Biomechanics.* 2002;35:1639-1646.

9. Reeves ND, Maganaris CN, Narici MV. Effect of strength training on human patella tendon mechanical properties of older individuals. *The Journal of Physiology* 2003;548:971-981.

10. Miller J, Pavlovski D, Shaemeva I. Orbit 1.8 gaze mechanics simulation. *San Francisco: Eidactics.* 1999.

11. Collins CC, Carlson MR, Scott AB, Jampolsky A. Extraocular muscle forces in normal human subjects. *Invest Ophthalmol Vis Sci.* 1981;20:652-664.

12. Quaia C, Ying HS, Nichols AM, Optican LM. The viscoelastic properties of passive eye muscle in primates. I: Static forces and step responses. *Plos One* 2009;4.

13. Robinson DA, O'Meara DM, Scott AB, Collins CC. Mechanical components of human eye movements. *Journal of Applied Physiology.* 1969;26:548-553.

14. Simonsz HJ. Force-length recording of eye muscles during local-anesthesia surgery in 32 strabismus patients. *Strabismus.* 1994;2:197-218.

15. Yoo L, Kim H, Gupta V, Demer JL. Quasilinear viscoelastic behavior of bovine extraocular muscle tissue. *Invest Ophthalmol Vis Sci.* 2009;50:3721-3728.

16. Yoo L, Reed J, Gimzewski JK, Demer JL. Mechanical interferometry imaging for creep modeling of the cornea. *Invest Ophthalmol Vis Sci* 2011;52:8420-8424.

17. Yoo L, Reed J, Shin A, et al. Characterization of ocular tissues using micro-indentation and hertzian viscoelastic models. *Invest Ophthalmol Vis Sci* 2011.

18. Boyce BL, Jones RE, Nguyen TD, Grazier JM. Stress-controlled viscoelastic tensile response of bovine cornea. *Journal of Biomechanics.* 2007;40:2367-2376.

19. Quaia C, Ying HS, Optican LM. The viscoelastic properties of passive eye muscle in primates. Ii: Testing the quasi-linear theory. *Plos One* 2009;4.

20. Yoo L, Gupta V, Lee C, Kavehpore P, Demer JL. Viscoelastic properties of bovine orbital connective tissue and fat: Constitutive models. *Biomechanics and Modeling in Mechanobiology* 2011;10:901-914.

21. Yoo L, Kim H, Shin A, Gupta V, Demer JL. Creep behavior of passive bovine extraocular muscle. *Journal of Biomedicine and Biotechnology* 2011.

22. Hinterdorfer P, Dufrene YF. Detection and localization of single molecular recognition events using atomic force microscopy. *Nature Method* 2006;3:347-355.

23. Pelling AE, Li Y, Shi W, Gimzewski JK. Nanoscale visualization and characterization of myxococcus xanthus cells with atomic force microscopy. *Proceedings of the National Academy of Sciences of the United States of America* 2005;102:6484-6489.

24. Rief M, Gautel M, Oesterhelt F, Fernandez JM, Gaub HE. Reversible unfolding of individual titin immunoglobulin domains by afm. *Science* 1997;276:1109-1112.

25. van der Mei HC, Busscher HJ, Bos R, de Vries J, Boonaert CJP, Dufrêne YF. Direct probing by atomic force microscopy of the cell surface softness of a fibrillated and nonfibrillated oral streptococcal strain. *Biophysical Journal* 2000;78:2668-2674.

26. Sokolov I. Atomic force microscopy in cancer cell research. *Cancer Nanotechnology* 2007;1-17.

27. Lin DC, Dimitriadis EK, Horkay F. Robust strategies for automated afm force curve analysis—i. Non-adhesive indentation of soft, inhomogeneous materials. *Journal of Biomechanical Engineering.* 2006;129:430-440.

28. Radmacher M. Measuring the elastic properties of biological samples with the afm. *Engineering in Medicine and Biology Magazine, IEEE.* 1997;16:47-57.

29. Lakes R. Advances in negative poisson's ratio materials. *Advanced Materials* 1993;5:293-296.

30. Chung SM, Yap AUJ, Koh WK, Tsai KT, Lim CT. Measurement of poisson's ratio of dental composite restorative materials. *Biomaterials* 2004;25:2455-2460.

31. Wu W, Sadeghipour K, Boberick K, Baran G. Predictive modeling of elastic properties of particulate-reinforced composites. *Materials Science and Engineering: A* 2002;332:362-370.

32. Pamenius M, Ohlson NG. The determination of elastic constants by dynamic experiments. *Dental Materials* 1986;2:246-250.

33. Spinner SAM. Elastic moduli of glasses at elevated temperatures by a dynamic method. *Journal of the American Ceramic Society* 1956;39:113-118.

34. D'Evelyn MP, Taniguchi T. Elastic properties of translucent polycrystalline cubic boron nitride as characterized by the dynamic resonance method. *Diamond and Related Materials* 1999;8:1522-1526.

35. Zhang M, Zheng YP, Mak AFT. Estimating the effective young's modulus of soft tissues from indentation tests—nonlinear finite element analysis of effects of friction and large deformation. *Medical Engineering & Physics* 1997;19:512-517.

36. van den Bedem SPW, Schutte S, Simonsz HJ, van der Helm FCT. Mechanical properties and functional importance of pulley bands or 'faisseaux tendineux'. *Vision Research* 2005;45:2710-2714.

37. Sumi C, Suzuki A, Nakayama K. Estimation of shear modulus distribution in soft tissue from strain distribution. *Biomedical Engineering, IEEE Transactions on* 1995;42:193-202.

38. Euler L. The rational mechanics of flexible or elastic bodies: Introduction to leonhardi euleri opera omnia, vol. X and xi, seriei secundae. *Orell Fussli.* 1638 - 1788.

39. Almqvist N, Bhatia R, Primbs G, Desai N, Banerjee S, Lal R. Elasticity and adhesion force mapping reveals real-time clustering of growth factor receptors and associated changes in local cellular rheological properties. *Biophysical Journal.* 2004;86:1753-1762.

40. Matzke R, Jacobson K, Radmacher M. Direct, high-resolution measurement of furrow stiffening during division of adherent cells. *Nature Cell Biology.* 2001;3:607-610.

41. Rotsch C, Braet F, Wisse E, Radmacher M. Afm imaging and elasticity measurements on living rat liver macrophages. *Cell Biology International.* 1997;21:685-696.

42. Rotsch C, Radmacher M. Drug-induced changes of cytoskeletal structure and mechanics in fibroblasts: An atomic force microscopy study. *Biophysical Journal.* 2000;78:520-535.

43. Sneddon IN. The relation between load and penetration in the axisymmetric boussinesq problem for a punch of arbitrary profile. *International Journal of Engineering Science.* 1965;3:47-57.

44. Yoo L, Reed J, Shin A, Demer JL. Atomic force microscopy determination of young's modulus of bovine extra-ocular tendon fiber bundles. *Journal of Biomechanics.* 2014;In Press.

45. Stolz M, Raiteri R, Daniels AU, VanLandingham MR, Baschong W, Aebi U. Dynamic elastic modulus of porcine articular cartilage determined at two different levels of tissue organization by indentation-type atomic force microscopy. *Biophysical Journal.* 2004;86:3269-3283.

46. Reese SP, Maas SA, Weiss JA. Micromechanical models of helical superstructures in ligament and tendon fibers predict large poisson's ratios. *Journal of Biomechanics* 2010;43:1394-1400.

47. Smith CW, Wootton RJ, Evans KE. Interpretation of experimental data for poisson's ratio of highly nonlinear materials. *Experimental Mechanics* 1999;39:356-362.

48. Vergari C, Pourcelot P, Holden L, et al. True stress and poisson's ratio of tendons during loading. *Journal of Biomechanics* 2011;44:719-724.

49. Alonso JL, Goldmann WH. Feeling the forces: Atomic force microscopy in cell biology. *Life Sciences.* 2003;72:2553-2560.

50. Dimitriadis EK, Horkay F, Maresca J, Kachar B, Chadwick RS. Determination of elastic moduli of thin layers of soft material using the atomic force microscope. *Biophysical Journal.* 2002;82:2798-2810.

51. Wenger MPE, Bozec L, Horton MA, Mesquidaz P. Mechanical properties of collagen fibrils. *Biophysical Journal.* 2007;93:1255-1263.

52. Rigby BJ, Hirai N, Spikes JD, Eyring H. The mechanical properties of rat tail tendon. *The Journal of General Physiology.* 1959;43:265-283.

53. Lynch HA, Johannessen W, Wu JP, Jawa A, Elliott DM. Effect of fiber orientation and strain rate on the nonlinear uniaxial tensile material properties of tendon. *Journal of Biomechanical Engineering.* 2003;125:726-731.

54. Quapp KM, Weiss JA. Material characterization of human medial collateral ligament. *Journal of Biomechanical Engineering.* 1998;120:757-763.

55. Yamamoto E, Hayashi K, Yamamoto N. Effects of stress shielding on the transverse mechanical properties of rabbit patellar tendons. *Journal of Biomechanical Engineering.* 2000;122:608-614.

56. Kirchner H, Thorpe SJ. Ultra-rapid object detection with saccadic eye movements: Visual processing speed revisited. *Vision Research.* 2006;46:1762-1776.

57. Lebedev S, Van Gelder P, Wai Hon T. Square-root relations between main saccadic parameters. *Investigative Ophthalmology and Visual Science.* 1996;37:2750-2758.

58. Cheng VT, Screen HC. The micro-structural strain response of tendon. *Journal of Materials Science* 2007;42:8957-8965.

Chapter 3

Independent Mechanical Behavior of Extraocular Muscle Compartments

3.1. Introduction

In skeletal muscles, there may exist multiple neuromuscular compartments that are controlled by different sets of motor neurons.[1-3] For example, transversus abdominis,[3] cricothyroid muscle,[4] and triceps brachii[5] are innervated independently by separate motor nerve branches. Similarly, EOM also has more motor units (defined as the set of muscle fibers innervated by a single motor neuron) than apparently required by conventional ocular motility mechanisms.[6, 7] Peng et al.[8] traced the intramuscular arborization of the abducens nerve (CN6) within the LR muscles of monkey and human, and found that the CN6 bifurcates and arborizes within non-overlapping superior and inferior zones throughout the EOM's length. As a sequential study, Costa et al.[9] confirmed Peng's report of compartmentalized LR innervation, and extended the study by tridimensional reconstruction of nerve arborizations to the IR, MR, and SR muscles of humans and monkeys. Based on the result, LR and MR EOM motor nerves bifurcated into two divisions that innervate; superior and inferior zones of EOM fibers in approximately equal size. In contrast, IR and SR EOM motor nerves were highly mixed throughout each EOM, proposing that differential innervation in horizontal rectus zones can potentially mediate previously unrecognized vertical oculorotary actions. Although Costa et al. did not suggest that the dual compartments of the horizontal rectus EOMs are always

differentially activated, these authors proposed that differential innervation might occur under some physiological conditions. Recently, functional evidence for differential compartmental activation of the human LR was obtained from magnetic resonance imaging during ocular counter-rolling induced by head tilt.[10]

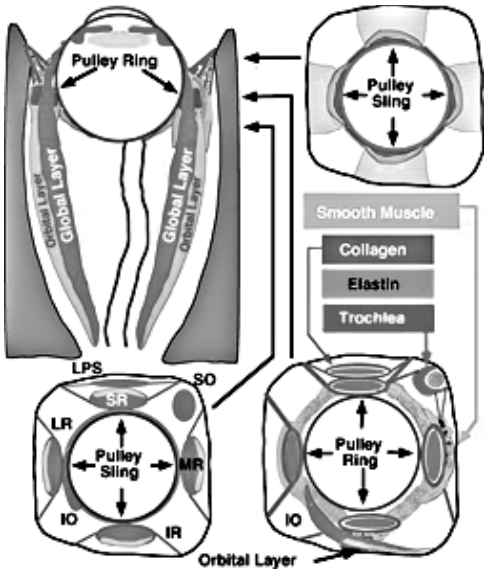

Fig. 3.1. Global (GL) and orbital (OL) layer structure (Demer et al.)[11]

Other than the compartments in horizontal rectus EOMs, an orthogonal compartmentalization of EOMs, the global (GL) and orbital layers (OL), has been established. The GL is continuous muscle layer from the annulus of Zinn to the tendinous insertion, and it rotates the eye containing three types of singly innervated fibers (SIFs) and one type of multiply innervated fiber (MIF). Meanwhile, the OL inserts on the pulley connective tissue not continuous to the tendon insertion, and contains one type of SIF and MIF each. The structure of GL and OL in the orbit is shown in Fig. 3.1. The active pulley hypothesis (APH) suggested that OL of EOMs

inserts in a pulley connective tissue ring through which pass the GL fibers that in turn insert on the sclera to rotate the eye. This laminar compartmentalization influences ocular kinematics: during EOM contraction, shifts in pulley positions influence EOM pulling directions by half the change in ocular orientation conforming Listing's Law (LL) ocular torsion.[11-15] The APH assumed that at least some degree of mechanical independence of fibers should exist in the OL vs. GL, since each layer is supposed to be independently controlled to maintain LL.

Anatomical basis for predicting the degree of mechanical independence of groups of EOM fibers does not exist yet. Skeletal muscles are considered to encompass four morphologies of fiber orientation: parallel, convergent, pennate, and sphincter.[16] Although EOMs are different in many respects from skeletal muscles, their roughly parallel arrangement of fiber organization might be supposed to have some independence among fibers. There are various claims regarding the anatomical degree to which EOM fibers are mutually coupled longitudinally and transversely. Observations based upon serial transverse sections of undisturbed, whole human and monkey orbits suggest that rectus EOM fibers are arranged in roughly parallel bundles.[17, 18] Mayr et al. studied teased fiber preparations of cat EOMs, and reported that while all OL fibers run from tendon to tendon, in the GL only the multiply-innervated fibers (MIFs) do so, while the singly-innervated fibers (SIFs) are usually arranged in series of two or three fibers interconnected by myomyous junctions with frequent fiber splitting.[19] They also observed end-to-side connections between SIFs and MIFs. In the approximately 22 mm long isolated superior rectus (SR) OL of a juvenile rabbit, Davidowitz et al. traced 94 fibers in four fascicles of the and found the singly-innervated fibers to extend 5 – 8 mm in length, and multiply-innervated fibers to extend 10 – 19 mm in length.[20] They observed several instances fiber splitting in multiply-innervated fibers. Based upon myosin expression in rabbit EOM, McLoon et al. proposed a complex variety of

fiber morphologies, with some extending the entire EOM length, and other shorter fibers in series arrangement.[21] Harrison et al., reported that individual EOM fibers or rabbit and monkey are shorter than the overall EOM, and in rabbit SR change their relationships with adjacent fibers along their longitudinal course.[22] Regardless of the arrangement of EOM fibers, and regardless of the presence of connective tissue within EOMs, anatomical studies cannot be decisive regarding the overall mechanical behavior of EOM subgroups considered on a larger scale. This issue can only be resolved by direct biomechanical measurements of EOM compartments that have not heretofore been available.

Materials engineering provides several approaches to characterize internal mechanical coupling. Coupling between normal and shear directional stresses or strains describes some of the moduli of anisotropic materials. The shear coupling ratio is defined as the ratio of the shear strain to normal strain associated with the axis of the normal strain.[23-25] Tensile or shear loading tests are performed to determine the shear coupling ratio of materials such as wood[26] or composites of graphite filaments embedded in epoxy resins.[27] Adhesive force measurement between composites could be considered similar to the coupling between EOM compartments, in terms of local force generation between two layers. Microbond techniques,[28-30] single-fiber fragmentation,[31-33] and micro-indentation/microdebonding techniques[34-36] have been employed for measuring fiber-matrix adhesion in composite materials. To date, none of these techniques has been employed to investigate the compartmental mechanical behavior of EOM.

Voluntary muscles such as skeletal or extraocular muscles are activated to contract by the innervation from the brain. In similar manner, artificial activation can be obtained by an electric stimulus delivered by an electrode. Coiled wire intramuscular electrodes have proven effective in research, but present two problems for clinical systems; the electrode is vulnerable to the

breakage due to the repeated bending,[37] and recruitment is dependent on muscle length with intramuscular stimulation, making control difficult.[38] Epimysial electrodes also have been tried for stimulation, but have the same recruitment problem.[39] As alternative, direct nerve stimulation through a nerve cuff electrode, was introduced that does not exhibit length dependent recruitment, nor would the electrode or its leads be subjected to the high degree of repeated bending. McNeal et al., using a rigid cuff electrode, showed that the ankle flexors and extensors could be activated selectively if the electrodes were in snug contact with the nerve.[40] Further, Veraart et al. also demonstrated the selective control of four different muscles in a cat (medial gastrocnemius, soleus, tibialis anterior, and extensor digitorum longus) using a cuff containing twelve dot electrodes.[41] This selective muscle activation technique might be utilized for activation of compartmentalized horizontal EOMs, although physiological innervational control needs to be understood to distinguish the contractile activity of EOM subparts.

From a biochemical perspective, it is generally accepted that interaction of myosin and actin in the presence of ATP represents the essential mechanism of muscle contraction[42], and calcium ion has a vital role as a main regulatory and signaling molecule. Filo et al. first described the relation between tension and calcium ion concentration using glycerinated skeletal and smooth muscles.[43] Hellam and Podolsky (1966) performed quantitative study of the calcium requirement using skinned fiber,[44] suggesting the threshold calcium concentrations for beginning (pCa 8.0-7.5) and maximum (pCa 6) muscle contraction. Specifically in EOM, calcium ion content is up to 40-fold higher than in limb skeletal muscle,[45] so that fast contracting, followed by rapid relaxation, can be generated to produce saccades, the fastest movements produced by the human body. Since calcium ionic solution has been proven as a catalyst of EOM contraction, it was employed for the active contraction experiments in this study.

Motivated by anatomical findings suggesting compartmentalized intramuscular innervation of horizontal rectus EOMs, and OL/GL compartmentalization in all EOMs, this study aimed to investigate the potential for independent mechanical behavior of EOM compartments in large and easily available bovine specimens. A finding of substantial mechanical coupling between EOM compartments during tensile and contractile movement would decisively exclude the Costa et al.[9] hypothesis of physiologically independent action of horizontal rectus EOM compartments, and would challenge the proposition of the APH that the OL is innervated differently from the GL in each of the anatomical EOMs. Conversely, a finding of substantial mechanical independence between compartments would allow the foregoing hypotheses to remain under consideration.

3.2. Method

3.2.1. Independent Passive Mechanical Behavior of EOM and EOT Compartments

Dual Channel Tensile Testing Apparatus. A custom dual channel micro-tensile load cell was constructed, consisting of two horizontally mounted, tensile loading devices capable of acting with <1 mm lateral spacing. In order to maintain high mechanical stiffness, all components were mounted, using heavy aluminum or steel hardware, to a 12.5 mm thick aluminum optical bench foundation plate. It was verified that the structure did not deform measurably during tissue loading, so that measurements reflected tissue properties without influence of instrument compliance. Each mechanical channel could be pulled independently while force was recorded independently in the corresponding channel. In each channel, a servo-

controlled electromagnetic linear motor (Ibex Engineering, Newbury Park, CA) capable of high speed (controllable to a maximum of 100 mm/sec) and fine resolution (20 nm) was mounted in line with an S-shaped semiconductor strain gauge (FUTEK Advanced Sensor Technology, Irvine, CA) having 5 mN resolution. This servomotor permits precise, independent control of both linear position and linear speed. Each strain gauge was in turn attached to a 127 mm long stainless steel tensile shaft that passed into a closed physiologic chamber through a frictionless air bearing that served as its mechanical support. Inside the physiologic chamber the tensile shaft was attached to a high friction, serrated stainless steel compression clamp to engage one end of the specimen under test. The other specimen end was similarly clamped to a tensile shaft fixed to the opposite end of the load cell. When the linear motor elongated one of the channels via the tensile shaft, the strain gauge indicated the tensile force in the corresponding channel.

Specimens under test were enclosed in a physiologic chamber with transparent walls whose lower portion contained a water bath heated under feedback control to maintain 100% humidity and 37°C temperature in the overlying air adjacent the specimen, as measured by a thermocouple. A high resolution video camera with 50 mm macro lens (Canon EOS 5D Mark II, Japan) was mounted above the specimen outside the physiologic chamber. Since the air in the physiologic chamber was saturated with water vapor to prevent evaporation from the specimen under test, the upper surface of the chamber was coated with an anti-condensation compound to inhibit fogging of the chamber wall during photography of the specimen. Fig. 3.2 illustrates the schematic drawing and photograph of the dual channel load cell.

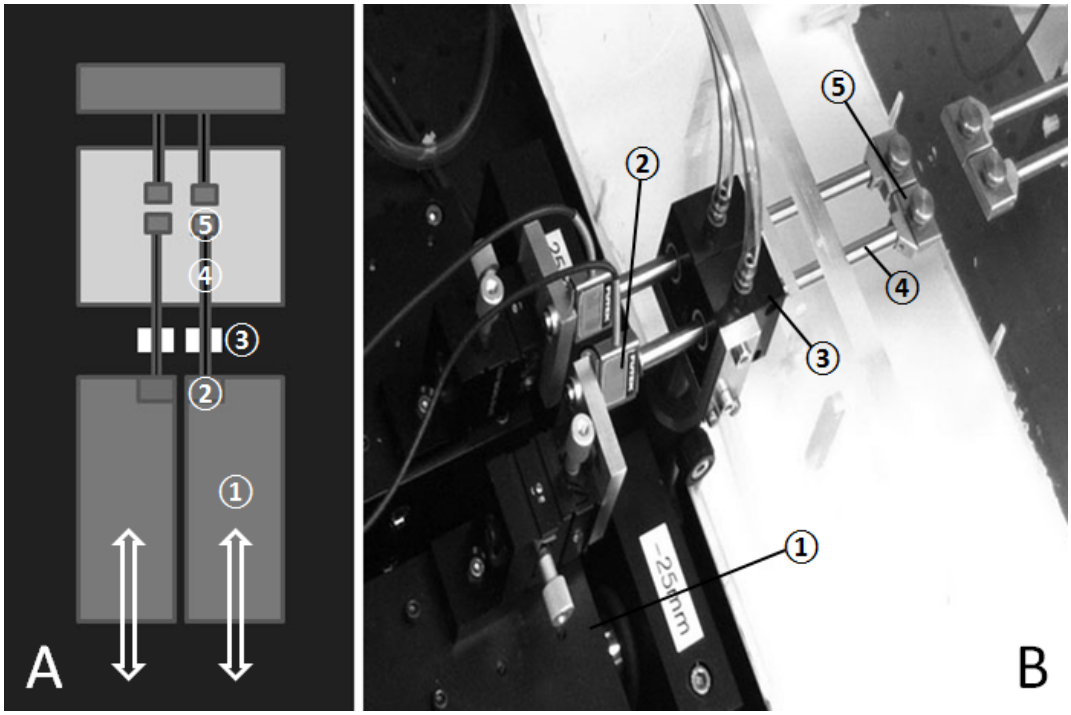

Fig. 3.2. Dual channel micro-tensile load cell.[46] A. Schematic cartoon. Two linear motors moved independently, and generated tensile forces in each compartment of the tissue placed in the clamps. B. Photograph of apparatus. In each adjacent channel, a strain gauge (②) attached to the linear motor (①) was connected to the specimen clamp (⑤) through a tensile shaft (④) that was supported by a frictionless air bearing (③).

Specimen Preparation. Fresh heads of cows aged 20 – 30 months were obtained immediately after slaughter from a nearby abattoir (Manning Beef LLC, Pico Rivera, CA). Transport time from abattoir to laboratory was approximately one hour, and one hour additionally elapsed for dissection and preparation of specimens in the laboratory. After extraction, specimens were maintained in lactated Ringer's solution at 37° C. For most experiments, any opaque tissue sheaths were carefully dissected away from the EOMs using micro-surgical instruments, so that surface fiducials could be optically imaged. In control

experiment, the connective tissue sheathes of some specimens were left intact to ascertain possible effect of the sheaths.

Transverse Compartments. Multiple specimens of all six anatomical EOMs were extracted and prepared for transverse compartment experiments. Tendons and a small amount of terminal GL were sharply excised to assure that specimens included both OL and GL. Varying with bovine age, average specimen length after tendon removal was 45±7 mm (standard deviation, SD). Depending upon the anatomical EOM, the ratio of length to greatest transverse width ranged from 2:1 to 5:1. Whole fresh EOM tissue is difficult to clamp uniformly because of its moisture and lack of intrinsic friction. It was critical to prohibit specimen slip relative to the clamp during experimental loading that would have introduced serious artifacts. For maximizing friction between the clamp and the specimen, a serrated clamp was fabricated of stainless steel using a computer-controlled mill. Prior to clamping, both broad surfaces of each specimen end were fixed using surgical suture and cyanoacrylate glue between 5 mm long layers of thin cardboard folded over the specimen's end to form an anchor that was placed in the clamp. Thus, the terminal 5 mm of each end of the specimen was contained within a clamp. The end of the specimen attached to moving clamps was sharply divided longitudinally (as, for example, between superior and inferior portions for horizontal rectus EOMs) using a scalpel over a short distance of 1–3 mm into the EOM and clamped separately to the two load cell channels, while the fixed end was clamped to one broad clamp. This short longitudinal division at the elongating end was the minimum length necessary to prevent the elongating portion of the specimen from folding onto the fixed portion clamp, and creating a collision artifact. Fig. 3.3 illustrates the arrangement for testing transverse compartmentalization of horizontal rectus EOMs.

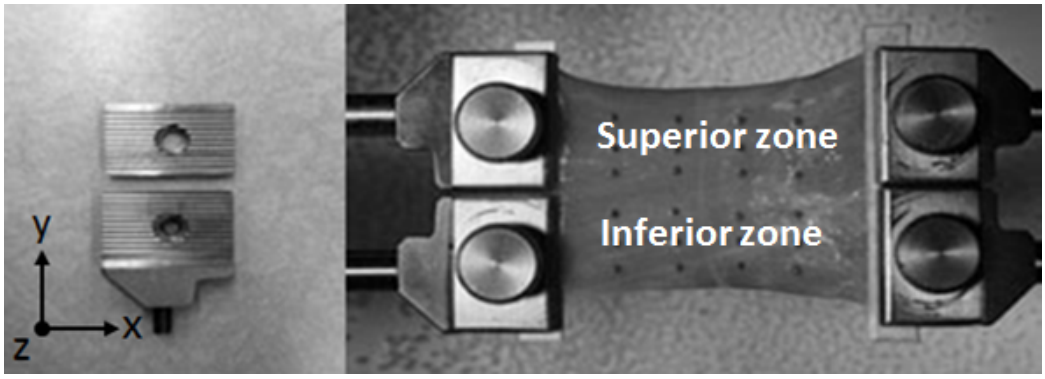

Fig. 3.3. Transverse compartment testing configuration of medial rectus EOM.[46] The specimen was aligned in the x-y plane. Metal bead fiducials are visible as an array of dots on the EOM global surface.

GL/OL Compartments. All EOMs consist of GL and OL that have scleral and pulley insertions, respectively. Since the OL is located on the EOM's orbital surface and inserts on pulley connective tissue, special care was necessary to isolate the OL insertion. First, the pulley tissue for each EOM was identified, and carefully dissected free of external attachments. Then, the GL tendon was detached from the scleral insertion, and the tendon itself was sharply excised from the GL. Excess tissue in the distal part of the OL attachment was trimmed to the width of the GL. The GL, and the OL attachment, were then glued using cyanoacrylate between folded layers of thin cardboard to provide secure mechanical anchors held in the clamps (Fig. 3.4). Since both OL and GL extend over the full width of each EOM, a wider clamp was necessary for the GL/OL experiments than was required for transverse compartment experiments (Fig. 3.4). Other details for specimen mounting were as for the transverse compartment experiment. Fig. 3.4 also illustrates specimen orientation for OL and GL experiments. Although the connective tissue contiguous with the OL insertion was expected to undergo some stretching

during tensile testing, this effect does not alter the tension measured in the OL since the tissues are in mechanical series with the strain gauge.

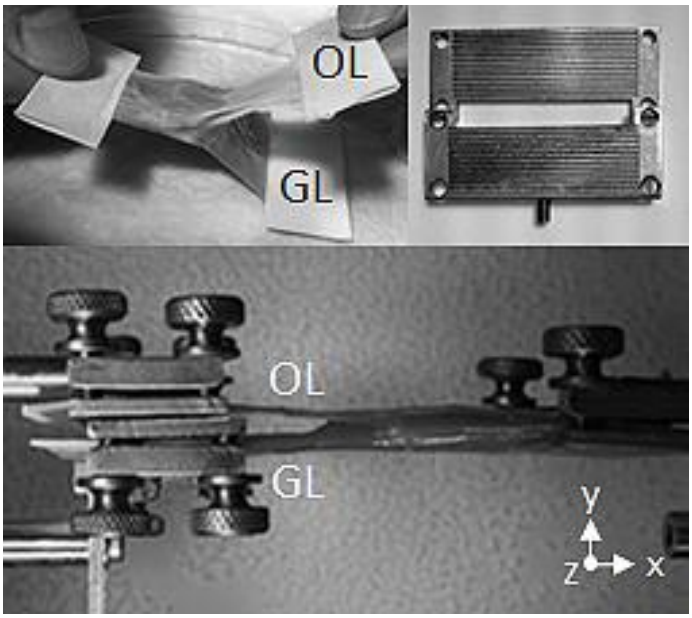

Fig. 3.4. GL/OL compartment testing arrangement.[46] A wider clamp was fabricated to span the entire tendon width. The specimen was aligned on the x-z plane. The abbreviations GL and OL indicate the points of force application that were coupled to these two layers; the cardboard marked OL was attached to connective tissue to which the OL fibers insert. The cardboard anchor on the OL's anchoring connective tissue was left long to avoid mechanical interference with the GL when mounted as in the illustration below.

Coupling Fraction and Displacement Ratio. To investigate coupling between adjacent compartments, two parameters were defined: Coupling Fraction (CF) and Displacement Ratio (DR). CF is defined as the maximum force in the stationary compartment (Fs) divided by the maximum force in the moving compartment (Fm).

$$\textbf{\textit{Coupling Fraction}}\ (\boldsymbol{CF}) = \frac{\textbf{Max. force in the stationary compartment (Fs)}}{\textbf{Max. force in the moving compartment (Fm)}} \qquad \text{Eq 3.1}$$

A value of CF=0 would imply that the two compartments are totally independent; a value of CF=1 implies totally dependent coupling, with identical forces in both layers. In an analogous manner, DR is defined as the maximum local displacement of any individual fiduicial marker of local strain in the stationary compartment (Ds) divided by the maximum displacement of the spatially corresponding fiducial in the moving compartment (Dm).

$$\textbf{\textit{Displacement Ratio}}\ (\boldsymbol{DR}) = \frac{\textbf{Displ. in the stationary compartment (Ds)}}{\textbf{Displ. in the moving compartment (Dm)}} \qquad \text{Eq 3.2}$$

Experimental Procedure. Pre-loading of approximately 20 gram force (gf) was applied to avoid slackness of specimens; ancillary experiments verified that the exact value of pre-load did not affect results appreciably. Only one channel at a time was extended in 3 mm increments for transverse compartment experiments, or 5 mm for GL/OL compartment experiments, while the other channel remained stationary during force recording in both channels. Because elongations were to fixed distances, resulting tensile forces reached an early peak and declined subsequently. Data were collected during the first 50 sec of each elongation, although analysis was confined to the first 5 sec. All six anatomic EOMs were tested at three different loading rates of 5, 20, and 100 mm/sec to investigate velocity dependence. During transverse compartment tests, fine reflective metal bead fiducials (1 mm diameter) were distributed in a regular array with unloaded spacing of 6 mm between columns and 3 mm between rows of metal bead fiducials

placed on the global surface for high definition video tracking to visualize local displacement throughout each EOM.

3.2.2. Independent Active Contractile Mechanical Behavior of EOM Compartments

Dual Channel Contraction Testing Apparatus. The dual channel contraction testing was assembled consisting of two vertically mounted strain gauges. Unlike the passive tensile compartment testing, force is actively generated by contraction induced by ionic calcium solution. Thus, only a force measurement system was built for the active contraction compartment testing. Since the force level generated from active contraction is lower than during passive tensile elongation, a finer resolution strain gauge (Grass Technology, Warwick, RI) having 0.02 mN minimum resolution was employed, and mounted using a fine height adjustment to measure isometric contraction force. Two types of muscle clamps were employed. The bottom end of the EOM specimen was placed in a broad, spring steel clamp to avoid rotation artifacts, and it was connected to a heavy anchor whose weight markedly exceeded all forces that might be generated by the EOM. The upper end of each portion of the specimen was connected via two metal hooks to a sensitive strain gauge using fine, stiff, monofilament nylon with breaking strength over 200 N. After condition by a bridge amplifier, the output of each strain gauge channel was low pass filtered and digitally sampled (10 Hz sampling rate) at 32 bit precision using LabVIEW (National Instruments Corporation, Austin, TX.) Specimens were initially configured in an empty glass beaker that was then filled with calcium solution pre-heated to 40°C temperature to allow for cooling during the experiment. Fig. 3.5 illustrates the photograph of the dual channel contraction testing apparatus.

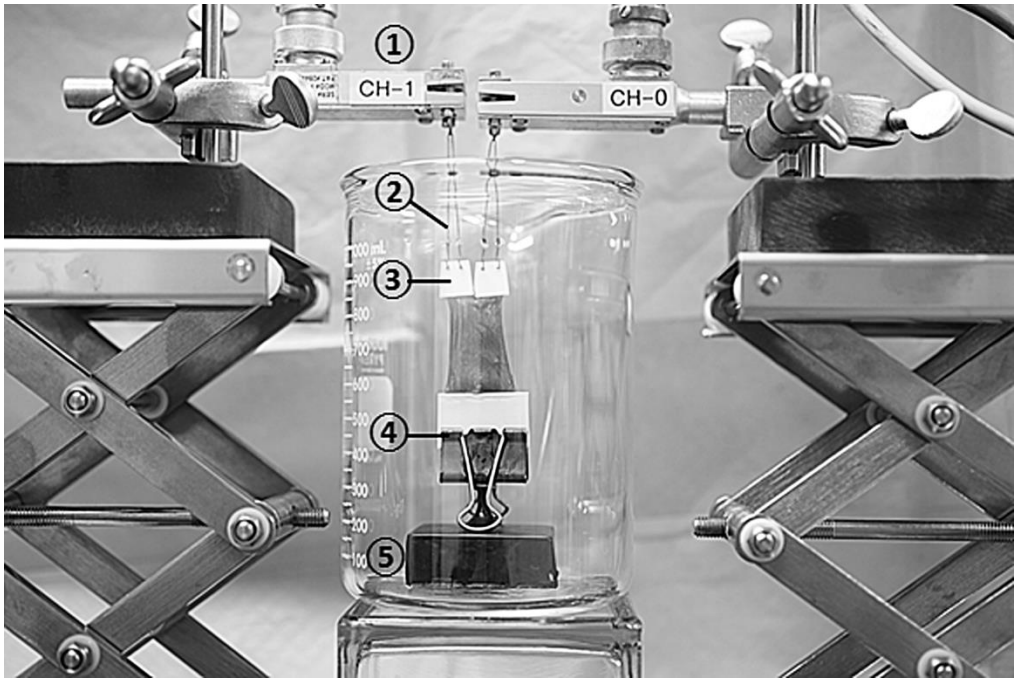

Fig. 3.5. Dual channel contraction testing apparatus. In each adjacent channel, two point sutures (②) connected the strain gauge (①) to the each EOM compartment (③). The common end of the EOM was clamped (④) to a heavy anchor weight resting on the bottom of the beaker (⑤). The contraction experiment was initiated by filling the beaker with calcium chloride solution to immerse the EOM specimen. Finely adjustable screw jack stands permitted separate pre-loading of each channel separately.

Muscle depolarization using calcium solution. Preliminary experiments were performed to confirm that bovine EOM can be contracted by ionic calcium solution. Various $CaCl_2$ concentrations from 5 mM to 100 mM were employed to maximize the degree of contraction of EOM. EOMs were immersed into varied $CaCl_2$ concentrations 5, 50, and 100 mM, and monitored the length change for an hour. After empirical investigation of various concentrations, optimum concentration for maximum EOM contraction was set at 50 mM. Every

EOM tested in more than 50 mM $CaCl_2$ solution contracted more than 20% of initial length. Fig. 3.6 shows an example of LR muscle that contracted 28.3% of initial length in one hour.

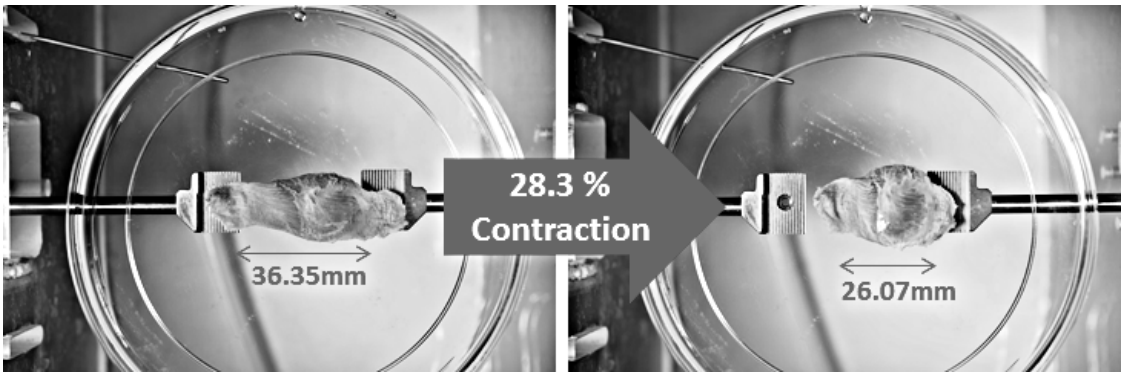

Fig. 3.6. Effect of $CaCl_2$ solution contraction on bovine LR muscle. The LR was immersed into 50 mM $CaCl_2$. After 1 hour, LR length had been reduced by 28.3% of initial length.

Compartment Isolation. Rather than elongating only one compartment in passive tensile testing, in the present experiment one compartment could be stimulated to actively contract by application of $CaCl_2$ solution, while isolating the other compartment with a water repellent coating. White petrolatum was used as the water repellent, and spread over the compartment designated not to be contracted, before the whole EOM was immersed in $CaCl_2$ solution. To verify compartmental isolation specificity, the aqueous soluble dye fluorescein sodium (Acid yellow, $C_{20}H_{10}O_5Na_2$) was added to the $CaCl_2$ solution. Fluorescein emits an apple-green fluorescence when excited by blue light. EOM specimens, either whole or transected, were photographed under blue light emitting diode illumination by a high resolution camera with 50 mm macro lens (Canon EOS 5D Mark II, Japan) equipped with yellow filter after immersion into 0.4 mM fluorescein-labeled $CaCl_2$ solution. In both transverse and GL/OL compartment experiments, fluorescein dye penetration was detected mostly in the exposed compartment, and

little fluorescein was evident in the isolated compartment, especially deep within the EOM. Fig. 3.7 illustrates the arrangement for testing transverse and GL/OL compartmentalization, and isolation of each compartment.

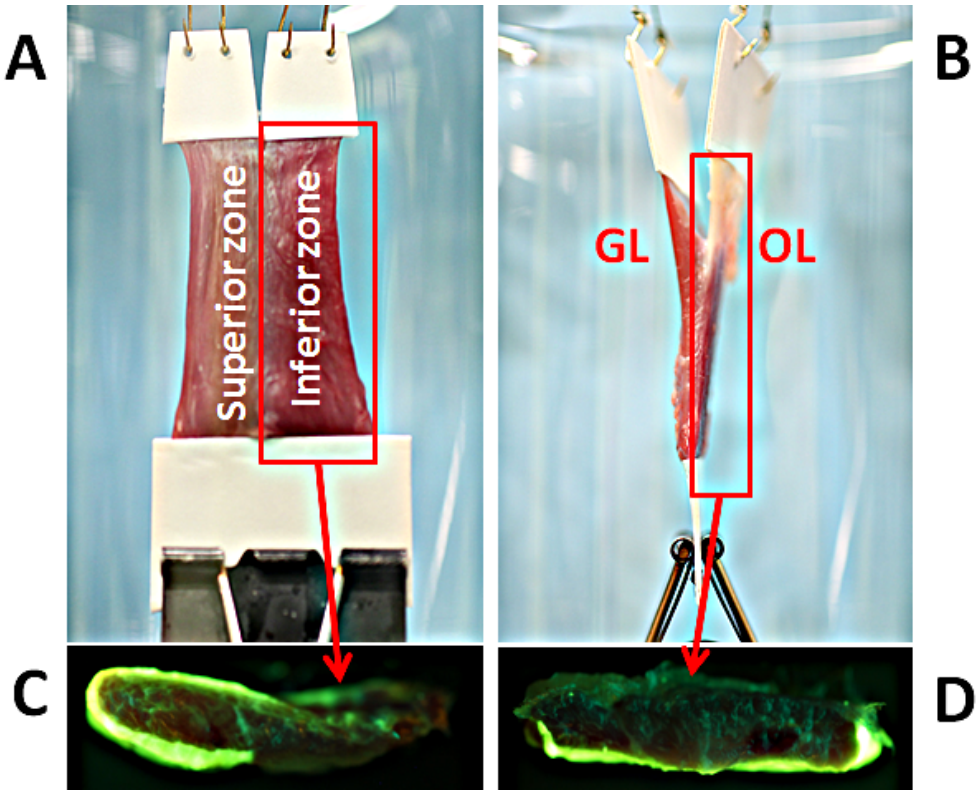

Fig. 3.7. Isolation of transverse and GL/OL compartments for chemical activation by 50 mM $CaCl_2$ labeled with 0.4 mM sodium fluorescein dye. Inferior (A) and OL (B) compartments were coated by water repellent white petrolatum. C, D. Cross sections of each compartment photographed in blue light using a yellow filter to demonstrate selective penetration of the fluorescein-labeled solution into the compartment not coated with petrolatum. After immersion in fluorescein-labeled $CaCl_2$ solution, superior (C) and GL (D, left) compartments were permeated with fluorescein marker, but inferior (C) and OL (D, bottom) compartments showed at most minimal fluorescence.

Experimental Procedure. As chosen, one OL/GL, or alternatively one transverse compartment, of a freshly excised bovine EOM specimen was coated with petrolatum to make resist penetration by aqueous $CaCl_2$ solution. One end of each compartment of the specimen was clamped to one channel of a sensitive strain gauge, while the common end of the specimen was clamped by a heavy anchor mass. The specimen and mass were inserted in a glass beaker. Since contraction force cannot be measured by the strain gauge if initial slackness exists, pre-loading of approximately 5 gram force (gf) was applied by elongation of the specimen ends at each strain gauge. Fluorescein-labeled 50 mM $CaCl_2$ solution pre-warmed to physiologic temperature was poured into the glass beaker, creating a slight reduction in tension due to buoyancy of the specimen. Thus, contraction of only one EOM compartment was activated for both the transverse and GL/OL compartment experiments, while the petrolatum-coated compartment was activated only minimally by what was assumed to be diffusion greatly hindered by the petrolatum coating. Force recording was performed continuously by strain gauges for in both channels.

Due to the buoyancy effect, reduced tension was detected immediately after EOM immersion in both channels, after which increased tension due to EOM contraction followed. Data were collected during 5 minutes for each experiment, although analysis was ultimately confined to the first 30 seconds. Since permeation of ionic solution between compartments, or through gaps in the petrolatum, eventually caused undesired contraction in the petrolatum-coated compartment after a period of time, force data in early 30 seconds were used to calculate the degree of mechanical independence between compartments.

3.3. Result

3.3.1. Independent Passive Mechanical Behavior of EOM and EOT Compartments

These results for the independent passive compartment behavior have been published in *Investigative Ophthalmology & Visual Science*.[46]

Transverse Compartment Coupling. The degree of mechanical coupling between the transverse compartments of 15 EOM specimens was tested at 5, 20, and 100 mm/sec loading rates to fixed extensions not exceeding 5 mm. Representative specimen photographs and time series data are illustrated in Fig 3.8. In the time series data, positive values indicate tensile force, and negatives values indicate relative compressive force. Force coupling to the stationary channel reduces its tensile force, thus appearing as relative compressive force. These experiments were performed for samples of all rectus and both oblique EOMs, all of which exhibited <10% CF under all testing conditions, and so reflecting a high degree of compartmental independence during tensile loading. For five specimens elongated to 3 mm at each loading rate, mean CF values for equal-sized compartments were 5.6 ± 0.3 %, 4.9 ± 0.1 %, and 4.1±0.1 %, respectively (Table 3.1). These findings indicate that CF varied inversely with loading rate, because of differences in the behavior of F_m and F_s. As loading rate increased, F_m increased (111.9, 133.1, and 142.4 gf respectively), but numerator F_s remained almost constant (6.3, 6.5, and 5.8 gf respectively), so their ratio decreased.

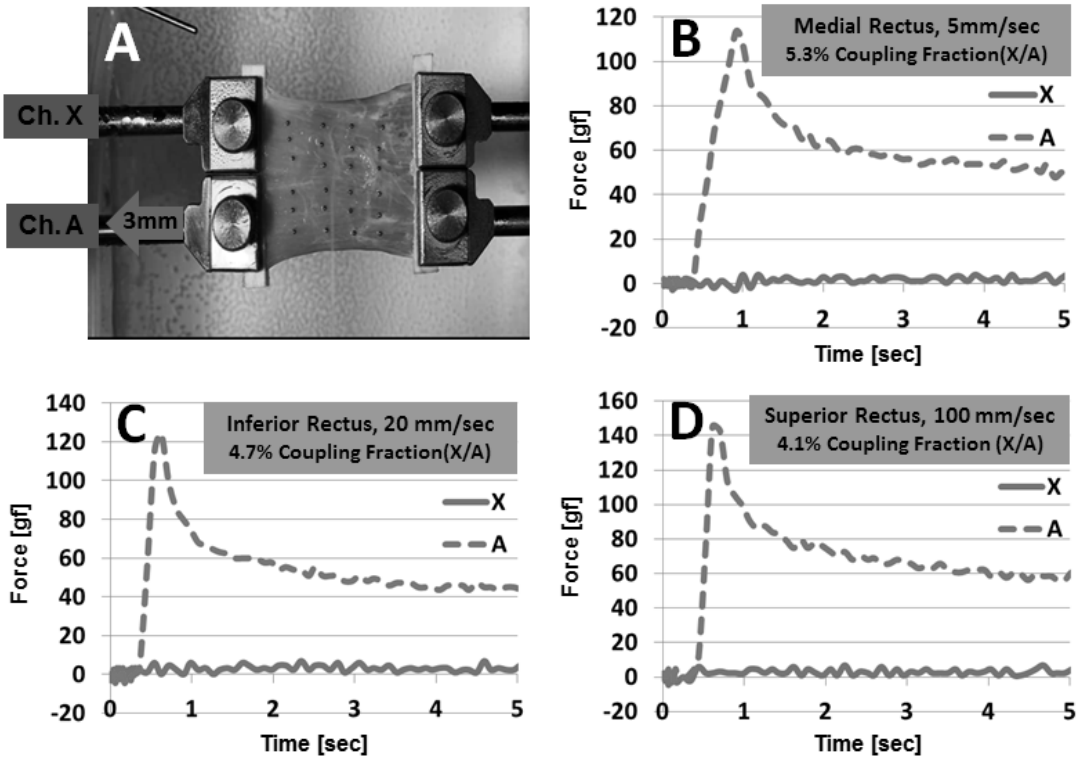

Fig. 3.8. Examples of transverse compartment testing of three rectus EOMs.[46] A. *En face* view of one rectus EOM specimen with metal bead fiducials lying on the global surface. Specimen appears broad relative to its length because the terminal tendon was excised and because 5 mm at each end was incorporated within the clamps. Channel A was elongated to 3 mm to the left, while channel X was stationary. Graphs plot forces in each layer at 5 (medial rectus, panel B.), 20 (inferior rectus, panel C), and 100 mm/sec (superior rectus, panel D) loading rates.

Local displacement information was also obtained from shifts of a rectilinear array with unloaded spacing of 6 mm between columns and 3 mm between rows of metal bead fiducials placed on the global surface of each EOM (Fig. 3.8). Locations of metal bead locations before and after tensile elongation were measured optically. Local displacements of each bead were computed as the two-dimensional differences between positions before and after elongation. Displacements of each fiducial distributed throughout the EOM were calculated for mapping the

displacement field. Fig. 3.9 illustrates an example displacement field obtained at the 5 mm/sec loading rate. Five specimens were tested and displacements were averaged in the x and y directions. The specimen at the fixed clamp necessarily has zero displacement, and the elongated end of the specimen at the moving clamp has the greatest displacement equal to that imposed by the load cell actuator. Therefore, displacement data in the first column near the moving clamps, which incorporates accumulated local displacements in the EOM, were used to determine average DR values in each compartment. Mean DR values were 5.4 ± 0.1 %, 5.4 ± 0.1 %, and 5.3 ± 0.1 % at the three loading rates, respectively (Table 3.1). As may be seen from Table 3.1, DR was about 5 %, independent of loading rate.

	5mm/sec	**20mm/sec**	**100mm/sec**
Coupling Fraction (CF)	5.6 ± 0.3 %	4.9 ± 0.1 %	4.1 ± 0.1 %
F_s / F_m	6.3 gf / 111.9 gf	6.5 gf / 133.1 gf	5.8 gf / 142.4 gf
Displacement Ratio (DR)	5.4 ± 0.1 %	5.4 ± 0.1 %	5.3 ± 0.1 %

Table 3.1. Transverse compartment coupling in EOMs at three loading rates.[46] Five specimens were tested at each loading rate (mean ± SD). F_s - maximum force in stationary compartment. F_s - maximum force in moving compartment.

From displacement fields (Fig. 3.9), local displacement can be analyzed in two-dimensions of linear position for each fiducial before and after loading. In each compartment, all local displacements in same column of fiducials were averaged, and compared along the EOM length for columns initially spaced 6 mm apart (Fig. 3.9). Since displacements in Fig. 3.9 are cumulative displacements summed from the right to the left columns, local displacements can be

calculated by subtraction between nearby column displacements. Local displacements for the moving compartment during five experiments averaged 792 ± 83 (SD), 522 ± 143, 521 ± 147, and 509 ± 87 μm, respectively, from first to fourth column. A similar computation was performed for the stationary compartment, resulting in 51 ± 98, 32 ± 64, 28 ± 34, and 14 ± 9 μm local displacements, respectively. The high SD values for the stationary compartment are caused by the shear force transfer described in the next paragraph. For both compartments, local displacement increased with distance from the fixed (origin) to the elongated specimen end (insertional tendon); of course as a boundary condition, there could have been no displacement at the fixed end clamp. The DRs from the first to fourth column were 5.4 ± 0.1 %, 4.8 ± 0.1 %, 4.2 ± 0.1 %, and 2.9 ± 0.1 %, respectively, indicating that the DR decreased from tendon end to origin.

In the displacement field for the stationary compartment, the fiducials mainly moved in the row closest to the boundary between compartments. Displacements of each row in the first column were 43 ± 11, 99 ± 12, and 235 ± 19 μm from top to bottom, respectively. This variation reflected shear force transfer. When the moving compartment elongated, shear force was generated at the boundary with the stationary compartment that is represented by the bottom row of fiducials. Since shear force declined with distance from the boundary, displacement declined accordingly.

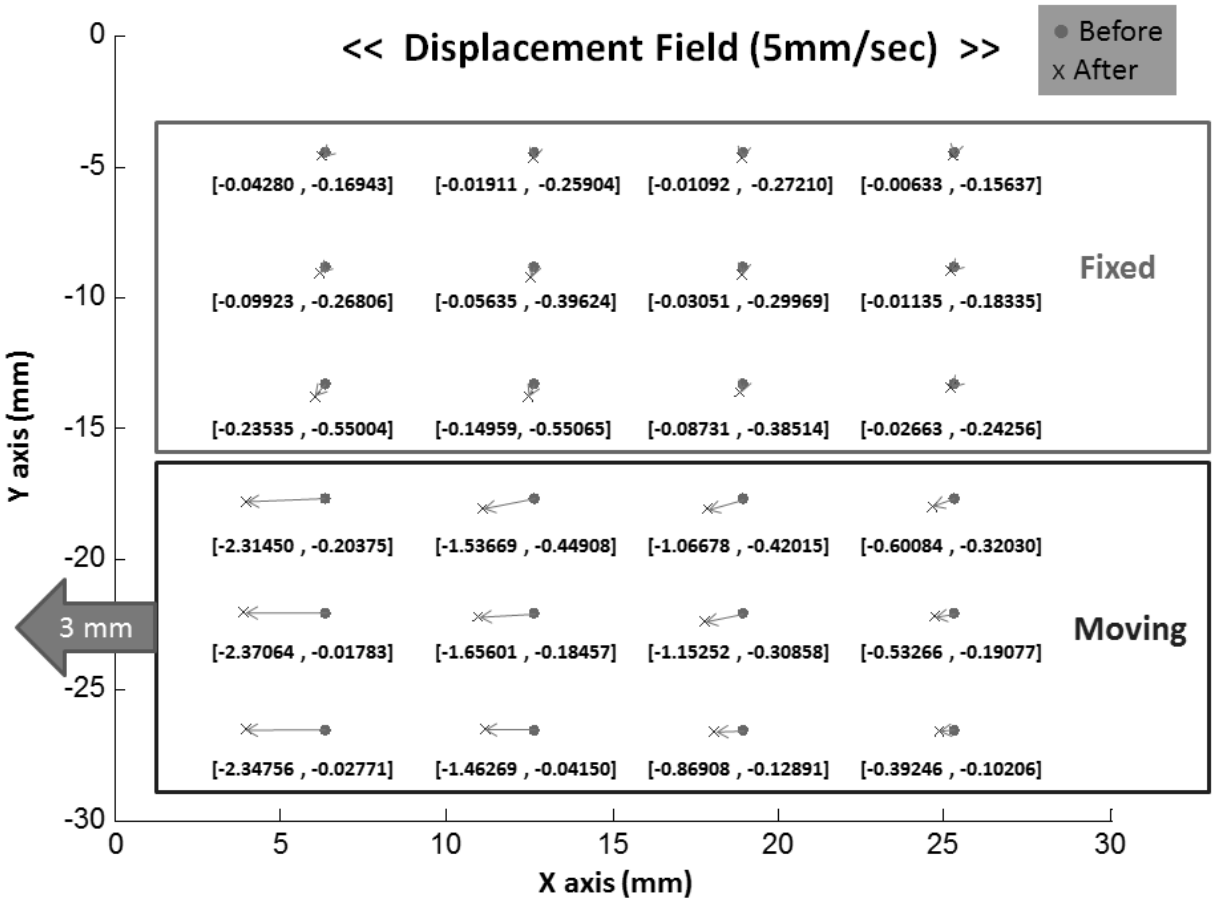

Fig. 3.9. Displacement field of 6 x 3 mm fiducial array for tensile elongations of bovine EOMs at 5 mm/s.[46] Five displacement results were averaged and visualized on the x-y plane.

Transverse Compartment Coupling in Six EOMs. Yoo et al.[47] have reported that the viscoelastic characteristics of all six bovine anatomical EOMs are similar, so it was of interest to compare compartmental coupling behavior among the anatomical EOMs. Three specimens of each anatomical EOM were subjected to 100 mm/sec tensile elongations using the foregoing experimental protocol. The observed CF values did not differ significantly among the six anatomical EOMs (Table 3.2, $P > 0.03$).

EOM	LR	MR	IR	SR	IO	SO
Transverse CF	4.1 ± 0.1 %	4.2 ± 0.1 %	4.5 ± 0.2 %	4.1 ± 0.1 %	4.5 ± 0.3 %	4.3 ± 0.2 %

Table 3.2. Mean (±SD) tensile force coupling from equal-sized elongating to stationary transverse compartments of each anatomical EOM.[46] Three specimens each were tested at 100 mm/sec loading rate. None of the differences was statistically significant (P > 0.03).

Coupling Between Transverse Compartments of Unequal Proportions. Since the transverse proportion of horizontal rectus EOMs that is exclusively innervated by a single motor nerve division averages 50:50,[9] it was reasonable to have conducted the foregoing experiments with equal sized elongating and stationary compartments. However, since the anatomical proportions observed among individual EOM specimens range from 40:60 to 60:40, the mechanical effects of unequal sized compartments were investigated. Transverse compartment coupling experiments were performed in which the moving compartment constituted 60% (60:40 ratio) and 80% (80:20 ratio) of transverse EOM width. Four different EOM specimens were elongated at 100 mm/sec for each of the two ratios, yielding CF values of 3.7 ± 0.2 %, and 3.0 ± 0.5 %.

GL/OL Compartment Coupling. Experiments evaluating mechanical coupling between the GL and OL were performed similarly to experiments for the transverse compartments, except for use of orthogonal specimen clamping in the x-z plane. Since the GL and OL each exist across the entire transverse width of rectus EOMs, the width of the clamp was approximately double that for transverse compartment experiments, and forces generated were higher. Fig. 3.10 illustrates GL/OL specimen placement and resulting force time series data. Twenty EOM specimens were tested at 5 and 100 mm/sec loading rates. For GL elongations, mean CF values

were 5.6 ± 0.4 % and 4.9 ± 0.1 %, respectively, while for OL elongations the mean CF values were 5.4 ± 0.4 % and 4.5 ± 0.4 % (Table 3.3). In each case, CF varied inversely to loading rate.

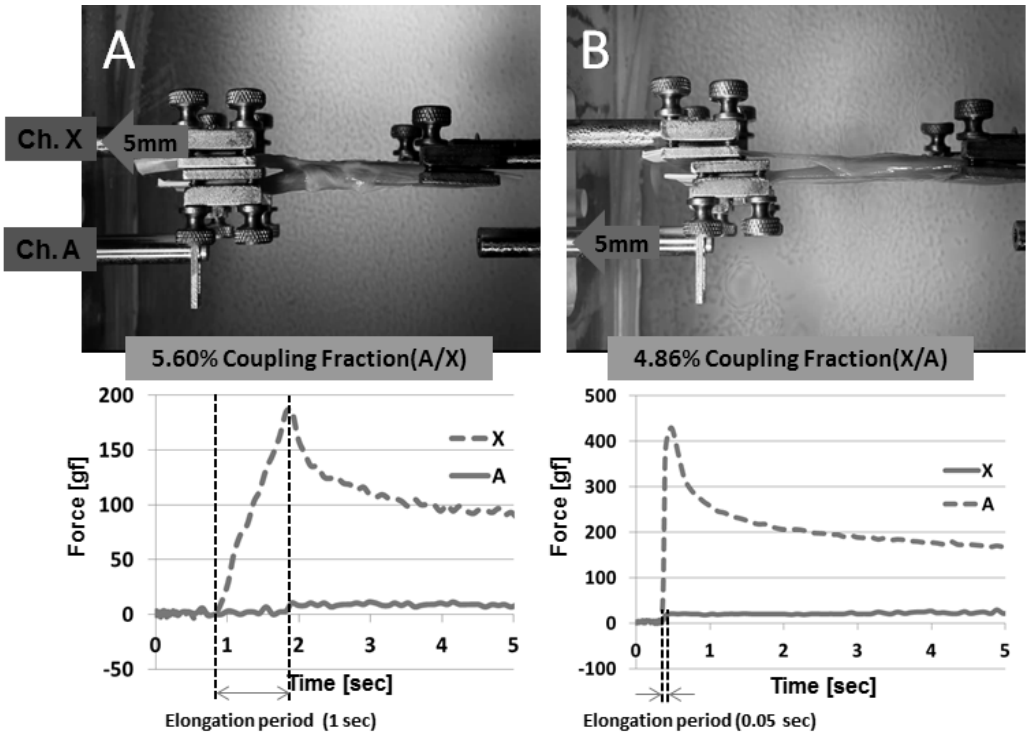

Fig. 3.10. Examples of GL/OL compartment loading of two rectus EOMs.[46] A. OL extension in lateral rectus, 5 mm/sec B. GL extension in medial rectus, 100 mm/sec.

Rate		5 mm/sec	100 mm/sec
Coupling Fraction (CF)	**OL Loading**	5.4 ± 0.4 %	4.5 ± 0.4 %
	GL Loading	5.6 ± 0.4 %	4.9 ± 0.1 %

Table 3.3. Mean coupling fraction (± SD) between GL/OL compartments during tensile loading.[46] Five specimens were tested at each loading rate.

Tendon Compartment Coupling. Considering that all human rectus and the SO EOMs insert on the globe via a tendon, mechanical coupling within tendon compartments was also investigated. For tendon compartment experiments, tendon from bovine horizontal rectus EOMs was sharply separated from the EOM bellies and subjected to the same experimental procedures as for transverse EOM compartments. Since tendon is stiffer than EOM, imposed elongations were smaller to avoid excessive tensile forces and specimen rupture. Five elongations of 0.2 or 0.3 mm at 5 mm/sec demonstrated an average CF of 3.3 ± 0.2 %, a slightly lower CF than for EOM belly.

Rubber Control Experiments. Since EOM is a highly orthotropic and flexible material, an isotropic and elastic rubber material (latex) was chosen as a control for the CF experiments. It was anticipated that the behavior of latex would differ substantially from that of EOM or tendon, because it was hypothesized that the independent mechanical behavior of the biological materials is related to their inhomogeneous internal structure. Samples with dimensions of 40 x 40 x 1.5 mm were prepared, with 1 mm elongation applied in the moving channel. The remaining experimental procedures were identical to those for EOM specimens. For rubber, mean CF values were 62.6 ± 1.6 %, 55.0 ± 0.7 %, and 50.0 ± 2.1 %, respectively, at loading rates of 5, 20, and 100 mm/sec. As loading rate increased, CF decreased, consistent with the findings from EOM transverse compartmental loading experiments.

Orthogonal Loading Control Experiments. It was hypothesized that independence between longitudinal transverse and GL/OL compartments is due to anisotropic orientation of EOM and tendon fibers whose long directions parallel the long axis of each of these tissues, with relatively little coupling due to connective tissues or fiber-to-fiber junctions between the roughly parallel fibers. Physiological loading is considered parallel to the lengths of the fibers. If that

interpretation were true, it was predicted that repetition of the CF experiments after 90° reorientation of the specimens to obtain non-physiological transverse loading would yield appreciably higher CF values than observed in the main experiment that employed longitudinal loading. Five specimens from lateral and inferior rectus EOMs were placed in the load cell so that their entire transverse widths, including both GL and OL, were incorporated into the adjacent fixed and moving sets of clamps. Since whole length of each EOM exceeds that of the clamp, excess EOM length was sharply excised. In each case, the posterior EOM was elongated by 3 mm orthogonal to the EOM's long axis, while force was recorded for the same direction in the stationary anterior EOM portion. The average orthogonal CF was 18.0±3.4% (range 12.0–21.0%), significantly greater than recorded under any condition during physiological longitudinal elongation in the transverse compartment or GL/OL compartment experiments ($P < 0.002$).

Effect of Perimuscular Connective Tissues. To determine if removal of even the scant perimuscular connective tissues influences CF between compartments, control experiments were performed using specimens with all enveloping connective tissues intact. Five different specimens were clamped without removal of connective tissues, and subjected to procedures otherwise identical to the original transverse compartment experiments. Average CF was 5.9±0.6%, which is similar to the result after removal of opaque enveloping connective tissue sheaths ($P > 0.3$), and confirming that the removal of this tissue did not influence the experimental results.

3.3.2. Independent Active Contraction of EOM Compartments

Transverse Compartment Coupling. The degree of mechanical coupling of actively-generated, internal force between the transverse compartments of five specimens was tested by active contraction using 50 mM $CaCl_2$. Representative specimen photographs and time series data are illustrated in Fig. 3.11. Since the strain gauge and specimen were aligned vertically in series, positive values indicate contraction force, and negatives values indicate relative relaxation force in the time series data. Force coupling to the stationary channel was appeared as relative compressive force. Because of the eventual permeation of ionic solution between compartments, force data in early 30 seconds were used to calculate the CF value. For calculating the degree of compartmental independence, the ratio of linear slope of each compartmental force was calculated having the same physical meaning as CF. All experiment data exhibited < 10% CF, reflecting a high degree of compartmental independence during active contraction that has the same tendency as passive tensile compartment testing. For five specimens, mean CF value was 6.03 ± 1.53 %.

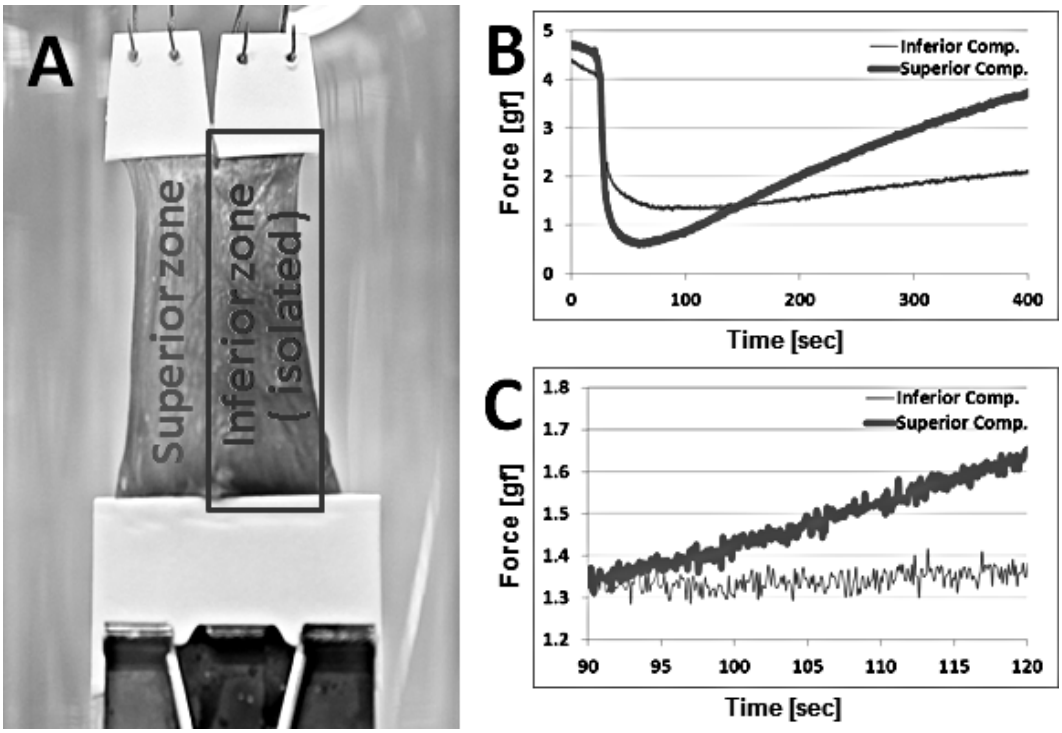

Fig. 3.11. Transverse compartment testing of bovine LR muscle. A. *En face* view of LR specimen with isolated inferior compartment using water repellent. B. Force transition of each compartment for five minutes. Initial force drop represents buoyancy effect of immersion in the aqueous solution. C. Early 30 seconds magnified view. Superior compartment force data have been shifted to align the ordinates for comparison.

GL/OL Compartment Coupling. GL and OL compartment active force coupling experiments were performed to evaluate the mechanical coupling between compartments similar to experiments for the transverse compartments. Throughout the passive tensile compartment testing, symmetry was shown, in that passive elongation of either the GL or OL compartment gives the same force coupling to the other compartment. Therefore, only GL compartment was activated using $CaCl_2$ solution since the OL has a much smaller and shorter portion of fibers than GL, and the superficially-located OL is easy to isolate with petrolatum coating. Fig. 3.12

illustrates GL/OL specimen placement and resulting force time series data. Five EOM specimens were tested for GL activation during OL isolation, and CF averaged 10.50 ± 3.28 %.

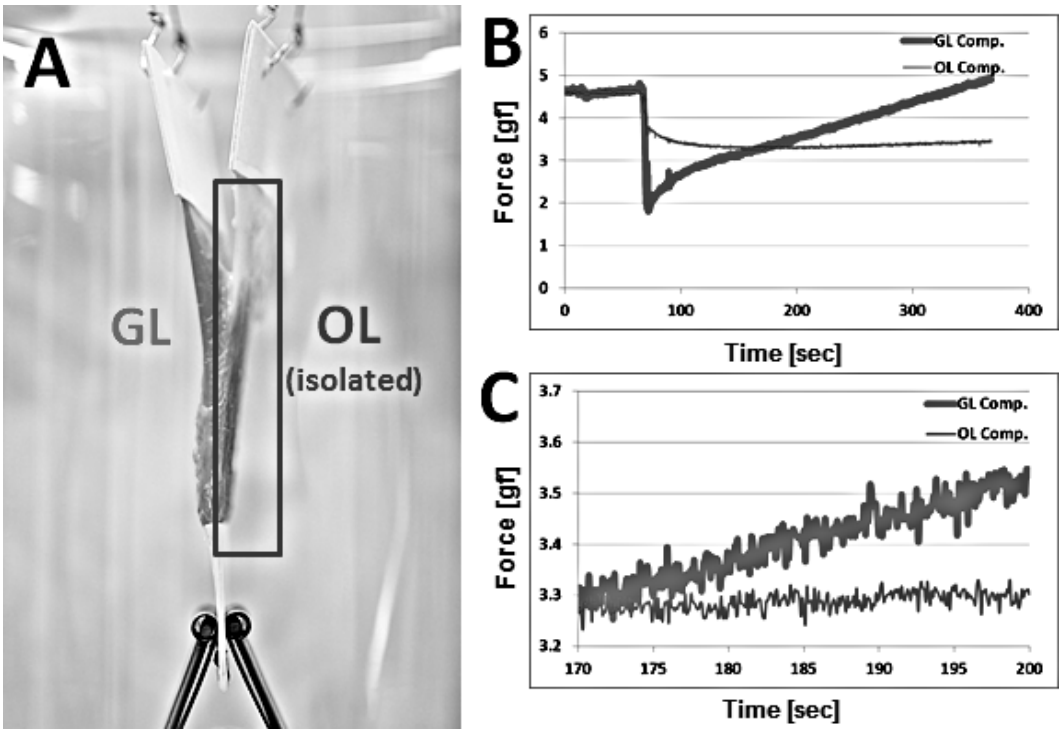

Fig. 3.12. GL/OL compartment testing of LR muscle. A. Front-back view of LR specimen with isolated orbital layer compartment using water repellent. B. Force transition of each compartment for five minutes. Initial force drop represents buoyancy effect. C. Early 30 seconds magnified view.

Control Active Contraction Experiments Without Compartment Isolation. Control experiments were performed in order to validate the active contraction using $CaCl_2$ solution, and effectiveness of the petrolatum isolation. For both transverse and GL/OL compartment experiments, whole EOM was immersed into 50 mM $CaCl_2$ solution without any petrolatum coating during dual channel force recording for five minutes. Fig. 3.13 shows resulting force in

transverse and GL/OL compartment specimens. In the transverse compartment experiment (Fig. 3.13A), both inferior and superior compartments showed similar contraction force behavior, suggesting that the calcium solution evenly penetrated into whole EOM and lead to contraction in the roughly equal sized compartments. However, for the case of GL/OL compartment experiment, data showed different magnitudes and temporal patterns of force in the GL and OL compartments. The anatomically larger GL compartment contracted to a higher force level than the smaller OL compartment.

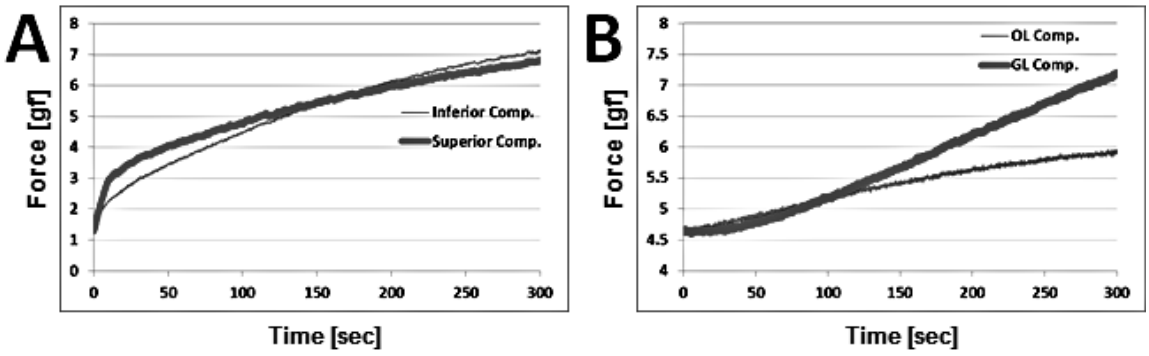

Fig. 3.13. Control experiment with simultaneous calcium activation of both transverse (A) and GL/OL (B) compartments. A. Transverse compartment force result of SR specimen. B. GL/OL compartment force result of IR specimen.

Totally independent compartmental behavior. In both passive tensile and active contraction experiments, the CF has been employed as an indicator of compartmental independence, and no CF value exceeded 10%. This implies considerable independence between transverse and GL/OL compartments. However, active contraction testing provides further evidence of compartment independence. Fig. 3.14 shows the contractile behaviors of each

compartment in transverse and GL/OL compartment experiments. In each figure, the arrow indicates the time interval between onset contraction in each compartment following conclusion of the buoyancy effect. During this period, tension in the two EOM compartments exhibited opposite trends: contraction in superior / GL compartments, but relaxation in inferior / OL compartments, implying totally opposite, independent compartmental mechanical behavior.

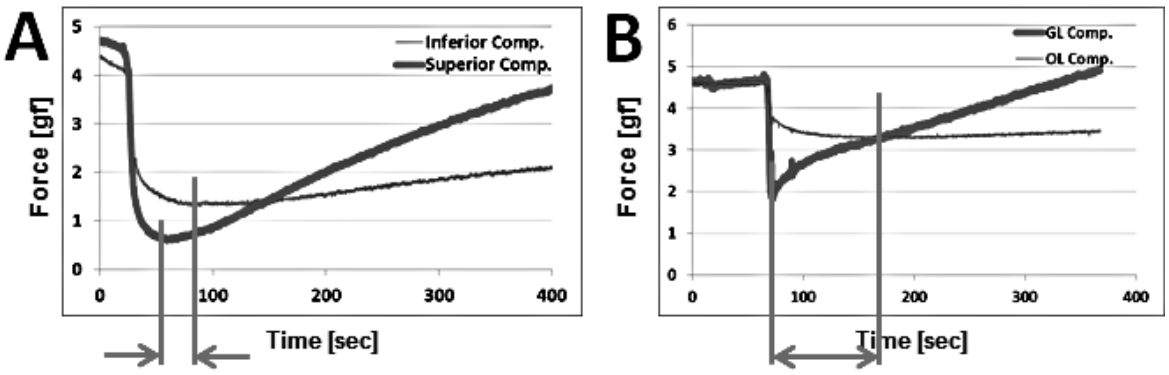

Fig. 3.14. Active contraction in transverse (A) and GL/OL (B) compartments. Initiation of a positive slope in the force curves indicates contraction onset. In each figure, the arrow indicates the time interval between asynchronous onsets of contraction in each compartment following conclusion of the buoyancy effect due to fluid immersion that reduced initial tensile force. A. Transverse compartment force with approximately 30 second time interval. B. GL/OL compartment force with time interval of about 100 seconds. During the interval, tension in each muscle compartment exhibited an opposite trend.

3.4. Discussion

These biomechanical experiments have demonstrated that adjacent but arbitrarily selected portions of EOMs and their tendons have a substantial degree of mechanical independence

during passive longitudinal loading: less than 10% (typically much less) of the longitudinal tension in any one compartment was transmitted to the complimentary compartment, whether during extension or contraction. This independence of tensile force in the physiologically generated, longitudinal direction was demonstrated between the OL and GL, as well as between transverse compartments of whole EOM and tendon ranging in ratio from 20:80, to 40:60 to 50:50 of transverse width. Compartmental independence was similar for all six anatomical EOMs. However, the same load cell apparatus demonstrated that this compartmentally independent, longitudinal mechanical behavior was quite different from the highly dependent behavior of an isotropic control material, latex rubber, implying that compartmental independence reflects the anisotropic structural properties of EOM and tendon. Further evidence that compartmental independence is related to tissue anisotropy is the finding that non-physiological, transverse loading of EOMs was associated with significantly less mechanical independence of adjacent regions.

Independence of longitudinal tensile force in transverse parsings of EOMs remained substantial and similar regardless of whether the transverse width of each EOM was arbitrarily divided into 50:50, 60:40, or 80:20 proportions. This suggests that any arbitrary groups of EOM fibers enjoy substantial mechanical independence from adjacent groups of fibers comprising the remainder of the EOM. It further implies that there is nothing special about mechanical intercoupling within adjacent groups of fibers that are mechanically tested together. While this biomechanical behavior was observed in all six anatomical EOMs, the biomechanical behavior only constitutes a condition necessary, but not itself sufficient, to permit physiologically independent compartmental function within an EOM. However, given the observed mechanical independence of these transverse grouping of EOM fibers, they could be coordinated into

physiologically integrated compartments by appropriate local innervation whose distribution is limited only to the transverse extent of each compartment. Such compartmental segregation of intramuscular innervation has been demonstrated for the horizontal rectus EOMs of humans, monkeys, and other mammals,[8, 9] but not in the vertical rectus EOMs. In other words, intramuscular motor nerve arborizations in the horizontal rectus EOMs do not cross transverse compartmental boundaries anywhere along the lengths of these EOMs, so the groups of EOM fibers separately innervated by the superior and inferior motor nerve trunks can constitute functionally independent superior and inferior muscle actuators whose tensions are delivered to separate insertions on the ocular sclera. Moreover, magnetic resonance imaging (MRI) has provided in-vivo evidence of selective contraction in the superior vs. inferior compartments of the human LR muscle during ocular counter-rolling, but not in the vertical rectus EOMs where intramuscular innervation is non-selective for compartments.[10, 48] There also is MRI evidence that selective compartmental function in the MR and to a lesser extent the LR may contribute to vertical duction in humans.[49] The markedly different electromyographic activity in the OL vs. the GL of the human MR is consistent with different function in these two layers.[50]

EOMs undergo both passive stretching and active contraction during agonist and antagonist action. In this study, passive stretching was replicated by micro-tensile setup while active contraction was induced by $CaCl_2$ solution setup. Highly independent contractile force in the transverse compartments, and OL/GL compartments, was demonstrated that is similar to that demonstrated for passive tensile loading. Since both tensile and contractile tests demonstrate similar results for the CF, observed CF values appear relevant to EOM force transfer transverse to the directions of active sarcomere action. However, the non-physiologic nature of $CaCl_2$ activation allows conclusions regarding slow, asymptotic active force coupling; presumably, the

similar findings for highly dynamic passive elongations would also be applicable to fast internal contractions under physiologic conditions.

It is notable that EOM compartments exhibit greater mechanical independence at higher, rather than lower, elongation velocities. As shown in Table 3.1, the relative intercompartmental coupling decreased as loading rate increased, while local strain, indicated by the displacement ratio, remained constant. This is primarily because maximum force in the moving compartment (F_m) increased with velocity due to viscous effects, while maximum displacement (D_m) was not altered by the loading speed. From Hook's law describing linear spring behavior, elastic force is proportional to displacement within the elastic limit. Consequently, EOM stiffness increased as loading rate increased, as is typical of any viscoelastic material. In addition, since there was minimal displacement in the fixed compartment, viscous effects were minimal there, so force changed little with loading rate. These findings further indicate that intercompartmental coupling is not appreciably mediated by viscous effects. Overall, this implies that compartmental independence between OL and GL is greater for fast eye movements such as saccades, than for steady fixations or slow movements such as pursuit. Furthermore, the current experiments demonstrated that portions of EOM tendon also exhibit substantial mechanical independence, permitting independent compartmental EOM contractile force to be transmitted independently to the globe.

Independence of tensile forces in EOM compartments was confirmed by observation of local displacement fields, for which there was also only about 5% coupling from the elongated to the stationary compartments. Modest variation in GL displacement fields along EOM lengths was probably caused by variation in EOM thickness. Since fusiform shaped, whole EOM was used for experiments, EOM thickness from anterior (tendon end) to posterior (origin end)

increased. Therefore, local displacements tended to be large in the thinner part, and smaller in the thick part. The displacement fields also showed shift transverse to the elongation. This may have reflected both the mechanical coupling between longitudinal and transverse strain inherent in any material, as recognized in the classic Poisson ratio, but may also have reflected a contribution from EOM anatomy. In addition to connective within the EOM, tissue sheaths envelope the outside of each EOM so as to couple the two compartments transversely. When the moving compartment was elongated, it also underwent transverse strain that was partially coupled to the stationary compartment via the particular configuration of the transverse connective tissue sheaths. This effect was probably small, but would exaggerate the apparent CF, such that EOM compartments are probably more independent longitudinally than CF measurements would indicate.

At least some degree of mechanical independence between OL and GL is required by the active pulley hypothesis (APH), which postulates that the OL translates pulley connective tissues to influence EOM pulling direction, and the GL generates oculorotary tension to rotate the globe in the corresponding direction.[12-15] The present findings easily fulfill requirements of the APH, and consistent with observations of marked structural, electrophysiological, hemodynamic, metabolic, and gene expression differences between OL and GL.[11-15]

The roughly parallel structure of EOM and tendon fibers probably is the dominant reason for the mechanical independence in compartments of EOM. Within EOM, fibers are arranged into fascicles of long, roughly parallel fibers. Anatomical studies have not been unanimous concerning the relative lengths of the fibers, or the configuration of their interconnections. In human and monkey, these fascicles extend most of the length of each rectus EOM, and exhibit few fiber-to-fiber junctions or fiber bifurcations when examined in serial sections stained by

Masson trichrome.[17, 18] While there have been reports of more myo-myous junctions in such as cat,[19] rabbit,[21] and squirrel monkey,[51] their biomechanical importance has not been demonstrated directly, and may be consistent with the low CF observed in the current study. Even if some anatomical couplings do occur among EOM fibers, the well-known compartmental specialization of numerous skeletal muscles demonstrates that partial couplings do not preclude substantially independent physiological actions. For example, gastrocnemius,[1] trapezius,[2] transversus abdominis,[3] cricothyroid,[4] and triceps brachii muscles[5] are comprised of multiple neuromuscular compartments that are controlled by independent motor neuron pools. The much higher CF observed for transverse as compared with longitudinal EOM elongations clearly demonstrate that fiber orientation plays a major role in force coupling among adjacent EOM regions.

While inducing contraction using $CaCl_2$ on a small scale has been reported in several studies, macro scale contraction such as shortening the whole EOM has not been reported previously. In order to find the optimum ion and concentration, preliminary experiments were performed with various calcium concentrations from 5 to 100 mM. With 50 mM calcium solution, EOM contracted enough for active contraction compartment experiments. In comparison with passive tensile loading for compartment testing, more physiological contraction loading by active contraction is more sensitive to specimen condition because $CaCl_2$ triggers the physiological myosin-actin interaction. Therefore, EOM condition is one of the important factors to obtain reasonable experiment data. In this study, elapsed time for every experiment was kept within two hours including specimen transport and preparation time in order to minimize the rigor mortis effect, which is a stiffening of muscle, beginning after three to four hours, reaching maximum stiffness after 12 hours, and gradually dissipating from approximately 24 hours after death.[52]

The current findings of substantial mechanical independence of adjacent portions of EOM tendon have clinical correlations. Tenotomy of only a portion of the fibers in vertical rectus EOM tendons has long been practiced for the treatment of small angle vertical strabismus,[53-56] and more recently of the horizontal rectus tendons for treatment of A and V pattern horizontal strabismus.[57] The present biomechanical findings permit the inference that surgical division from the scleral insertion of a portion of the fibers of a rectus tendon would release the tension in those fibers, while maintaining nearly unchanged the tension in the fibers that remain attached to the sclera. This interpretation is consistent with the finding of a predictable relationship between the percentage of vertical rectus tenotomy and the degree of correction of vertical strabismus in humans.[58] Selective regional surgery on the broad SO tendon has long been practiced to selectively manipulate the vertical actions effected by the posterior tendon fibers, versus torsional actions effected by the anterior fibers.[59-64]

Taken together, the current findings indicate that EOM and tendon have sufficient biomechanical independence to support the proposed functional diversity of actions in distinct neuromuscular compartments of the horizontal rectus EOMs, and following regionally selective surgical manipulations in rectus and oblique EOT. Since biomechanical independence only affords the opportunity, and not the obligation, of physiological independence of groups of fibers within any given EOM, it remains to be determined the extent to which innervational control coordinates or distinguishes the contractile activity of EOM subparts during the physiological and pathological ocular motor repertoire.

3.5. References

1. English AW, Wolf SL, Segal RL. Compartmentalization of muscles and their motor nuclei: The partitioning hypothesis. *Phys. Ther.* 1993;73:857-867.

2. Holtermann A, Roeleveld K, Mork PJ, et al. Selective activation of neuromuscular compartments within the human trapezius muscle. *J Electromyogr Kinesiol.* 2009;19:896-902.

3. Urquhart DM, Hodges PW. Differential activity of regions of transversus abdominis during trunk rotation. *Eur Spine.* 2005;14:393-400.

4. Mu L, Sanders I. The human cricothyroid muscle: Three muscle bellies and their innervation patterns. *J Voice.* 2009;23:21-28.

5. Lucas-Osma AM, Collazos-Castro JE. Compartmentalization in the triceps brachii motoneuron nucleus and its relation to muscle architecture. *J Comp Neurol.* 2009;516:226-239.

6. Goldberg SJ, Wilson KE, Shall MS. Summation of extraocular motor unit tensions in the lateral rectus muscle of the cat. *Muscle Nerve.* 1997;20:1229-1235.

7. Goldberg SJ, Meredith MA, Shall MS. Extraocular motor unit and whole-muscle responses in the lateral rectus muscle of the squirrel monkey. *J. Neurosci.* 1998;18:10629-10639.

8. Peng M, Poukens V, da Silva Costa RM, Yoo L, Tychsen L, Demer JL. Compartmentalized innervation of primate lateral rectus muscle. *Invest Ophthalmol Vis Sci.* 2010;51:4612-4617.

9. Costa RMdS, Kung J, Poukens V, Yoo L, Tychsen L, Demer JL. Intramuscular innervation of primate extraocular muscles: Unique compartmentalization in horizontal recti. *Invest Ophthalmol Vis Sci.* 2011;52:2830-2836.

10. Clark RA, Demer JL. Differential lateral rectus compartmental contraction during ocular counter-rolling. *Invest Ophthalmol Vis Sci.* 2012;53:2887-2896.

11. Demer JL, Oh SY, Poukens V. Evidence for active control of rectus extraocular muscle pulleys. *Invest Ophthalmol Vis Sci.* 2000;41:1280-1290.

12. Demer JL. The orbital pulley system: A revolution in concepts of orbital anatomy. *Ann NY Acad Sci.* 2002;956:17-32.

13. Demer JL. Pivotal role of orbital connective tissues in binocular alignment and strabismus. The friedenwald lecture. *Invest Ophthalmol Vis Sci.* 2004;45:729-738.

14. Demer JL. Current concepts of mechanical and neural factors in ocular motility. *Curr Opin Neurol.* 2006;19:4-13.

15. Demer JL. Mechanics of the orbita. *Dev Ophthalmol.* 2007;40:132-157.

16. Martini FH, Timmons MJ, Tallitsch RB. Human anatomy (6th edition). *San Francisco: Benjamin Cummings; 2008.*

17. Lim KH, Poukens V, Demer JL. Fascicular specialization in human and monkey rectus muscles: Evidence for anatomic independence of global and orbital layers. *Invest Ophthalmol Vis Sci.* 2007;48:3089-3097.

18. Demer JL, Poukens V, Ying H, Shan X, Tian J, Zee DS. Effects of intracranial trochlear neurectomy on the structure of the primate superior oblique muscle. *Invest Ophthalmol Vis Sci.* 2010;51:3485-3493.

19. Mayr R, Gottschall J, Gruber H, Neuhuber W. Internal structure of cat extraocular muscle. *Anat. Embryol.* 1975;148:25-34.

20. Davidowitz J, Philips G, Breinin GM. Organization of the orbital surface layer in rabbit superior rectus. *Invest Ophthalmol Vis Sci.* 1977;16:711-729.

21. McLoon LK, Rios L, Wirtschafter JD. Complex three-dimensional patterns of myosin isoform expression: Differences between and within specific extraocular muscles. *Journal of Muscle Research and Cell Motility* 1999;20:771-783.

22. Harrison AR, Anderson BC, Thompson LV, McLoon LK. Myofiber length and three-dimensional localization of nmjs in normal and botulinum toxin–treated adult extraocular muscles. *Invest Ophthalmol Vis Sci.* 2007;48:3594-3601.

23. Tsai SW, Hahn HT. Introduction to composite materials. *Lancaster, Pa. : Technomic Publishing Company.* 1980.

24. Lekhnitskii SG. Theory of elasticity of an anisotropic elastic body. *San Francisco: Holden-Day; 1963.*

25. Vasiliev VV. Mechanics and analysis of composite materials. *Amsterdam ; New York : Elsevier; 2001*.

26. Liu JY. Effects of shear coupling on shear properties of wood. *Wood Fiber Sci.* 2000;32:458-465.

27. Whitney JM. Elastic moduli of unidirectional composites with anisotropic filaments. *J Compos Mater.* 1967;1:188-193.

28. Broutman LJ. Measurement of the fiber-polymer matrix interfacial strength. *Interfaces in Composites, ASTM STP 452.* 1969;27-41.

29. Takaku A, Arridge RC. The effect of interfacial radial and shear stress on fibre pull-out in composite materials. *J Phys D Appl Phys.* 1973;6:2038-2047.

30. Gray RJ. Analysis of the effect of embedded fibre length on fibre debonding and pull-out from an elastic matrix. *J Mater Sci.* 1984;19:861-870.

31. Kelly A, Tyson WR. Tensile properties of fibre-reinforced metals: Copper/tungsten and copper/molybdenum. *Journal of the Mechanics and Physics of Solids.* 1965;13:329-350.

32. Cox HL. The elasticity and strength of paper and other fibrous materials *Brit J Appl Phys.* 1952;3:72-79.

33. Amirbayat J, Hearle JWS. Properties of unit composites as determined by the properties of the interface. Part i: Mechanism of matrix-fibre load transfer. *Fibre Sci Technol.* 1969;2:123-141.

34. Mandell JF, Chen J-H, McGarry FJ. A microdebonding test for in-situ fiber-matrix bond and moisture effects. *Cambridge: Dept Mater Sci & Eng, MIT, 1980.*

35. Grande DH, Mandell JF, Hong KCC. Fibre-matrix bond strength studies of glass, ceramic, and metal matrix composites. *J Mater Sci.* 1988;23:311-328.

36. Netravali AN, Stone D, Ruoff S, Topoleski LTT. Continuous micro-indenter push-through technique for measuring interfacial shear strength of fiber composites. *Composites Science and Technology.* 1989;34:289-303.

37. Marsolais EB, Kobetic R. Implantation techniques and experience with percutaneous intramuscular electrodes in the lower extremities. *J Rehabil Res Dev.* 1986;23:1-8.

38. Crago PE, Peckham PH, Thrope GB. Modulation of muscle force by recruitment during intramuscular stimulation. *Biomedical Engineering, IEEE Transactions on.* 1980;BME-27:679-684.

39. Grandjean PA, Mortimer JT. Recruitment properties of monopolar and bipolar epimysial electrodes. *Ann Biomed Eng.* 1986;14:53-66.

40. McNeal DR, Bowman BR. Selective activation of muscles using peripheral nerve electrodes. *Medical and Biological Engineering and Computing.* 1985;23:249-253.

41. Veraart C, Grill WM, Mortimer JT. Selective control of muscle activation with a multipolar nerve cuff electrode. *IEEE Trans Biomed Eng* 1993;40:640-653.

42. Szent-Gyorgyi A. Chemistry of muscular contraction, 2nd edition. *Academic Press; New York; 1951*.

43. Filo RS, Borm DF, Ruegg JC. Glycerinated skeletal and smooth muscle: Calcium and magnesium dependence. *Science.* 147:1581-1583.

44. Hellam DC, Podolsky RJ. The relation between calcium concentration and isometric force in skinned frog muscle fibers. *Federation Prec.* 1966;25:466.

45. Porter JD, Karathanasis P. The development of extraocular muscle calcium homeostasis parallels visuomotor system maturation. *Biochem Biophys Res Commun* 1999;257:678-683.

46. Shin A, Yoo L, Chaudhuri Z, Demer JL. Independent passive mechanical behavior of bovine extraocular muscle compartments. *Invest Ophthalmol Vis Sci* 2012;53:8414-8423.

47. Yoo L, Kim H, Gupta V, Demer JL. Quasilinear viscoelastic behavior of bovine extraocular muscle tissue. *Invest Ophthalmol Vis Sci.* 2009;50:3721-3728.

48. Demer JL, Clark RA, da Silva Costa RM, Kung J, Yoo L. Expanding repertoire in the oculomotor periphery: Selective compartmental function in rectus extraocular muscles. *Ann N Y Acad Sci* 2011;1233:8-16.

49. Clark RA, Demer JL. Functional morphometry of horizontal rectus extraocular muscles during horizontal ocular duction. *Invest Ophthalmol Vis Sci.* 2012;53:7375-7379.

50. Collins CC. The human oculomotor control system. Basic mechanisms of ocular motility and their clinical implications. G. Lennerstrand and p. Bach-y-rita. *New York, Pergamon.* 1975:145-180.

51. Shall MS, Dimitrova DM, Goldberg SJ. Extraocular motor unit and whole-muscle contractile properties in the squirrel monkey. *Exp. Brain Res.* 2003;151:338-345.

52. Saladin KS. Anatomy & physiology: 6th edition. *McGraw-Hill; New York; 2010.*

53. Wright KW. Mini-tenotomy procedure to correct diplopia associated with small-angle strabismus. *Trans Am Ophthalmol Soc.* 2009;107:97-102.

54. Yim HB, Biglan AW, Cronin TH. Graded partial tenotomy of vertical rectus muscles for treatment of hypertropia. *Trans Am Ophthalmol Soc.* 2004;102:169-175; discussion 175-166.

55. Von GA. Beitrage zur lehre vorn schielen und den schiel operationen. *Arch Ophtalmol.* 1857;3:177-386.

56. Howe L. Partial tenotomy. In: Howe l, ed. The muscles of the eye. London/new york: Gp putnam's sons / the knickerbocker press. 1908:304-308.

57. van der Meulen-Schot HM, van der Meulen SB, Simonsz HJ. Caudal or cranial partial tenotomy of the horizontal rectus muscles in a and v pattern strabismus. *Br. J. Ophthalmol.* 2008;92:245-251.

58. Chaudhuri Z, Demer JL. Graded rectus tenotomy in small angle hypertropia due to sagging eye syndrome. *J AAPOS* 2013;17:e3.

59. Vempali VM, Lee JP. Results of superior oblique posterior tenotomy. *J. AAPOS.* 1998;2:147-150.

60. Gobin M. [posterior tenotomy of the superior oblique muscle in a-pattern squint]. *Bull Soc Belge Ophtalmol.* 1978;182:104-113.

61. Graf M, Krzizok T, Kaufmann H. [combined oblique muscle operation with transposition of the insertion in strabismus sursoadductorius]. *Klin Monbl Augenheilkd.* 1994;205(6):329-335.

62. Souza-Dias C, Uesugui C. Efficacy of different techniques of superior oblique weakening in the correction of the "a" anisotropia. *J Pediatr Ophthalmol Strabismus.* 1986;23(2):82-86.

63. Yagasaki T, Nomura H, Koura T, Sato M, Awaya S. Posterior tenotomy of the superior oblique at the scleral insertion for a-pattern deviations. *Jpn J Ophthalmol.* 1995;39(1):83-88.

64. Kushner BJ. Effect of ocular torsion on a and v patterns and apparent oblique muscle overaction. *Archives of Ophthalmology* 2010;128:712-718.

Chapter 4

Biomechanics of Z-tenotomy and Z-myotomy

4.1. Introduction

The SO muscle is the longest and thinnest of the six EOMs, and it has relatively broad insertion to the scleral attachment. One of the roles of the SO is infraduction (downward rotation), which is maximal when the eye is adducted (rotated towards the midline). Overdepression in adduction is associated with A-pattern strabismus (outward deviation of the eyes in downward gaze) that may be treated by SO weakening surgery. Several surgical technique have been advocated for lengthening and weakening of the SO, including recession,[1-3] tenectomy,[4, 5] tendon-lengthening using either a silicone tendon expander,[6-8] nonabsorbable suture,[9] or autologous fascia,[10] tenotomy,[11-14] and marginal Z-tenotomy.[15-18] A recent report advocated Z-tenotomy for treating mild to moderate A-pattern strabismus associated with overdepression in adduction.[19] This report claimed that 70-80% SO Z-tenotomy effectively collapses the A-pattern collapse and normalizes versions. However, the biomechanical effects of Z-tenotomy have heretofore been uncharacterized.

Z-tenotomy is performed by making overlapping incisions, spaced along the length of the EOT, from opposite sides of the tendon. For z-tenotomy exceeding 50%, no individual tendon fibers remain continuous along the length of the EOM across the two tenotomy incisions, implying that any post-operative force transmission by the tendon would be due to transverse

coupling between tendon fiber bundles. This is relevant to the previous chapter of independent mechanical behavior of EOM and EOT compartments, since transverse coupling might be analogous to inter-compartmental coupling. If fiber bundles are independent from other in the transverse direction, even 50% Z-tenotomy would reduce transmitted force maximally, because all fibers would be divided. In this light, it is puzzling that 70-80% Z-tenotomy of the SO is reportedly necessary to treat A-pattern strabismus associated with overdepression in adduction. Therefore, the mechanical effect of various doses Z-tenotomy of the SO tendon must be investigated.

Z-myotomy is done by the same technique as Z-tenotomy. The only difference is the application for EOMs in Z-myotomy, versus EOTs in Z-tenotomy. Lee et al. proposed that IO muscle Z-myotomy is an effective surgical procedure for treatment of "IO overaction."[20] Since geometry after either Z-tenotomy or Z-myotomy becomes complicated, cross sections of a specimen are not uniform along the longitudinal direction, simple stress-strain analysis would be difficult to investigate and interpret. However, if we can convert the geometry from an irregular pattern to a simple prism shape, systematic biomechanical characterization of Z-myotomy might be possible, especially for characterizing viscoelastic behavior of EOM tissue. Also, in Z-myotomy tensile tests, interaction between the intact and incised fiber bundles determines the shear coupling effect that is highly relevant to study of independent mechanical behavior of EOM compartments.

4.2. Method

Custom Micro-tensile Testing. A custom, horizontally mounted micro-tensile load cell was constructed using heavy aluminum and steel hardware, on a 12.5 mm thick aluminum foundation plate so that the structure did not deform measurably during tissue loading. A servo-controlled electromagnetic linear motor (Ibex Engineering, Newbury Park, CA) capable of high speed (controllable to 100 mm/s maximum) and 20 nm resolution was mounted in line with an S-shaped semiconductor strain gauge (FUTEK Advanced Sensor Technology, Irvine, CA) having 5 mN force resolution (equivalent to 1.962 gram force), providing precise control of both position and speed. The strain gauge was attached to a 127 mm long stainless steel tensile shaft that passed into a closed physiologic chamber through a frictionless air bearing that served as its mechanical support. Inside the physiologic chamber the tensile shaft was attached to a serrated stainless steel compression clamp to engage one end of the specimen under test. The other specimen end was similarly clamped to a tensile shaft fixed to the opposite end of the load cell. When the linear motor displaced the tensile shaft, the strain gauge indicated the corresponding force.

Specimens under test were enclosed in a physiologic chamber with transparent walls whose lower portion contained a water bath heated under feedback control to maintain 100% humidity and 37°C temperature in the overlying air, as measured by a thermocouple. A high resolution video camera with 50 mm macro lens (Canon EOS 5D Mark II, Japan) was mounted to photograph the specimen from above through a transparent cover that was coated with an anti-

condensation compound to inhibit fogging during photography of the specimen. Figure 1 illustrates the photograph of the load cell and components.

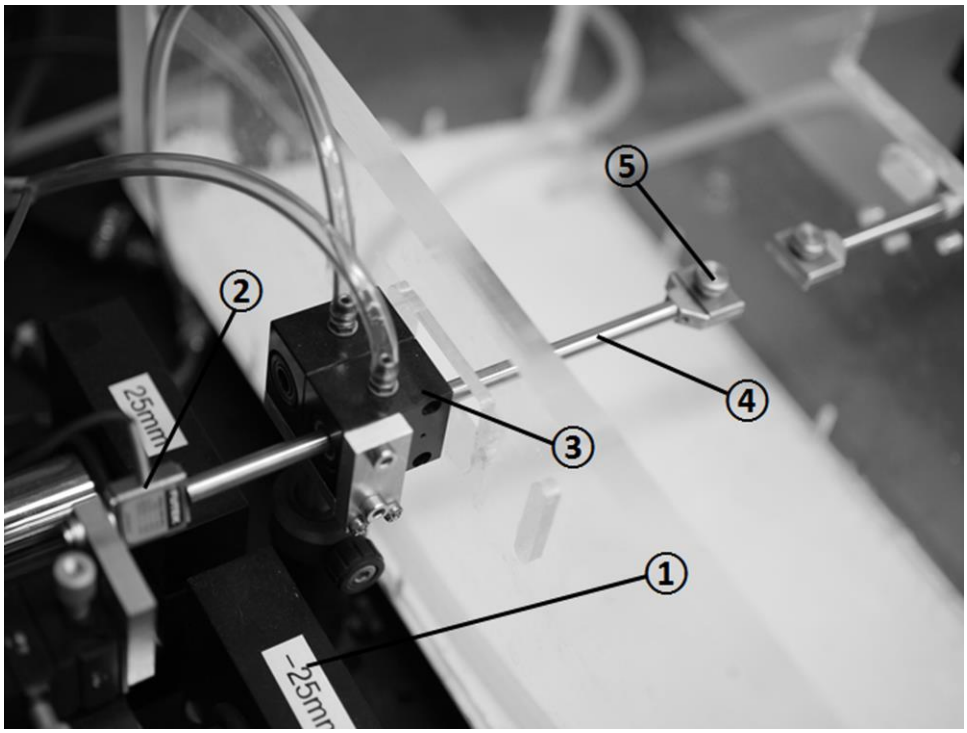

Fig. 4.1. Micro-tensile load cell.[21] Photograph of apparatus. A strain gauge (②) attached to the linear motor (①) was connected to the specimen clamp (⑤) through a tensile shaft (④) that was supported by a frictionless air bearing (③).

Wiechert Viscoelastic Model. Viscoelastic materials, ranging from polymers to biological tissues, can be modeled for describing their stress or strain interactions, and their temporal dependencies. There are two basic models for linear viscoelastic modeling: Maxwell and Voigt.[22] The Maxwell model uses a purely viscous damper and a purely elastic spring connected in series, so that it can predict relaxation very well, but not creep. On the contrary, the Voigt model consists of a Newtonian damper and Hookean elastic spring connected in parallel that can

describe creep accurately, but is poor for predicting relaxation. For the purpose of compensating limitations of each model, several models have been established by linear combination of springs and dashpots. Among them, the Wiechert model[23, 24] can have as many spring-dashpot elements as needed illustrated in Fig 4.2, so that the viscoelastic behavior of the material can be described satisfactorily. Also, the Wiechert model is an appropriate choice if a finite element analysis using ANSYS is to be performed for the material. In the case where the stress relaxation tests are conducted, the total stress σ(t) transmitted by the Wiechert constitutive model is given by[25]

$$\sigma(t) = \left[E_0 + \sum_{i=1}^{n} E_i \exp\left(-\frac{t}{\tau_1}\right)\right] \varepsilon_0 \qquad \text{Eq. 4.1}$$

where t is the time, E_i (i=0, 1, . . .) the relaxation modulus of the ith spring, τ_i (i=1, 2,. . .) the relaxation time of the ith dashpot, and ε_0 is the constant strain applied to the material during the stress relaxation test. Eq. 4.1 can be divided by ε_0 in both left and right terms, then the equation becomes

$$E_{rel}(t) = E_0 + \sum_{i=1}^{n} E_i \exp\left(-\frac{t}{\tau_i}\right) \qquad \text{Eq. 4. 2}$$

where E_{rel} is called as the time-dependent relaxation modulus.

A Wiechert model for a viscoelastic material is determined by seeking appropriate constants E_i (i=0, 1, . . ., n), and τ_i (i=1, 2,. . ., n) in the Prony series of Eq. 4. 2.

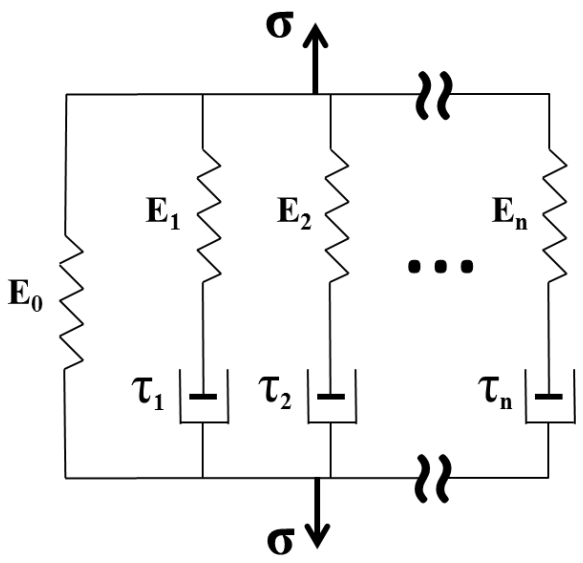

Fig. 4.2. Wiechert model diagram. The Wiechert model consists of as many spring-dashpot elements as needed. Thus, the viscoelastic behavior of the material can be described as precisely as required.

Specimen Preparation. Fresh heads of cows aged 20-30 months were obtained immediately after slaughter from a nearby abattoir (Manning Beef LLC, Pico Rivera, CA). Transport time from abattoir to laboratory was approximately one hour, and one hour additionally elapsed for dissection and preparation of specimens in the laboratory. After extraction, specimens were maintained in lactated Ringer's solution at 37° C. Dimensions of tendon specimen for Z-tenotomy were set at 20 x 10 mm. Since EOM thickness is not negligible, specimen thickness needs to be controlled, so that the muscle specimen for Z-myotomy was 20 x 10 x 2 mm. To minimize axial damage to EOT and EOM fibers, each specimen was initially reduced to 25 mm in length, by cutting the longer dimension parallel to fibers. This left 2.5 mm margin in length for clamping at each end.

Z-tenotomy with Control Material Isotropic Rubber. Isotropic latex rubber (abrasion-resistant natural latex rubber 1/16 inch thick, McMaster-Carr, Santa Fe Springs, CA) was used a control material. Specimens were prepared measuring 30 mm long, and 20 mm wide. Unlike tendon specimens, only 20% elongation was applied in latex tensile testing since this is well characterized, linearly elastic material, and force behavior is linear like a spring, so that maximum force transition for various Z-tenotomy ratios should correspond to failure force transition of EOM. Each of three specimens was tested for 5 different Z-tenotomy ratios from 0, 20, 40, 60, 80% specimen width at 1 mm/s loading rate.

Uniaxial Tensile Experiment with Z-tenotomy and Z-myotomy. Pre-loading was applied to EOT and EOM specimens to avoid slackness. Tensile testing was performed under the physiological conditions by subjecting specimens to increasing tension until failure. Before tensile loading, Z-tenotomy was performed by making two transverse incisions, each from opposite sides of the specimen, spaced 8 mm apart (Fig. 4.3A). In different specimens, Z-tenotomy was performed from each tendon margin at 0, 20, 40, 50, 60, and 80% tendon width. Fig. 4.3B illustrates 20% z-tenotomy.

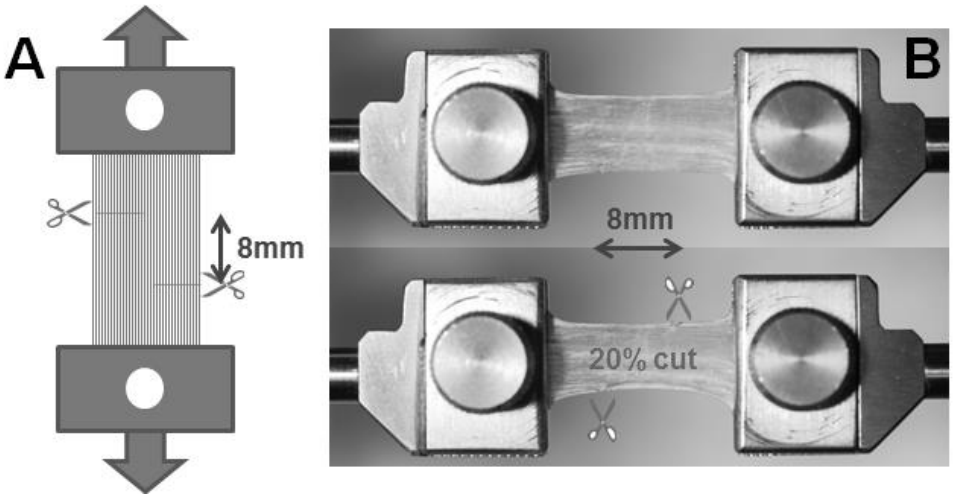

Fig. 4.3. Experimental approach to Z-tenotomy.[21] A. Schematic drawing of Z-tenotomy experiment. EOTs were clamped in both ends and pre-loading was applied for avoiding slackness. Then, specimen was incised from two opposite margins at pre-determined distances (20, 40, 50, 60, and 80% of total EOT width). The distance between two incisions was 8 mm. B. 20% A-tenotomy of SO tendon. After clamping the specimen (top), 20% of tendon width was incised from both margins with 8 mm longitudinal spacing between incisions (bottom).

The Z-myotomy tensile experiment protocol was the same as for the Z-tenotomy tensile experiment. Since all six EOMs exhibit similar time-dependent nature and elastic properties,[26] LR and SR EOMs, easy to extract, were prepared for Z-myotomy experiments. Before tensile loading, Z-myotomy was performed from each EOM margin at 0, 20, 40, 50, 60, and 80% width.

Z-myotomy Equivalence Tensile Testing. There is a geometric problem for performing mathematical modeling of viscoelastic mechanical behavior involving the irregular cross sectional areas produced by Z-tenotomy and Z-myotomy. Although there are analytic solutions for crack in fracture mechanics,[27] discontinuous cross section along the EOM or EOT specimen makes it difficult to formulate mathematical models for viscoelastic analysis that customarily

assume regular cross sectional area. By matching the failure force of irregular to regular cross section specimens, viscoelastic modeling of the former can be plausibly inferred from the latter.

Uniaxial tensile tests were performed with EOM specimens ranging from 1 to 10 mm wide, in 1 mm increments, having same length x thickness (20 x 2 mm) as Z-myotomy specimens. Then, the behavior of each Z-myotomy specimen from 20 to 80% was matched to a specimen with a continuous cross section. Fig. 4.4 illustrates the equivalence between Z-myotomy and non-Z-myotomy specimen.

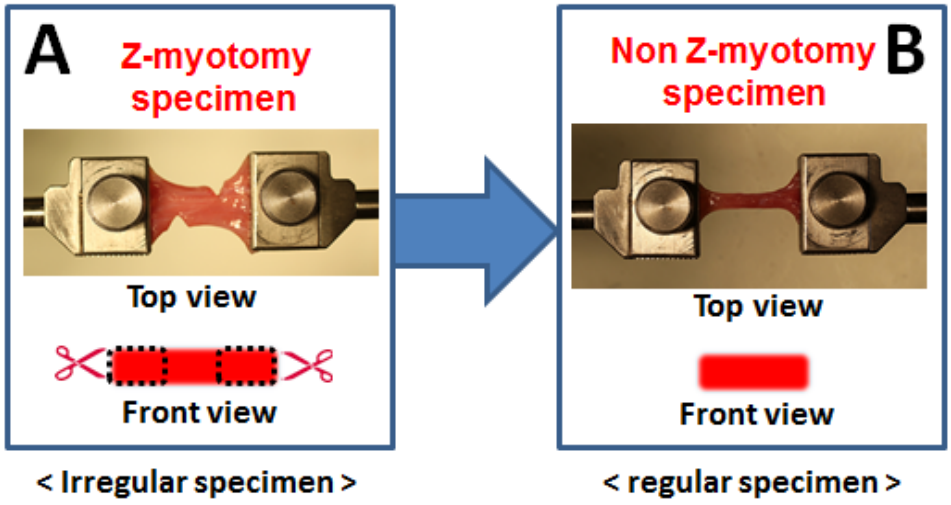

Fig. 4.4. Schematic illustration of equivalence. Z-myotomy specimens (A) have irregular cross sections along the specimen length, thus viscoelastic modeling cannot be performed. After matching the failure force of each Z-myotomy specimen to a non-Z-myotomy specimen (B), mathematical viscoelastic modeling can be executed.

Stress Relaxation Testing of EOM and Viscoelastic Modeling. Stress relaxation experiments were performed using the micro-tensile load cell with equivalent Z-myotomy EOM specimens. Each sample was elongated to 30% in deformation with the highest speed of 100 mm/sec. It then left for over 100 seconds while recording the force output. The Wiechert model was employed for viscoelastic characterization of each Z-myotomy equivalence specimen.

4.3. Result

Results for Z-tenotomy were published in *Journal of AAPOS*.[21]

Z-tenotomy with Control Material Isotropic Rubber. Isotropic latex rubber control tests were performed. Each of 3 bovine EOT specimens was elongated until 20% of initial length at 1 mm/sec loading. Representative specimen photographs and result data according to 5 different Z-tenotomy ratios are illustrated in Fig 4.5. As may be seen in Fig. 4.5A, the latex between incisions became distorted to slanted by path by shear force. There was a linear trend of decreasing maximum force with increasing percentage Z-tenotomy, as shown in Fig. 4.5B. This reflects the combined effect of tensile and shear forces. Theoretically, as tenotomy percentage increases, tensile force would be expected to decrease and reaches to zero at 50% Z-tenotomy, because of decreasing cross section area for tensile loading. However, this effect is offset by shear force that increases and peaks at 50% Z-tenotomy, before decreasing progressively for greater tenotomy. Consequently, the experimental data, reflecting the sum of tensile and shear forces, exhibited a linearly-decreasing, isotropic coupling effect. The graph in Fig. 4.5B extrapolates to nearly zero force at about 90% Z-tenotomy.

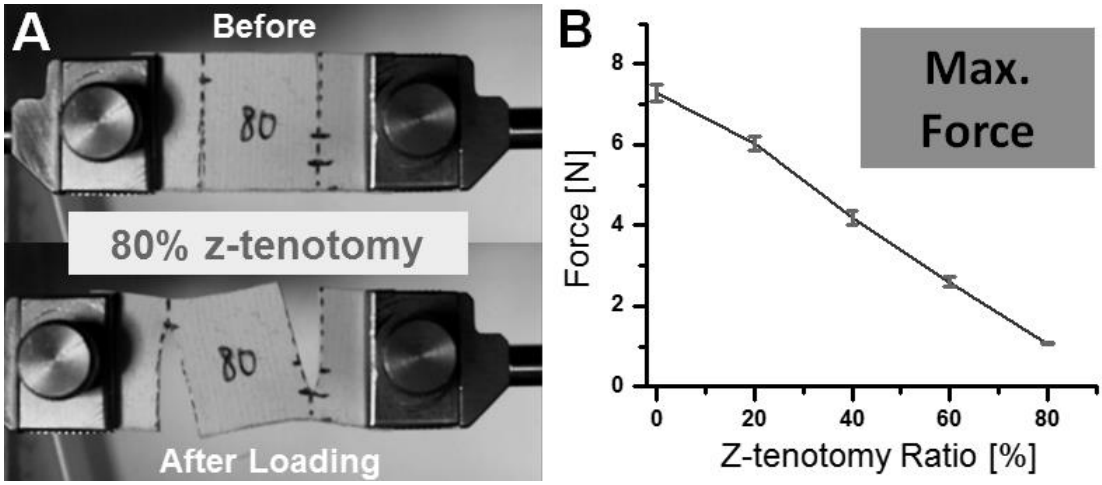

Fig. 4.5. Z-tenotomy of latex.[21] A. Photographs of 80% z-tenotomy tensile testing (before and after elongation). Middle part of specimen was distorted affected by the shear force caused by Z-tenotomy following tensile loading. B. Maximum force transition from 0 to 80% Z-tenotomy. Maximum force declined linearly with the Z-tenotomy ratio. Error bars indicate SD.

SO Z-tenotomy Tensile Testing. A total of 30 bovine SO tendon specimens were elongated until failure at 1 mm/s loading rate, including 6 different Z-tenotomy ratios. Representative specimen photographs before and after loading, and failure force data for each Z-tenotomy ratio are illustrated in Fig. 4.6 Tendon failure force exhibited two significant trends varying with the amount of Z-tenotomy (Fig. 4.6 D). For less than 50% SO Z-tenotomy, failure force declined with a parabolic shape, rather than linearly as observed for latex rubber. In more striking contrast, for more than 50% Z-tenotomy, SO force transmission was reduced to a roughly constant value of nearly zero (0.46, 0.42, and 0.42N at 50, 60, and 80% Z-tenotomy, respectively). Consequently, the SO tendon showed a parabolic response to increasing Z-tenotomy until 50%, but virtually no tensile force after 50% Z-tenotomy. Although tensile forces

in latex rubber were all measured at 20% elongation from initial length rather than at failure for the same range of Z-tenotomies as employed in tendons (Fig. 4.5 B), comparison between the linear trend in rubber and nonlinear pattern in EOT is valid since force transition in linear elastic rubber should be similar at any elongation point up to failure.

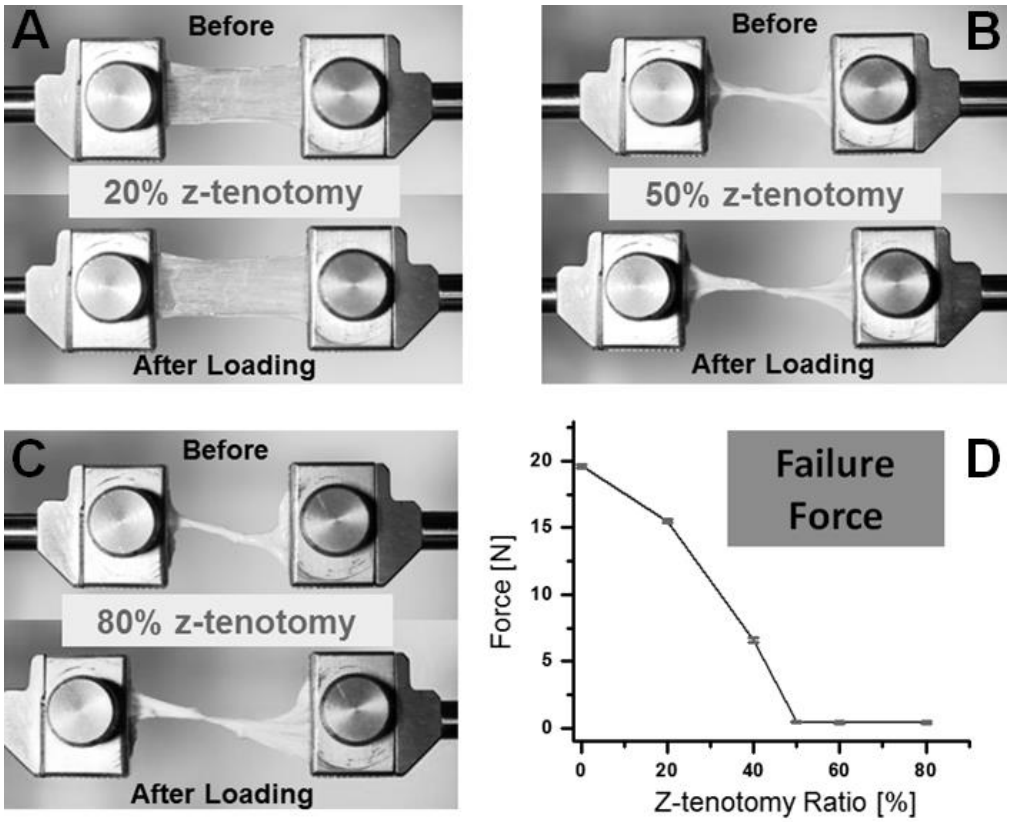

Fig. 4.6. Tensile testing after SO Z-tenotomy.[21] A. 20% Z-tenotomy (before and after elongation). B. 50% Z-tenotomy. C. 80% Z-tenotomy. D. Failure force transition from 0 to 80% Z-tenotomy. Error bars indicate SD.

Superior Rectus (SR) Z-tenotomy. Tensile testing of bovine SR tendons was performed identically to the method for SO tendons. Representative specimen photographs

before and after loading, and failure force are illustrated in Fig 4.7 As may be seen by comparing Fig. 4.6 D and 4.7 D, Z-tenotomy had similar effect for both the SO and SR tendons. In both cases, tensile testing to failure demonstrated progressively steep, nonlinear decline for less than 50% Z-tenotomy, and almost zero residual force for more than 50%.

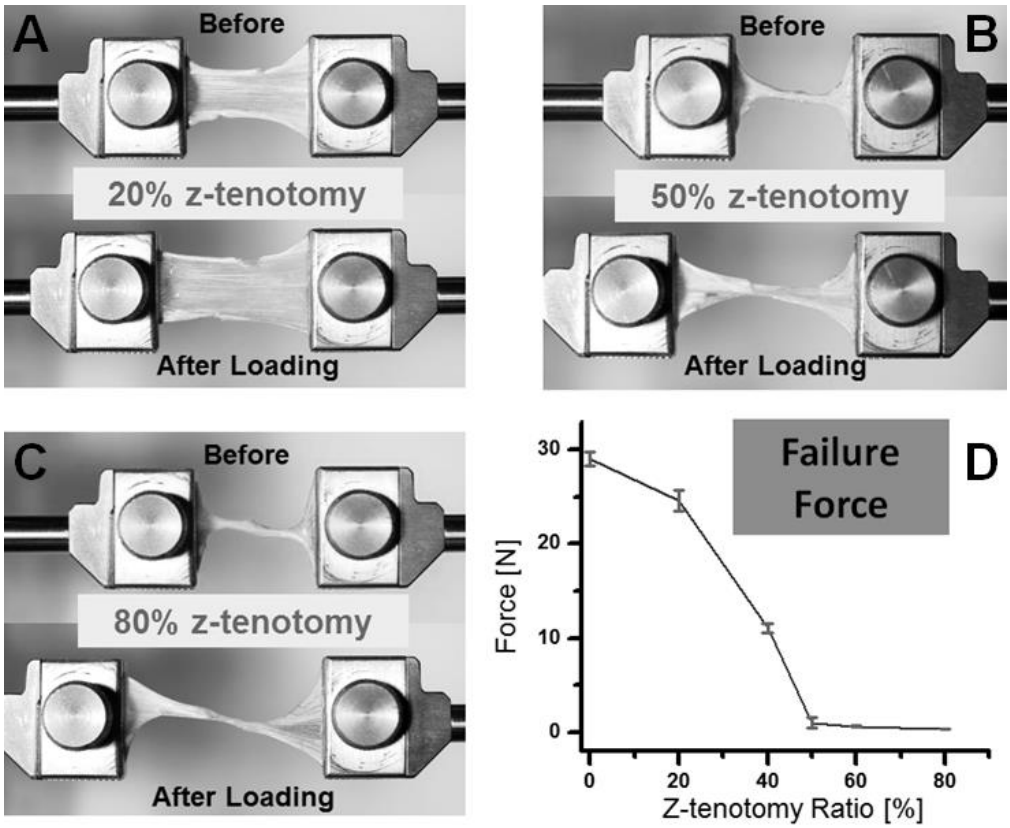

Fig. 4.7. Z-tenotomy of superior rectus tendon.[21] A. 20% Z-tenotomy before and after elongation. B. 50% Z-tenotomy before and after elongation. C. 80% Z-tenotomy before and after elongation. D. Failure force transition from 0 to 80% Z-tenotomy results. Failure force was reduced to near zero for 50% or greater Z-tenotomy. Error bars indicate SD.

Z-myotomy Tensile Testing. Tensile testing was carried out using bovine EOM specimens with Z-myotomy in the same procedure as Z-tenotomy tensile testing. Five specimens were tested for each Z-myotomy ratio from 0 to 80% incision. Thus, a total 30 specimens were elongated until failure at 1 mm/s loading rate. Muscle failure force exhibited similar trend as Z-tenotomy, but there was a slight difference. While the threshold incision ratio was 50% for Z-tenotomy, minimum failure force was reached at 60% for Z-myotomy (1.04, and 1.01N, at 60, and 80% Z-myotomy, respectively). Consequently, EOM showed a parabolic response to increasing Z-myotomy until 60%, but reached the minimum tensile force after 60% Z-myotomy. Fig 4.8 illustrates the failure force trend.

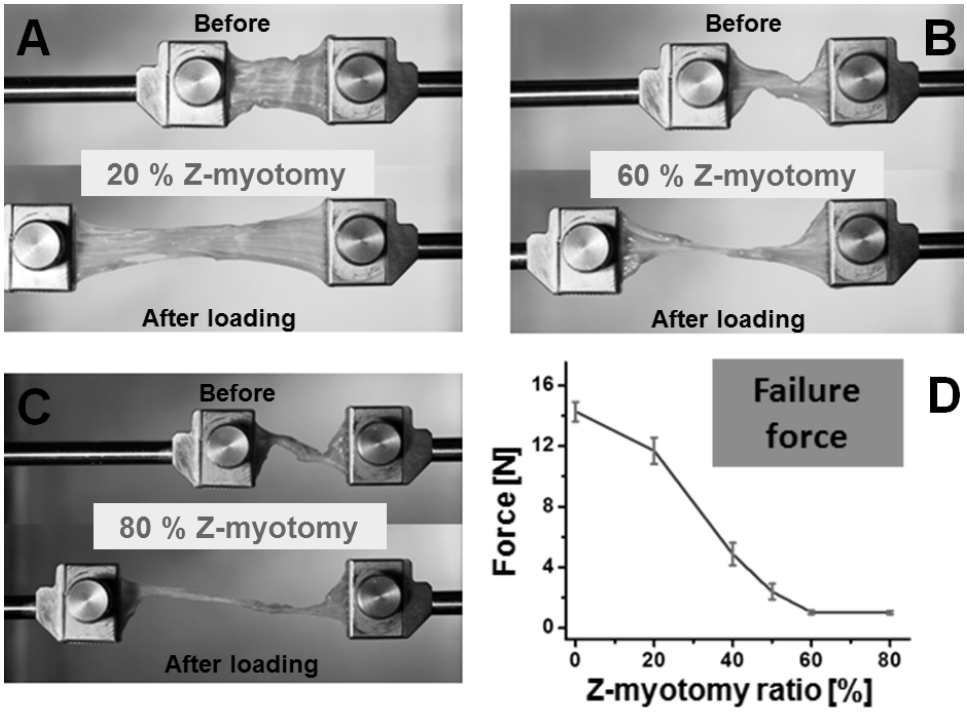

Fig. 4.8. Tensile testing after Z-myotomy. A. 20% Z-myotomy before and after elongation. B. 60% Z-myotomy. C. 80% Z-myotomy. D. Failure force transition from 0 to 80% Z-myotomy. Failure force was reduced to minimum for 60% or greater Z-tenotomy. Error bars indicate SD.

Z-myotomy Equivalence Tensile Testing. Z-myotomy equivalence tensile testing was examined for substitution from irregular to regular cross section specimens. In total, 30 specimens were tested. Three specimens were elongated until failure for each width from 1 to 10 mm with identical length and thickness. The failure force trend is illustrated in Fig 4.9.

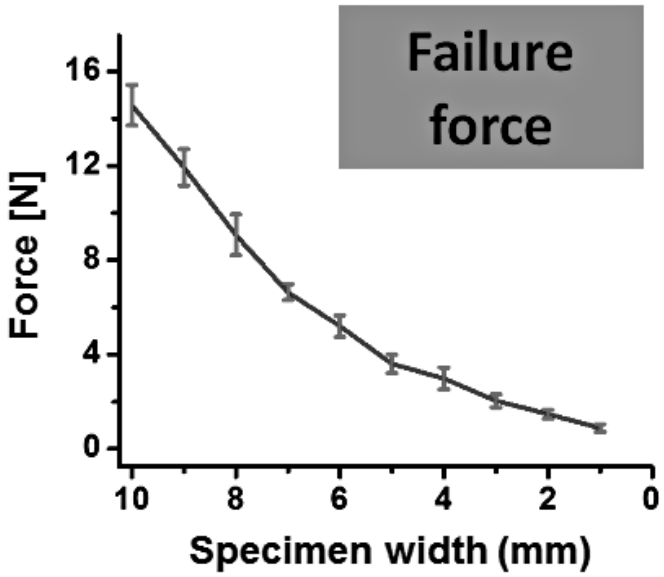

Fig. 4.9. Failure force of bovine EOM specimens of varying widths for comparison with Z-myotomy equivalence. Failure force transition of regular shaped EOM specimens of widths varying from 1 to 10 mm. Error bars indicate SD.

Linear interpolation of force values between widths was used to estimate intermediate values and matched to the force value observed for Z-myotomy specimens, meaning that irregular Z-myotomy specimens were replaced by regular, non-Z-myotomy EOM specimens suitable for viscoelastic characterization. Widths of non-Z-myotomy specimens having continuous cross

sections were calculated. Table 4.1 shows the equivalent widths for 5 different Z-myotomy ratios from 20 to 80 %.

Z-myotomy ratio	**20 %**	**40 %**	**50 %**	**60 %**	**80 %**
Equivalent width	8.9 mm	5.8 mm	3.4 mm	1.3 mm	1.2 mm

Table 4.1. Equivalent width for each Z-myotomy ratio. Failure force was matched between Z-myotomy and regular-shaped specimens, and resulting widths of non Z-myotomy specimens having continuous cross sections was calculated. Other dimensions of specimen were held constant at 20 mm in length, and 2 mm in thickness.

Stress Relaxation Testing of EOM and Viscoelastic Modeling. For stress relaxation testing in each equivalent width, three specimens were tested from 8.9 to 1.2 mm width; therefore, 15 specimens total were elongated to 30% of initial length. A similar relaxation trend was exhibited in both 1.3 and 1.2 mm wide, corresponding to the failure force data as 60 and 80 % Z-myotomy. Thus, experimental behavior of the 1.3 and 1.2 mm width specimens was regarded as the same. Fig. 4.10 illustrates averaged relaxation data of each equivalent width. Relaxation moduli at 30% strain were 1308, 1347, 1489, and 1625 kPa, corresponding to 8.9, 5.8, 3.4, and 1.3 and 1.2 mm widths, respectively.

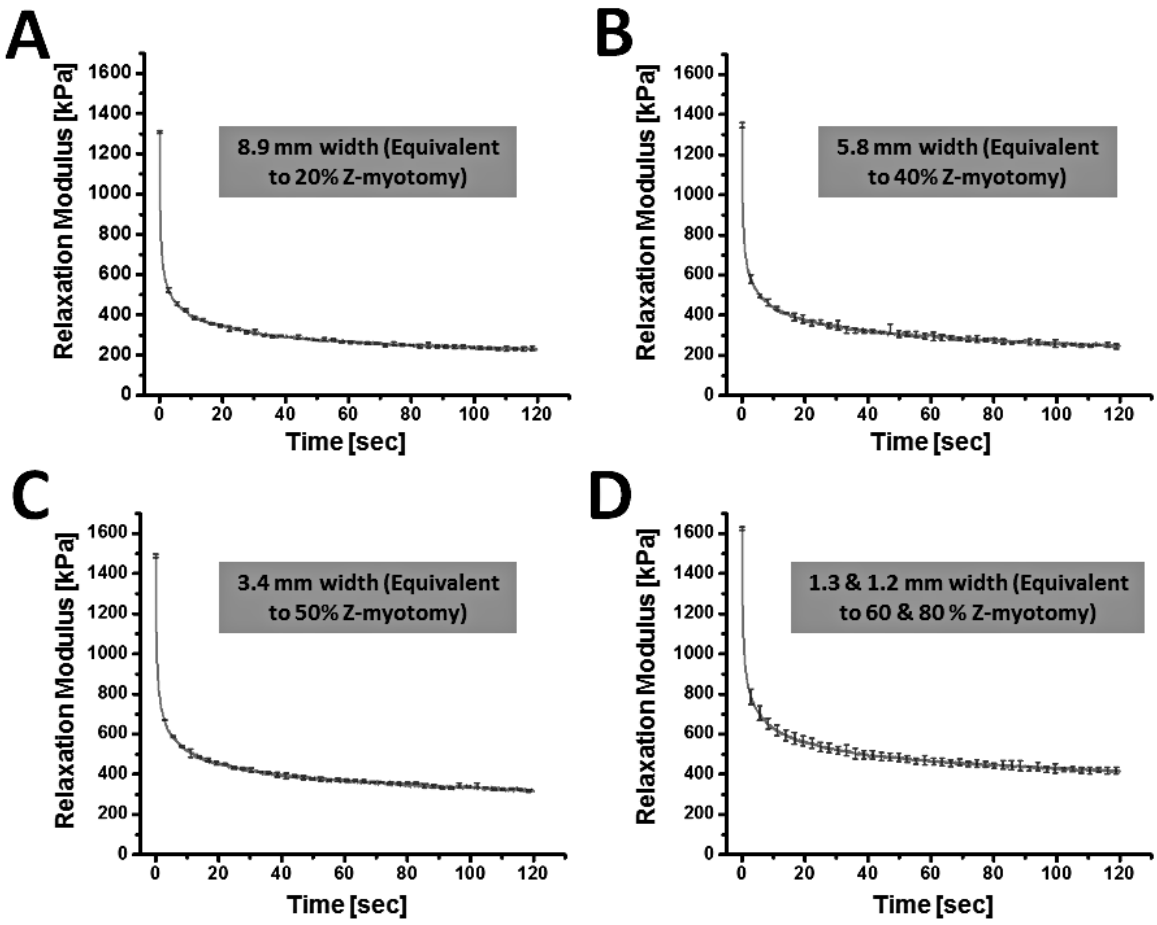

Fig. 4.10. Stress relaxation testing of each equivalent specimen. A. 8.9 mm width corresponding to 20% Z-myotomy. B. 5.8 mm width (40% Z-myotomy). C. 3.4 mm width (50% Z-myotomy). D. 1.3 and 1.2 mm width (60 and 80% Z-myotomy). Error bars indicate SD.

In this study, three spring-dashpot elements of a Wiechert viscoelastic model were chosen for good approximation. Then Eq. 4.2 can be rewritten as

$$E_{rel}(t) = E_0 + E_1\, exp\left(-\frac{t}{\tau_1}\right) + E_2\, exp\left(-\frac{t}{\tau_2}\right) + E_3\, exp\left(-\frac{t}{\tau_3}\right) \qquad \text{Eq. 4. 3}$$

Using the nonlinear data analysis software (OriginLab, Northampton, MA), curve fittings were performed on averaged relaxation curves of four different type specimens. All parameters for Eq. 4.3 were extracted from the fitting data and are shown in Table 4.2.

	E_0	E_1	E_2	E_3	τ_1	τ_2	τ_3	R^2
8.9 mm	222.85	202.06	250.57	647.32	37.79	3.79	0.34	0.9976
5.8 mm	230.33	284.99	206.96	613.13	4.92	50.68	0.37	0.9970
3.4 mm	306.09	678.73	296.62	212.73	0.41	4.78	48.20	0.9967
1.3 & 1.2 mm	404.35	678.78	310.67	235.50	0.40	4.58	44.42	0.9981

Table 4.2. Curve fitting parameters for each stress relaxation data. Parameters for Wiechert viscoelastic equation from averaged stress relaxation curves were extracted. E_0, E_1, E_2, and E_3 are relaxation modulus of the each spring, and τ_1, τ_2, and τ_3 are relaxation time of each dashpot. R^2 values are indicated for each curve fit.

4.4. Discussion

These biomechanical experiments confirm that Z-tenotomy and Z-myotomy incisions weaken both artificial material, as well as EOT, and EOM in graded fashion. However, the effect depends strongly on the structure of the material subjected to Z-tenotomy and Z-myotomy. A control experiment using isotropic rubber demonstrated a linear decline of maximum force according to the dose of cutting ratio. As the ratio increased, tensile force decreased because the amount of intact latex was reduced. At the same time, a coupling effect developed and progressively increased in the latex specimen, converting force transmission from pure axial

along the axis of elongation, to an increasing Z-shaped slant. Since latex rubber material has an isotropic structure throughout, shear force is efficiently transferred through the remaining specimen bridging the two incisions. It is therefore intuitive that a roughly linear reduction of maximum force as a function of cutting ratio occurs as a result of isotropic coupling effect.

Surgical advocates of Z-tenotomy appear to have implicitly assumed that EOT is an isotropic material like latex, because tenotomy percentages substantially exceeding 50% have been advised for effective SO weakening.[19] But, in the current experiments, neither SO nor SR tendon exhibited mechanical responses to progressively increasing Z-tenotomy that resembled latex. For both EOM tendons, failure force declined at an accelerating rate with progressive tenotomy until at or above 50%, there was hardly any force transmission at all. Z-tenotomy of 50% or more divides all continuity between parallel fibers extending the full length of the EOT, so any remaining resistance to failure force would be attributable to transverse coupling between adjacent fibers. Understandably, this residual failure force must be very low since transverse coupling between fibers has been shown the preceding dual channel tensile experiments to be very low. Putting it another way, Z-tenotomy or 50% or more is mechanically very nearly the same as complete, unguarded tenotomy. The difference in biomechanics reflects the internal structure of EOT.

More detailed analysis can be performed using viscoelastic characterization of Z-myotomy. When we compare the relaxation modulus, $E_{rel,}$ at the peak 30% strain for four different widths, relaxation modulus increased (1308, 1347, 1489, and 1625 kPa) as cross section area of specimen decreased (8.9, 5.8, 3.4 to 1.3 and 1.2 mm) meaning that a smaller residual EOM width reflects a larger tensile modulus. There has been similar reports that the tensile modulus of a small piece of tendon is greater than that of whole tendon.[28, 29] Butler et al. suggests

that the modulus of a small specimen of tendon may be more descriptive of the collagen in the tendon since the fascicle initial length and cross section can be more accurately determined and fiber bundles tend to be more parallel than in whole tissue.[30] The decreasing amount of connective tissues in smaller tendon also could be another reason for increasing modulus.[31, 32] Danylchuk et al. suggested that a precise definition of the tensile strength of ligament ought to take into account the relative contributions of collagen fasciculi and connective sheaths.[31] This study showed that EOM follows the same trend as tendon and ligament.

Another interesting comparison could be performed in terms of relaxation rate. For comparison purpose, each relaxation data was normalized by divided with maximum relaxation modulus. Fig 4.11 shows normalized relaxation curves in each Z-myotomy equivalence case.

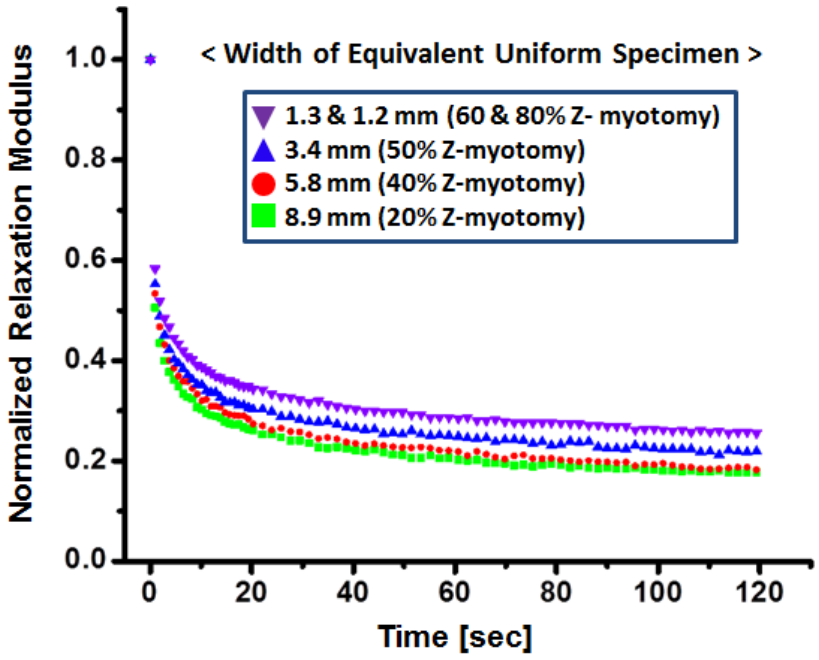

Fig. 4.11. Normalized stress relaxation of each Z-myotomy equivalent specimen. All four relaxation data sets were normalized to their corresponding maxima. As Z-myotomy ratio increased, specimens relaxed less and slower.

Results illustrate that as the specimen became smaller, it relaxed slower, and the asymptotic modulus increased. Atkinson et al. reported the similar tendency in human patellar tendon.[33] Large tendon specimens relaxed faster and more than smaller specimens. Greater fluid inside a large specimen could be the reason for greater relaxation due to high permeability to it. Also, large specimen exhibits a longer toe region representing straightening of the crimped fibrils at the beginning of the tensile phase. This longer toe suggests that tissue can be reoriented to align with the load, and squeezed more, and thus relax faster after reaching peak force. EOM can be analyzed in the same manner because of its similar structure to EOT. Both tensile modulus and relaxation rate trends according to specimen size can be rewritten in terms of Z-myotomy ratio; as Z-myotomy ratio increases, tensile modulus of the specimen increases, and relaxation rate decreases.

The biomechanics of EOT and EOM differ from isotropic latex since EOT and EOM do not have isotropic structures. An isotropic structure is the same in all directions. Tendon and muscle have orthotropic structure, the same in one direction – along the length of the fibers – but different transverse to the length of the fibers. Unlike latex rubber, EOT and EOM are composed of strong parallel fibers aligned in the longitudinal direction, thinly woven with sparse, thin transverse fibers and a small amount of viscous extrafibrillar matrix filled between fiber bundles. Our measurements by atomic force microscopy indicate that the individual longitudinal tendon fibers behave with pure elasticity of high stiffness, without significant viscosity.[34] Dual-channel load cell experiments have demonstrated that tensile elongation of any arbitrary proportion of EOT or EOM fibers within any EOM results in only about 5% coupling force transmission to the remainder of the fibers.[35] Poor transfer of shear force in EOT and EOM corresponds to substantial force decoupling between transverse layers, and represents the greatest biomechanical

difference from a material such as isotropic latex. These findings are especially relevant for Z-tenotomy exceeding 50% and Z-myotomy over 60%. A 50% or greater Z-tenotomy and Z-myotomy render discontinuous all of the stiff tendon fibers that normally transmit longitudinal force, leaving the minimal mechanism of shear force coupling as the only means of force transmission. It is particularly notable that transverse force coupling in EOT and EOM, which is low even for static elongations, declines even further in the dynamic case for elongations of increasing speed.[35] Of course, the current experiments were performed in vitro and deliberately isolated the EOTs and EOMs from sheaths and other tissues that would be present in vivo, so that biomechanics could be studied without confounding by these other tissues. However, the in vivo biomechanical coupling of other tissues to EOM or EOT is probably relatively small at most, so findings in vitro should not be much different from in vivo.

Since 70-80% Z-tenotomy of the SO has been advocated as necessary surgical technique,[19] the current data indicate that the operation as performed is mechanically equivalent to completely dividing all fibers of the EOT. The latter is likely to be technically simpler and faster to perform.

4.5. References

1. Caldeira JA. Graduated recession of the superior oblique muscle. *Br J Ophthalmol.* 1975;59:553-559.

2. Romano P, Roholt P. Measured graduated recession of the superior oblique muscle. *J Pediatr Ophthalmol Strabismus.* 1983;20:134-140.

3. Drummond GT, Pearce WG, Astle WF. Recession of the superior oblique tendon in a-pattern strabismus. *Can J Ophthalmol.* 1990;25:301-305.

4. Prieto-Diaz J. Posterior tenectomy of the superior oblique. *J Pediatr Ophthalmol Strabismus.* 1979;16:321-323.

5. Shin GS, Elliott RL, Rosenbaum AL. Posterior superior oblique tenectomy at the scleral insertion for collapse of a-pattern strabismus. *J Pediatr Ophthalmol Strabismus.* 1996;33:211-218.

6. Wright KW. Superior oblique silicone expander for brown syndrome and superior oblique overaction. *J Pediatr Ophthalmol Strabismus.* 1991;28:101-107.

7. Wright KW, Min BM, Park C. Comparison of superior oblique tendon expander to superior oblique tenotomy for the management of superior oblique overaction and brown syndrome. *J Pediatr Ophthalmol Strabismus.* 1992;29:92-97; discussion 98-99.

8. Seawright AA, Gole GA. Results of treatment of superior oblique overaction by silicone tendon-expander technique. *J Pediatr Ophthalmol Strabismus.* 1998;35:33-37.

9. Suh DW, Guyton DL, Hunter DG. An adjustable superior oblique tendon spacer with the use of nonabsorbable suture. *J. AAPOS.* 2001;5:164-171.

10. Talebnejad MR, Eghtedari M, Owji N, Alavi A. Superior oblique tendon elongation with fascia lata. *J. AAPOS.* 2008;12:507-509.

11. Berke RN. Tenotomy of the superior oblique for hypertropia. *Trans Am Ophthalmol Soc.* 1946;44:304-342.

12. Velez G. Graduated tenotomy of superior oblique by temporal approach for a-pattern anisotropia: A report of 49 cases. *Binocul Vis.* 1987;2::217-220.

13. Reynolds J, Wackerhagen M. Bilateral superior oblique tenotomy for a-pattern strabismus in patients with fusion. *Binocul Vis.* 1988;3:33-39.

14. Vempali VM, Lee JP. Results of superior oblique posterior tenotomy. *J. AAPOS.* 1998;2:147-150.

15. Jampolsky A. Oblique muscle surgery of the a-v patterns. *J. Pediatr. Ophthalmol. Strabismus.* 1965;2:31-36.

16. McNeer KW. Untoward effects of superior oblique tenotomy. *Ann. Ophthalmol.* 1972;4:747-750.

17. Crawford JS. Surgical treatment of true brown's syndrome. *Am. J. Ophthalmol.* 1976;81:289-295.

18. Souza-Dias C, Uesugui C. Efficacy of different techniques of superior oblique weakening in the correction of the "a" anisotropia. *J Pediatr Ophthalmol Strabismus.* 1986;23(2):82-86.

19. Brooks DR, Morrison DG, Donahue SP. The efficacy of superior oblique z-tenotomy in the treatment of overdepression in adduction (superior oblique overaction). *J. AAPOS.* 2012;16:342-344.

20. Lee SY, Cho HK, Kim HK, Lee YC. The effect of inferior oblique muscle z myotomy in patients with inferior oblique overaction. *J Pediatr Ophthalmol Strabismus.* 2010;47:366-372.

21. Shin A, Yoo L, Demer JL. Biomechanics of superior oblique z-tenotomy. *J AAPOS* 2013;17:612-617.

22. Fung YC. Biomechanics: Mechanical properties of living tissues, second edition. *Springer; New York.* 1993.

23. Wiechert E. Ueber elastische nachwirkung. *Dissertation, Königsberg University; Germany.* 1889.

24. Wiechert E. Gesetze der elastischen nachwirkung für constante temperatur. *Annalen der Physik.* 1893;286, 335–348, 546–570.

25. Roylance D. Mechanics of materials. *John Wiley & Sons; New York.* 1996.

26. Yoo L, Kim H, Gupta V, Demer JL. Quasilinear viscoelastic behavior of bovine extraocular muscle tissue. *Invest Ophthalmol Vis Sci.* 2009;50:3721-3728.

27. Anderson TL. Fracture mechanics: Fundamentals and applications, third edition. *Taylor & Francis; London, UK.* 2004.

28. Butler DL, Noyes FR, Walz KA, Gibbons MJ. Biomechanics of human knee ligament allograft treatment. *Transactions of the 33rd Annual Meeting of the Orthopedic Research Society San Francisco, CA.* 1987.

29. Stouffer DC, Butler DL, Hosny D. The relationship between crimp pattern and mechanical response of human patellar tendon-bone units. *Journal of Biomechanical Engineering* 1985;107:158-165.

30. Butler DL, Kay MD, Stouffer DC. Comparison of material properties in fascicle-bone units from human patellar tendon and knee ligaments. *J Biomech* 1986;19:425-432.

31. Danylchuk KD, Finlay JB, Krcek JP. Microstructural organization of human and bovine cruciate ligaments. *Clin Orthop Relat Res* 1978;294-298.

32. Yahia LH, Drouin G. Collagen structure in human anterior cruciate ligament and patellar tendon. *Journal of Materials Science* 1988;23:3750-3755.

33. Atkinson TS, Ewers BJ, Haut RC. The tensile and stress relaxation responses of human patellar tendon varies with specimen cross-sectional area. *Journal of Biomechanics* 1999;32:907-914.

34. Yoo L, Reed J, Shin A, Demer JL. Atomic force microscopy determination of young's modulus of bovine extra-ocular tendon fiber bundles. *Journal of Biomechanics.* 2014;In Press.

35. Shin A, Yoo L, Chaudhuri Z, Demer JL. Independent passive mechanical behavior of bovine extraocular muscle compartments. *Invest Ophthalmol Vis Sci* 2012;53:8414-8423.

Chapter 5

Conclusions

5.1. Biomechanical Studies of EOT

Nano-indentation of EOT fiber bundles analyzed within the Hertzian framework effectively characterized the transverse Young's modulus, a critical mechanical parameter, for bovine EOT fiber bundles. Transverse Young's modulus for fiber bundles from lateral, inferior, medial, superior recti, inferior and superior oblique EOTs were computed to be about 60 MPa, and did not vary significantly according to the anatomical EOM from which the EOTs were obtained. Single fibers from EOT exhibited much higher stiff and purely elastic, rather than viscoelastic, behavior.

A precise estimate of the PR of bovine EOTs was calculated using an OCT technique. The PR averaged 0.542 ± 0.011 for all six anatomical EOMs, implying that volume decreased, and density increased, during tensile loading. Considering that PR values for soft tissues have been reported to be between 0.35 and 0.49, EOTs have an unusual PR value among soft tissues. The volume change may be due to internal rearrangement of the fiber structure, which consists of a helical organization of fibrils within crimped fibers. The precise PR value for EOT determined in the present study should facilitate quantitative modeling of ocular motor biomechanics and is represented in a theoretical framework practical for graphical simulation of quasistatic ocular motility using FEM.

5.2. Independent Mechanical Behavior of EOM Compartments

Mechanical evidence for independent compartmental movement was investigated. Extensive experimental study was performed to examine the independent passive mechanical behavior of transverse and GL/OL EOM compartments using a dual channel micro-tensile load cell. Independent contractile behavior of EOM compartments was also demonstrated by calcium-induced contractile experiments. The current findings indicate that EOM and EOT have sufficient biomechanical independence to support the proposed functional diversity of actions in distinct neuromuscular compartments of the horizontal rectus EOMs, and following regionally selective surgical manipulations in rectus and oblique EOT. Since biomechanical independence only affords the opportunity, and not the obligation, of physiological independence of groups of fibers within any given EOM, it remains to be determined the extent to which innervational control coordinates or distinguishes the contractile activity of EOM subparts during the physiological and pathological ocular motor repertoire.

5.3. Biomechanics of Z-tenotomy and Z-myotomy

Biomechanical effects of Z-tenotomy and Z-myotomy were characterized using tensile loading. EOT and EOM failure force exhibited two significant trends varying with the amount of Z-tenotomy and Z-myotomy. For less than 50 and 60 % Z-tenotomy and Z-myotomy, failure force declined with a parabolic shape, rather than linearly as observed for latex rubber. In contrast, for more than 50 % Z-tenotomy and more than 60% Z-myotomy, force transmission

was reduced to the minimum not changing further with additional incision. Consequently, tendon and EOM showed a parabolic response to increasing Z-tenotomy and Z-myotomy, but minimum tensile force after 50% Z-tenotomy and 60% Z-myotomy. Since EOT and EOM have orthotropic structure, a 50% or greater cut renders discontinuous all of the EOT and EOM fibers that normally transmit longitudinal force, leaving the minimal mechanism of shear force coupling as the only means of residual force transmission.

Additional viscoelastic characterization was performed using Z-myotomy equivalence experiments, matching irregular Z-myotomy specimens to regular non-Z-myotomy specimens. After performing stress relaxation experiments with Wiechert viscoelastic mathematical modeling, we concluded that as Z-myotomy ratio increases, the tensile modulus of the specimen increases, and relaxation rate decreases. These biomechanical approaches and findings regarding Z-tenotomy and Z-myotomy will be helpful to clinicians and surgeons as a reference before Z-tenotomy and Z-myotomy treatment.